Copyright Warning & Restrictions

The copyright law of the United States (Title 17, United States Code) governs the making of photocopies or other reproductions of copyrighted material.

Under certain conditions specified in the law, libraries and archives are authorized to furnish a photocopy or other reproduction. One of these specified conditions is that the photocopy or reproduction is not to be "used for any purpose other than private study, scholarship, or research." If a, user makes a request for, or later uses, a photocopy or reproduction for purposes in excess of "fair use" that user may be liable for copyright infringement,

This institution reserves the right to refuse to accept a copying order if, in its judgment, fulfillment of the order would involve violation of copyright law.

Please Note: The author retains the copyright while the New Jersey Institute of Technology reserves the right to distribute this thesis or dissertation

Printing note: If you do not wish to print this page, then select "Pages from: first page # to: last page #" on the print dialog screen

ABSTRACT

SOURCE LOCALIZATION VIA TIME DIFFERENCE OF ARRIVAL

by
Ciprian Romeo Comsa

Accurate localization of a signal source, based on the signals collected by a number of receiving sensors deployed in the source surrounding area is a problem of interest in various fields. This dissertation aims at exploring different techniques to improve the localization accuracy of non-cooperative sources, i.e., sources for which the specific transmitted symbols and the time of the transmitted signal are unknown to the receiving sensors. With the localization of non-cooperative sources, time difference of arrival (TDOA) of the signals received at pairs of sensors is typically employed.

A two-stage localization method in multipath environments is proposed. During the first stage, TDOA of the signals received at pairs of sensors is estimated. In the second stage, the actual location is computed from the TDOA estimates. This later stage is referred to as hyperbolic localization and it generally involves a non-convex optimization. For the first stage, a TDOA estimation method that exploits the sparsity of multipath channels is proposed. This is formulated as an ℓ_1-regularization problem, where the ℓ_1-norm is used as channel sparsity constraint. For the second stage, three methods are proposed to offer high accuracy at different computational costs. The first method takes a semi-definite relaxation (SDR) approach to relax the hyperbolic localization to a convex optimization. The second method follows a linearized formulation of the problem and seeks a biased estimate of improved accuracy. A third method is proposed to exploit the source sparsity. With this, the hyperbolic localization is formulated as an an ℓ_1-

regularization problem, where the ℓ_1-norm is used as source sparsity constraint. The proposed methods compare favorably to other existing methods, each of them having its own advantages. The SDR method has the advantage of simplicity and low computational cost. The second method may perform better than the SDR approach in some situations, but at the price of higher computational cost. The ℓ_1-regularization may outperform the first two methods, but is sensitive to the choice of a regularization parameter. The proposed two-stage localization approach is shown to deliver higher accuracy and robustness to noise, compared to existing TDOA localization methods.

A single-stage source localization method is explored. The approach is coherent in the sense that, in addition to the TDOA information, it utilizes the relative carrier phases of the received signals among pairs of sensors. A location estimator is constructed based on a maximum likelihood metric. The potential of accuracy improvement by the coherent approach is shown through the Cramer Rao lower bound (CRB). However, the technique has to contend with high peak sidelobes in the localization metric, especially at low signal-to-noise ratio (SNR). Employing a small antenna array at each sensor is shown to lower the sidelobes level in the localization metric.

Finally, the performance of time delay and amplitude estimation from samples of the received signal taken at rates lower than the conventional Nyquist rate is evaluated. To this end, a CRB is developed and its variation with system parameters is analyzed. It is shown that while with noiseless low rate sampling there is no estimation accuracy loss compared to Nyquist sampling, in the presence of additive noise the performance degrades significantly. However, increasing the low sampling rate by a small factor leads to significant performance improvement, especially for time delay estimation.

SOURCE LOCALIZATION
VIA TIME DIFFERENCE OF ARRIVAL

by
Ciprian Romeo Comsa

A Dissertation
Submitted to the Faculty of
New Jersey Institute of Technology
in Partial Fulfillment of the Requirements for the Degree of
Doctor of Philosophy in Electrical Engineering

Department of Electrical and Computer Engineering

January 2012

.

APPROVAL PAGE

SOURCE LOCALIZATION
VIA TIME DIFFERENCE OF ARRIVAL

Ciprian Romeo Comsa

Dr. Alexander M. Haimovich, Dissertation Advisor — Date
Professor of Electrical and Computer Engineering, NJIT

Dr. Yeheskel Bar-Ness, Committee Member — Date
Distinguished Professor of Electrical and Computer Engineering, NJIT

Dr. Ali Abdi, Committee Member — Date
Associate Professor of Electrical and Computer Engineering, NJIT

Dr. Osvaldo Simeone, Committee Member — Date
Assistant Professor of Electrical and Computer Engineering, NJIT

Dr. Hana Godrich, Committee Member — Date
Postgraduate Research Associate of Electrical Engineering, Princeton University

BIOGRAPHICAL SKETCH

Author: Ciprian Romeo Comsa

Degree: Doctor of Philosophy

Date: January 2012

Undergraduate and Graduate Education:

- Doctor of Philosophy in Electrical Engineering,
  New Jersey Institute of Technology, Newark, NJ, 2012

- Master of Science in Electrical Engineering,
  Technical University "Gheorghe Asachi" of Iasi, Romania, 2001

- Bachelor of Science in Electrical Engineering,
  Technical University "Gheorghe Asachi" of Iasi, Romania, 2000

Major: Electrical Engineering

Presentations and Publications:

C. R. Comsa and A. M. Haimovich, "Performance Bound for Signal Parameters Estimation from Low Rate Samples," to be submitted to the IEEE Transactions on Signal Processing.

C. R. Comsa, A. M. Haimovich, S. Schwartz, Y. H. Dobyns, and J. A. Dabin, "Source Localization using Time Difference of Arrival within a Sparse Representation Framework," in the International Conference on Acoustics, Speech and Signal Processing (ICASSP), 2011, May 22-27, Prague, Czech Republic, pp. 2872-2875.

C. R. Comsa, A. M. Haimovich, S. Schwartz, Y. H. Dobyns, and J. A. Dabin, "Time Difference of Arrival Based Source Localization within a Sparse Representation Framework," in the 45th Annual Conference on Information Sciences and Systems (CISS), 2011, March 23-25, Baltimore, MD, USA, pp. 1-6.

C. R. Comsa, J. Luo, A. M. Haimovich, and S. Schwartz, "Wireless Localization using Time Difference of Arrival in Narrow-Band Multipath Systems," in the IEEE International Symposium on Signals, Circuits and Systems (ISSCS), 2007, July 12-13, Iasi, Romania, vol. 2, pp. 469 - 472.

Destinul omului este creația
Lucian Blaga

E ușor a scrie versuri cand nimic nu ai a spune
Mihai Eminescu

Căci dacă dragoste nu am, nimic nu-mi folosește
Sf. Ap. Pavel

Eu nu strivesc corola de minuni a lumii
şi nu ucid
cu mintea tainele, ce le-ntâlnesc
în calea mea
în flori, în ochi, pe buze ori morminte.
Lumina altora
sugrumă vraja nepătrunsului ascuns
în adâncimi de întuneric,
dar eu,
eu cu lumina mea sporesc a lumii taină –
şi-ntocmai cum cu razele ei albe luna
nu micşorează, ci tremurătoare
măreşte şi mai tare taina nopţii,
aşa îmbogăţesc şi eu întunecata zare
cu largi fiori de sfânt mister
şi tot ce-i neînţeles
se schimbă-n neînţelesuri şi mai mari
sub ochii mei –
căci eu iubesc
şi flori şi ochi şi buze şi morminte.
Lucian Blaga

ACKNOWLEDGMENT

This dissertation is the result of extensive research carried within the CWCSPR group at NJIT. This would not have been possible without the tremendous support and guidance of my adviser, Dr. Alexander M. Haimovich, whose contribution to my evolution as researcher I heartily appreciate. It is my pleasure then to thank Dr. Yeheskel Bar-Ness, Dr. Ali Abdi, Dr. Osvaldo Simeone, and Dr. Hana Godrich for the honor they gave me by serving as my dissertation committee members. A special thought I will always keep for Dr. Stuart C. Schwartz from Princeton University, whose experience, wisdom, and warm personality I also had the chance to benefit from.

I would also like to thank to the Ross Memorial Fellowship fund for partial financial support during my doctoral studies. Special thanks go to the staff of the graduate studies and international students' offices and to the faculty and staff of the ECE department for their advice and support. Among them, I owe my deepest gratitude to Ms. Marlene Toeroek who always had the right solution to every problem I dealt with.

I would equally like to show my gratitude to all my colleagues at CWCSPR and NJIT for becoming my friends and for all the moments we shared. I am also indebted to my colleagues from the Technical University "Gheorghe Asachi" of Iasi, Romania, for their support and assistance during my leave of absence at NJIT. Special thanks go to Dr. Paul Cotae, who made it possible for me to come at NJIT in the first place.

Finally, I am grateful to the many wonderful people who contributed to my intellectual formation before my PhD studies. I would also like to thank my parents and my family for their support and sacrifice that made it possible for me to accomplish high jumps in life, especially my beloved wife, Viorica, son and daughter, Kevin and Karina.

TABLE OF CONTENTS

TABLE OF CONTENTS
(Continued)

Chapter **Page**

LIST OF FIGURES

LIST OF FIGURES
(Continued)

Figure **Page**

LIST OF FIGURES
(Continued)

Figure **Page**

LIST OF SYMBOLS

$\boldsymbol{X}^T$	Transpose of matrix $\boldsymbol{X}$
$\boldsymbol{X}^H$	Transpose conjugate of matrix $\boldsymbol{X}$
$\boldsymbol{X}^*$	Conjugate of matrix $\boldsymbol{X}$
tr{·}	Trace of
Re{·}	Real part of
Im{·}	Imaginary part of
var{·}	Variance of
$\mathbb{E}\{\cdot\}$	Expected value of
AE	Amplitude Estimation
AOA	Angle of Arrival
AWGN	Additive White Gaussian Noise
CC	Cross-correlation
CDMA	Code-Division Multiple Access
CRB	Cramer Rao Bound
DFT	Discrete Fourier Transform
DOA	Direction of Arrival
DTFT	Discrete Time Fourier Transform
ESPRIT	Estimation of Signal Parameters via Rotational Invariance
FCC	Federal Communications Commission
FIM	Fisher Information Matrix
FRI	Finite Rate of Innovation

LIST OF SYMBOLS
(Continued)

GDOP	Geometrical Dilution of Precision
GMSK	Gaussian Minimum Shift Keying
GPS	Global Positioning System
LOS	Line of Sight
LR	Low Rate
LS	Least Squares
MIMO	Multiple Input Multiple Output
ML	Maximum Likelihood
MPDR	Minimum Power Distortionless Response
MS	Mobile Station
MSE	Mean Squared Error
MUSIC	Multiple Signal Classification
MXTM	Mini-max Total MSE
NLOS	Non Line of Sight
NLS	Nonlinear Least Squares
PDF	Probability Density Function
PSD	Power Spectral Density
RMSE	Root Mean Squared Error
ROI	Rate of Innovation
RSS	Received Signal Strength
SDP	Semidefinite Programming

LIST OF SYMBOLS
(Continued)

SDR	Semidefinite Relaxation
SNR	Signal-to-Noise Ratio
SPE	Signal Parameters Estimation
TDE	Time Delay Estimation
TDOA	Time Difference of Arrival
TOA	Time of Arrival
ULA	Uniform Linear Array
WLAN	Wireless Local Area Network
WLS	Weighted Least Squares
ZZB	Ziv-Zakai Bound

CHAPTER 1

INTRODUCTION

1.1 Source Localization in Wireless Systems

The localization of a signal source has been a problem of interest in various fields such as wireless communications, radar, sonar, navigation, acoustics, geophysics, or other sensor networks for the past few decades, due to technology advances, [1-6], and new requirements in terms of accuracy and operating environments, [7]. For example, in the USA, it is required now by the Federal Communications Commission (FCC) that the wireless service providers must report the call initiating mobile station (MS) location to an Emergency 911 (E-911) at the public safety answering point with an accuracy of 100 meters for 67% of all wireless E-911 calls. It is still expected that the required precision will be higher. But accurate localization is also desirable in many other applications. The wide range of applications, as well as that of conventional localization techniques, is summarized in many overviews in the literature, [8-20].

Localization techniques of wireless sources can be viewed as falling into two main categories, namely mobile-based (or forward link) localization systems, and network-based (or reverse link) localization systems, [15]. In the first case, the MS (serving as a receiver) determinates its own location by measuring the signal parameters of an external system such as the cellular system it operates on or the global positioning system (GPS). In the second case, the system determinates the position of the MS (as signal source) by measuring its signal parameters at the base stations (receiving sensors). The sensors measure the received signal and relay it to a fusion center for processing and estimation of the source location, as illustrated in Figure 1.1. The technique relies on

existing networks, e.g., cellular or wireless local area networks (WLAN). Network-based systems have the advantages of lower cost, size and battery consumption at the mobile device over the mobile-based systems. Also, in the GPS case, the mobile device needs signals from at least four satellites of the current network of 24 GPS satellites, albeit a hybrid method based on both GPS technology and the cellular infrastructure can also be used. Generally speaking, the GPS-based approach has a relatively higher accuracy, but it degrades in urban environments. All these considerations serve as motivation to seek improvements in network-based techniques for source localization.

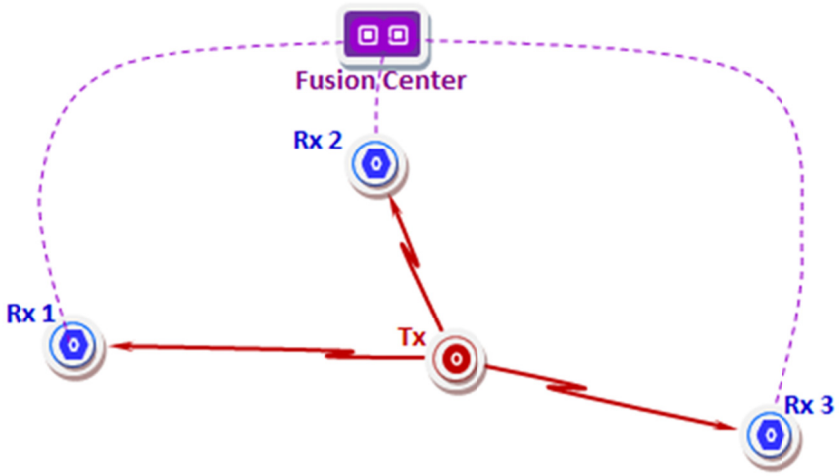

Figure 1.1 Localization system layout. The signal transmitted by the source Tx is received by sensors Rx1, Rx2, Rx3. The sensors relay the received signals to a fusion center, where the source location is estimated by processing the received signals.

With the network-based methods for source localization, the processing is performed based on some parameters of the signal received by the sensors, such as angle of arrival, signal strength, time of arrival, time difference of arrival, and combinations of these leading to hybrid techniques. Using these parameters, the actual source location is computed by triangulation. The angle of arrival (AOA) (or direction of arrival (DOA)) method involves measuring angles of the source as seen by several sensors; the received

signal strength (RSS) technique calculates the distance measuring the energy of the received signal; the time of arrival (TOA) procedure is based on measurements of travel time of the signal converted into distance, while the time difference of arrival (TDOA) is different from TOA by utilizing a reference sensor. These methods can all be used depending on specific applications and environments, each of them having their own advantages and drawbacks: e.g., the AOA method requires antenna arrays at each sensor, which make it costly; for RSS the channel (path-loss) model needs to be known, while TOA requires synchronization with the source clock.

The focus in this research is on the network-based localization within a plane. The source location space where the source is expected to be located is limited to some surveillance area, a priori known. The source is placed in the near-field of the sensors, i.e., the sensors are widely dispersed over the surveillance area. This means that both the bearing and range can be estimated for source localization, as opposed to the far-field case when only bearing (DOA) is typically estimated. Such source localization can be achieved either in one or two stages.

1.2 Two-Stage Source Localization

Typically, the source location is estimated in two stages. During the first stage, a measure of the received signal, usually the propagation time delay, is estimated at each sensor, [7, 10, 21-28]. In the second stage, the actual location is computed from the time delay estimates. Time delay estimation (TDE) becomes challenging in multipath propagation environments, where the line-of-sight (LOS) signal component becomes obscured by multipath reflections. Hence, accurate localization requires techniques capable of resolving the LOS signal component, [29-33]. When the transmitted signal and its

transmission time are known at a sensor, the TOA can be estimated by a variety of techniques. A classical method is to estimate the TOA from the timing of the peak of the cross-correlation (CC) between the transmitted and received signals, [21, 34]. The resolution of the TOA estimated in this case is limited by the width of the main lobe of the time autocorrelation function of the transmitted signal. This limitation makes the method unable to distinguish between the LOS signal and a reflected component when they are spaced closer than the resolution limit. Over the years, various techniques have been proposed to overcome this limitation. An example is the root-MUSIC method, belonging to a larger class called super-resolution methods due to their high resolution capabilities, [6, 9, 35-39].

Recently, some potentially even higher resolution estimation techniques have been proposed, based on the observation that many propagation channels associated with multipath environments tend to exhibit a sparse structure in the time domain, i.e., the number of multipaths is much smaller than the number of samples of the received signal. This sparsity has been exploited in TOA estimation, [40], and other TOA-related applications, such as compressed channel sensing, [41, 42], underwater acoustic channel deconvolution, [43], or channel response estimation in CDMA systems, [44]. TOA estimation requires the transmitted signal to be known to the sensors. In many applications, the source may be non-cooperative or otherwise the signal and timing information may not be available at the receiving sensors. The common approach for such a case is to take one of the sensors as reference and measure the TDOA at each of the other sensors with respect to the chosen reference sensor. A method for TDOA estimation for sparse non-negative acoustic channels is presented in [45], based on the

cross-relation introduced in blind channel identification [46-48]. Similar method has been presented in [49] and [50]. However, a discussion about the conditions under which this method works was included in [51].

In the current work, a method for high resolution TDOA estimation for complex-valued sparse multipath channels is developed and applied to source localization. The proposed method casts the TDOA estimation as a convex optimization problem that can be efficiently solved by conventional algorithms, [52]. In particular, the problem is formulated as an ℓ_1-regularization problem, i.e., the ℓ_1-norm is used to impose a sparsity-constraint on the channel. While the proposed approach does not require the transmitted signal to be known at the sensors side, as it is the case in [40-43], the pulse shape is assumed known. Also, for simplicity, the reference sensor is considered single-path, i.e., the reference sensor receives only LOS signal component.

For any pair of sensors, given their locations, the TDOA estimated at the first stage localizes the source on a hyperboloid with constant range difference between the two sensors. Since the source can occupy only a single point on the hyperbolic curve, TDOA measurements from the other sensors are used to resolve the location ambiguity. The process of finding a solution of the intersection of the hyperbolic curves is the second stage of the source localization, also referred to as hyperbolic localization, and is equivalent to solving a system of non-linear equations, [53], i.e., it is a non-convex optimization. Traditional solutions proposed in the literature for hyperbolic localization have generally poor robustness to errors in the TDOA estimates. More recent methods, which relax the non-convex problem to a convex optimization by applying a semi-definite relaxation (SDR) method, were found to be more robust to TDOA errors than the

traditional methods. However, the SDR methods are not optimal in general. In this dissertation, three convex optimization methods with different computational costs are proposed to improve the hyperbolic localization accuracy. The first method takes an SDR approach to relax the hyperbolic localization to a convex optimization. The second method follows a linearized formulation of the problem and seeks a biased estimate of improved accuracy. The first two methods perform comparably when the source is inside the convex hull of the sensors. When the source is located outside, the second approach performs better, at the cost of higher computation. A third method is proposed by exploiting the source sparsity. With this, the hyperbolic localization is formulated as an ℓ_1-regularization problem, where the ℓ_1-norm is used as source sparsity constraint. Computer simulations show that the ℓ_1-regularization can offer further improved accuracy, but at the cost of additional computational effort.

1.3 Single-Stage Source Localization

Aside from the two-stage approach, the source location can be also estimated directly, in a single stage, by making use of the signal parameters without estimating them as an intermediary step. Conventional single-stage methods generally apply the maximum likelihood (ML) approach to exploit amplitude and/or time delay information contained in the envelope of the received signals, [6, 54-62]. RSS, TOA, and TDOA based are among the well-known localization techniques. Since these exploit only the envelope of the received signals, they are collectively referred to as non-coherent. An alternative approach, which is referred to as the coherent localization, is to additionally exploit the carrier phases of the received signals among pairs of sensors. This is possible when the carrier phase of the received signals is preserved and mutual time and phase

synchronization is achieved across sensors. The localization is accomplished by formulating a localization metric which is a joint statistic that incorporates the time delay and phase information contained in the received signals as if transmitted from various points of the source two-dimensional location space. In the non-coherent case, the phase information is not exploited.

The two-stage and the single-stage localization approaches have in general comparable performance. However, the later requires higher computational effort. For example, the source location is typically estimated based on a grid search and the number of grid points, say N_g, is very high for a good resolution of the estimate. With the two-stage approach most of the computational effort is spent to estimate a small number of TDOAs, proportional to the number of sensors, say M. Estimation of each TDOA involves one search among N_g points, i.e., the overall computational effort is proportional to MN_g. With the single-stage approach, the computational effort is proportional to N_g^2 since a bi-dimensional search grid is required for location estimation. Nevertheless, with the modern computation capabilities, nowadays both two-stage and single-stage approaches are feasible. When comparing the one-stage non-coherent approach to the (one-stage) coherent one, the later can offer much higher accuracy, justifying the higher computational effort spent over the two-stage approach.

The potential for significant accuracy gain of coherent processing over the non-coherent has been shown in recent work on target localization employing active sensors, such as in MIMO (multiple input multiple output) radar systems [63-66]. As opposed to passive systems (of interest for the current problem) where all sensors receive the signal transmitted by the source to be located, in active systems, the signal usually travels a

round trip, i.e., a known signal transmitted by one sensor is reflected by the target and measured by the same or different sensor. The round trip and the reflectivity of the target make the received signal to noise ratio (SNR) lower than if the same receiving sensors would have to passively locate a signal source instead of the target. The great improvement in accuracy with coherent processing, particularly at high SNR, is due to the fact that the accuracy in coherent localization, as expressed by the Cramer Rao lower bound (CRB), is inverse proportional to the carrier frequency of the received signal, whereas for non-coherent localization, the accuracy is inversely proportional to the bandwidth of the received signal, [55, 63, 64, 67, 68]. This is referred to as coherency advantage in [64]. Beside the number of sensors, the localization accuracy is also strongly reliant on the received SNR and the relative geographical spread of the array sensors versus the source location. This dependence is referred to as spatial advantage.

While coherent processing can facilitate source localization with very high accuracy, the localization technique has to contend with high peak sidelobes in the coherent localization metric [69-73]. At high SNR, these sidelobes have limited impact on the performance, but bellow a threshold SNR value, performance degrades quickly, being affected by large errors [26, 27, 74-77]. Thus, while at high SNR the localization performance can be predicted by using the CRB, at low SNR other lower bounds have to be used, e.g. the Ziv-Zakai bound (ZZB), [77]. The coherent localization also requires precise knowledge of the sensor locations and phase synchronization across sensors, [78-81], which, although they are assumed given in this work, in practice may require additional self-calibration techniques.

1.4 Signal Parameters Estimation from Low Rate Samples

In many localization applications the signals can be uniquely described by a small number of parameters, [1]. For example, a stream of short pulses of known shape can be fully defined by the time delays of the pulses and their amplitudes. Since the number of parameters describing these signals is small, such signals are referred to as signals of finite rate of innovation (FRI). The number of parameters describing the FRI signals determines the rate of innovation of the signals, which is usually much smaller than the number of signal samples taken at the Nyquist rate. This observation was exploited to set the grounds for sampling at rates lower than the Nyquist rate. To this end, a mechanism to sample at low rates streams of Diracs can be found in [82], [83], and the references therein. A scheme for recovering the original stream from the samples was also proposed. A set of more recent works, e.g., [84] and [85], generalizes the approach to sampling at low rates streams of pulses of arbitrary shape. Furthermore, by contrast to [83], where the minimum sampling rate is dictated by the bandwidth of a sampling filter, the minimum sampling rate in [84] is given by the signal's rate of innovation (ROI). ROI can be easily illustrated for a signal $x_R(t)$ for which any of its segments of length T is uniquely determined by no more than $2K$ parameters, e.g., K time delays and K amplitudes. Thus, $x_R(t)$ is said to have FRI. Specifically, its local ROI is $2K/T$, i.e., it has no more than $2K$ degrees of freedom every T seconds. The sampling scheme developed in [84] for such FRI signals takes samples at a rate as low as $2K/T$. It is then shown that from these samples the original signal can be perfectly recovered by some signal processing technique. However, it was found in [86] that the performance of the signal recovery from low rate (LR) samples can deteriorate in the presence of noise substantially more

than the recovery from samples taken at the Nyquist rate would deteriorate. However, with conventional Nyquist sampling, if the noise is continuous time, i.e., it is generated prior to sampling, oversampling does not help. By contrast, when sampling at ROI, increasing the sampling rate brings substantial signal recovery performance improvement.

This dissertation investigates, among others, the performance of time delay and amplitude estimation from samples taken at low rates in the presence of additive noise affecting the transmission channel. To this end, a CRB is developed in general and particular settings. With low rate sampling in noise, the CRB shows higher performance degradation than if samples would be taken at the Nyqist rate. However, increasing a low sampling rate by a small factor leads to considerable performance improvement. For the particular setting considered, this improvement is proportional to the cube of the increase factor. The resolvability of two close paths is also shown to improve with the sampling rate and inter-path separation.

1.5 General Framework and Signal Model

With passive localization, the unknown x-y location ξ_0 of an emitting source has to be estimated based on the signals collected by a number M of sensors. The source is assumed to transmit an unknown lowpass signal $s_0(t)$ modulating a carrier frequency f_c. The signal is assumed narrow-band in the sense that the carrier frequency is much higher than the signal's bandwidth. The sensors are widely dispersed within a surveillance area, at precisely known arbitrarily fixed locations ξ_k, forming a distributed sensor array. The source is in the near-field of the distributed array in the sense that it has a different bearing, and possibly a different range, with respect to each of the sensors. Ideal mutual

time and phase synchronization are assumed across the sensors. These allow complete source localization by coherent processing, i.e., by processing both the envelope and the carrier phase measurements at the sensors. Complete source localization is also possible by non-coherent processing, i.e., by processing only the envelope information at the sensors. The processing can be performed in two stages or in a single stage and is all carried out at a fusion center assumed linked via ideal communication links to the sensors. Both the envelope and the carrier phase measurements are related to the source location by the embedded time delay. The time delay between the source at ξ_0 and a sensor at ξ_k is given by

$$\tau_k(\xi_0) = \frac{1}{c} d_k(\xi_0) = \frac{1}{c}\sqrt{(x_k - x_0)^2 + (y_k - y_0)^2}\ , \tag{1.1}$$

where c is the speed of light and $d_k(\xi_0)$ is the travelled distance between the two locations.

When the propagation environment is multipath free, i.e., the sensors receive only the LOS component, the model for the signal received at a sensor is expressed

$$r_k(t) = \alpha_k s_0\big(t - \tau_k(\xi_0)\big) + w_k(t)\ , \tag{1.2}$$

where α_k is the complex-valued channel gain (pathloss due to source-sensor separation plus carrier phase shift) and $w_k(t)$ is additive white Gaussian noise (AWGN), with variance σ^2, $w_k(t) \sim \mathcal{N}(0, \sigma^2)$. The system is assumed stationary over the observation time interval such that α_k and τ_k are time invariant over the aforementioned interval. The complex gain is expressed

$$\alpha_k = g_k e^{-j\omega_c \tau_k(\xi_0)}\ , \tag{1.3}$$

where $\omega_c = 2\pi f_c$ and g_k is the real-valued gain (in fact attenuation) of the transmitted signal through the propagation channel from the source to a sensor. With the assumption that the signal arrives at a sensor through the LOS path from the source, g_k depends only on the free space propagation path loss, which varies with the source location. For example, for the free-space propagation the attenuation of the LOS component is typically related to the distance between transmitter and receiver as in [87]:

$$g_k = \frac{c}{4\pi f_c} d_k^{-1}(\xi_0) \ . \tag{1.4}$$

The carrier phase term $e^{-j\omega_c \tau_k(\xi_0)}$ in (1.3) is a demodulation residue and it depends on the carrier frequency and the unknown propagation delay, and thus on the source location. The variation of g_k with the source location is observed to be much slower than that of the phase term. Furthermore with the signal model (1.2), g_k can be roughly determined, for example by direct measurement of the received power (with respect to the transmitted power).

Since source localization relies on the relation between the received signal parameters and the travel distance, for accurate localization it is desirable the travel path to be the LOS path. However, in many cases the propagation environment is multipath, meaning that the received signal is a superposition of signal components, each of them arriving with different delay, attenuation and phase shift. In general, the LOS component may be present among these or it may be missing due to some physical obstruction. It was shown in [31] that the non-line-of-sight (NLOS) components cannot help to source localization unless some a priori knowledge about them, e.g., their statistical distribution, is known. Otherwise, it is better to discard the NLOS components. Thus, one challenge is to separate the LOS component from the NLOS ones. If the LOS component is missing

completely, the only option to perform accurate source localization is to exploit the a priori knowledge about the NLOS components. Identifying and dealing with the NLOS-only case was discussed in a number of publications, e.g., [32, 33]. Throughout the current work, whenever dealing with multipath propagation, it assumed that the received signal consists of a sum of the LOS and NLOS components:

$$r_k(t) = \alpha_k s_0(t - \tau_k) + \sum_{p=2}^{P_k} \beta_{kp} s_0\left(t - \tau_{kp}\right) + w_k(t)\,, \tag{1.5}$$

where P_k is the number of multipath components (LOS and NLOS) impinging the k^{th} receiver. The LOS component parameters are the same as for the model (1.2), while for each of the p^{th} NLOS component, the signal parameters are the time delay τ_{kp} and the complex channel gain,

$$\beta_{kp} = h_{kp} e^{j\phi_{kp}}, \tag{1.6}$$

with the attenuation h_{kp}, and the phase shift ϕ_{kp}. Note that for the NLOS components the phase shift doesn't depend only on the carrier frequency f_c and the travel time τ_{kp}, but it suffers from additional (difficult to predict) shifts caused by physical propagation phenomena, such as scattering.

1.6 Outline

This dissertation addresses the passive localization in plane of wireless non-cooperative sources, i.e., sources for which the actual signal and the time and phase of the transmitted signal are unknown to the sensors. The source is placed in the near-field of the sensors, meaning that both the bearing and range can be estimated for source localization. The

location processing is carried out at a fusion center assumed to have ideal communication links to the sensors. Mutual time synchronization across sensors is also required for non-coherent processing. For coherent processing both time and phase synchronization across sensors is needed. The location is estimated based on the source-to-sensors distance information embedded into the received signal parameters. Thus for accurate localization the LOS signal component is assumed to reach all the sensors. These are the major assumptions used to approach the source localization problem.

The aim of the Chapter 1 of the dissertation is to provide an introduction to the source localization problem. In order to bring a motivation for addressing this topic, a brief overview of the source localization techniques approached in the literature and their limitations is provided. The methods studied in this dissertation are also introduced, followed by the general framework for the source localization, including systemic aspects, main assumptions, and signal models.

Chapter 2 discusses the two-stage localization approach and introduces new methods that exploit the sparse structure of multipath channels and of source location space. Each of the two stages is formulated employing standard convex optimization tools. The proposed methods are shown to deliver higher accuracy and robustness to noise, compared to existing conventional two-stage source localization methods. The main results of this chapter were also included in [88] and [89].

The single-stage source localization is treated in Chapter 3. The coherent localization is explored. A location estimator is constructed based on a maximum likelihood metric. The potential of accuracy improvement by the coherent approach is shown through the Cramer Rao lower bound. However, the technique has to contend with

high peak sidelobes in the localization metric, especially at low SNR. Employing a small antenna array at each sensor is one approach to minimize the sidelobes level. Some results of this chapter were also included in [24].

In Chapter 4, the performance of time delay and amplitude estimation from samples of the received signal taken at rates lower than the conventional Nyquist rate is evaluated. To this end, a Cramer Rao lower bound is developed and its variation with system parameters is analyzed. It is shown that while with noiseless low rate sampling there is no estimation accuracy loss compared to Nyquist sampling, in the presence of additive noise the performance degrades significantly. However, increasing a low rate sampling by a small factor leads to significant performance improvement, especially for time delay estimation. The main results of this chapter will be included also in [90].

Overall concluding remarks and avenues for future work are given in Chapter 5.

CHAPTER 2

TWO-STAGE SOURCE LOCALIZATION

Typically, the source location is estimated in two stages. During the first stage, a measure of the received signal, usually the propagation time delay, is estimated at each sensor. In the second stage, the actual location is computed from the time delay estimates. In Figure 2.1 the layout of the source localization system based on TOA measurements is illustrated within the general framework described in the Chapter 1. The system based on TDOA measurements is similar, except that the source location is given by a intersection of hyperbolas instead of circles.

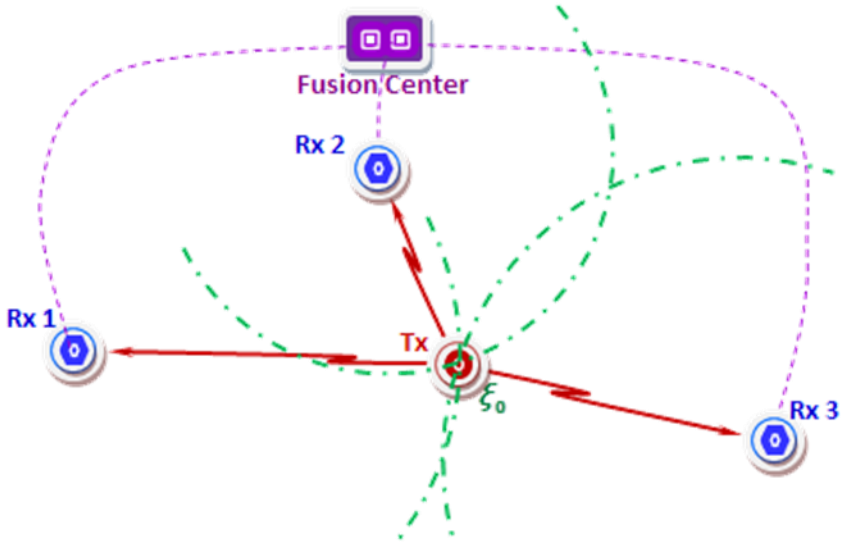

Figure 2.1 Two-stage localization system layout. The fusion center estimates the TOAs at the three receiving sensors. The values of each TOA localizes the source on circle, thus the location of the source is given by the intersection of the three circles.

2.1 TDOA Estimation

2.1.1 Signal Model

Within the general framework presented, the model for the signal received at any sensor is expressed as the convolution between the transmitted signal, $s_0(t)$, and the channel impulse response (CIR), $h_k(t)$:

$$r_k(t) = (s_0 * h_k)(t) + w_k(t), \tag{2.1}$$

where $w_k(t)$ is additive white Gaussian noise (AWGN), with variance σ^2. Time delay estimation is particularly challenging in multipath environments. For the two-stage approach, in general the carrier phase information is discarded, [26], so the multipath channel is modeled

$$h_k(t) = g_k\delta(t-\tau_k) + \sum_{p=2}^{P_k} \beta_{kp}\delta\big(t-\tau_{kp}\big), \tag{2.2}$$

where $\delta(\cdot)$ denotes the delta function, P_k is the number of paths of the channel observed at sensor k, g_k is the LOS component real valued attenuation, and β_{kp} is the complex valued channel gain of the NLOS components. The channel parameters P_k, g_k and β_{kp} are unknown to the sensors.

The localization method proposed in this chapter is based on the estimation of the TDOA at pairs of sensors, $\Delta\tau_{kl}(\xi_0) = \tau_k(\xi_0) - \tau_l(\xi_0)$. The LOS propagation delay between the source located at ξ_0 and any sensor at ξ_k, $\tau_k(\xi_0)$, is proportional to the source-to-sensor distance: $\tau_k(\xi_0) = (1/c)\sqrt{(x_k - x_0)^2 + (y_k - y_0)^2}$, where c is the speed of light. A TDOA measurement localizes the source on a hyperboloid with a constant range difference between the two sensors, k and l. Since the source can occupy

only one point on the hyperbolic curve, TDOA measurements from the other sensors are used to resolve the location ambiguity. One of the sensors, say $l = 1$, is chosen as reference such that the sensor pairs used for TDOA estimation are $\{k, 1\}$, for $k = 2, \dots, M$.

2.1.2 Conventional TDOA Estimation

For the estimation of the TDoAs, which is the first stage, one natural approach is using the ML estimation, which implies a maximization is performed for all the delays TDOA, e.g., [60]. It has been shown in [21] that for single path channel models this approach is equivalent to applying the generalized cross-correlation (GCC) technique with a Hannan-Thomson (HT) processor. This takes the received signals r_i, filters them by some function $H_i(f)$ specified in [21], v_i, $i \in \{k, l\}$ being the signals obtained after filtering. Then it takes the cross-correlation $R_{v_k v_l}$ of the results and searches for its maxima. The corresponding time lag represents the TDOA. The cross-correlation $R_{v_k v_l}(\tau)$ is $\int_{-\infty}^{\infty} \psi_g(f)\, G_{v_k v_l}(f) e^{j2\pi f\tau} df$, where $\psi_g(f) = H_k(f) H_l^*(f)$ is the HT processor and $G_{v_k v_l}(f)$ is the cross power spectral density function (the Fourier transform of the cross-correlation $R_{v_k v_l}(\tau)$) of the received signals $r_k(t)$ and $r_l(t)$. In practice, instead of the actual cross-correlation $R_{v_k v_l}$, an estimate is obtained from the finite observations r_k and r_l.

Aside from HT, other processors $\psi_g(f)$ have been suggested in the literature and tested for multipath channel models too, including the simple cross-correlator (CC), which assumes $\psi_g(f) = 1$. The CC has the advantage of simple implementation, but unfortunately, it may lead to relative large biases, especially when it is used in narrow-

band systems operating in a dense multipath environment. The ML estimator is asymptotically optimal (achieves the CRB bound, which by definition is the lower limit of the variance of an unbiased estimate [91, 92], asymptotically as SNR or the number of signal samples goes to infinity). However, it should be pointed out that in order for the ML estimator to achieve optimal performance, not only that the sample space should be large enough, but the environment should be multipath free. Furthermore, the spectra of the noise signals have to be known a priori. If anyone of these conditions is not satisfied, the ML algorithm becomes suboptimal, like other GCC members, [23].

Another option available for TDOA estimation is the application of super-resolution techniques, e.g., [35]. The basic idea is to estimate the noise subspace through eigen-decomposition, and then to estimate the signal parameters by utilizing the fact that the signal vector is orthogonal to the noise subspace. Based on this, an objective function, say $\mathcal{S}$, is constructed such that its first largest, say L' peaks offer a way to find the unknown parameter of interest, the TDOA, in this case. Root-MUSIC is one such technique that seems to offer good performance, especially at low SNR. In this case, the objective function takes the form of a polynomial, and it is necessary to find the L' roots with the largest magnitude (closest to the unit circle) [1]. Root-MUSIC is computationally attractive since it employs only a one-dimensional search, compared to the ML estimation which requires a multi-dimensional search.

However, in practical situations there are some difficulties that have to be overcome, [35]. First, the correlation matrix of the received signals is needed. The objective function for estimating the time delay is constructed based on the eigenvalues and eigenvectors of this correlation matrix. In practice, the correlation matrix has to be

estimated from the measured data samples. Limited length of the data snapshot results in accuracy loss in estimating the correlation matrix. Second, additional processing, e.g., forward-backward spatial smoothing, [93-95], is needed to decorrelate the signal components to fit the assumptions in MUSIC. Third, one of the most important difficulties is estimating the number of signal components, L', because it has decisive influence on the time delay estimation by MUSIC-like algorithms. Conventional order selection algorithms, e.g., AIC, MDL, hypothesis testing, Gerschgorin radii, or support vector machine, may be used, but their performance is still questionable, [35, 96-101].

2.1.3 TDOA Estimation for Sparse Channels

Regardless of the difficulties enumerated with the super-resolution approaches, recent work has shown that channel estimation in general, and time delay estimation in particular, can be improved through sparsity regularization, [40-44]. In this section, an ℓ_1-regularization method for TDOA estimation is proposed, exploiting the sparsity of multipath channels.

The ℓ_1-regularization method

Assuming for simplicity of presentation that the time-delays of the CIR are integer multiples of the sampling rate, define the received signal vector $\boldsymbol{r}_k = [r_k(1), \dots, r_k(Q+L-1)]^T$, the CIR vector $\boldsymbol{h}_k = [h_k(1), \dots, h_k(L)]^T$, and the noise vector $\boldsymbol{w}_k = [w_k(1), \dots, w_k(Q+L-1)]^T$, where $Q+L-1$, L, and Q are the lengths of the received signal vector, channel and transmitted signal vector, respectively. With these, the signal model (2.1) can be written as

$$\boldsymbol{r}_k = \boldsymbol{S}\boldsymbol{h}_k + \boldsymbol{w}_k, \tag{2.3}$$

where $\boldsymbol{S}$ is the $(Q + L - 1) \times L$ matrix relating the received signal vectors $\boldsymbol{r}_k$ to the channel vectors $\boldsymbol{h}_k$. Since typically $L \gg P_k$, the CIR, $\boldsymbol{h}_k$, is a sparse vector. Sparsity of the CIR vector can be enforced by minimizing its ℓ_0-norm, i.e., the number of non-zero elements. Minimization of the ℓ_0-norm of $\boldsymbol{h}_k$ is a non-convex optimization problem and it is NP-hard, which means that no known algorithm for solving this problem is significantly more efficient than an exhaustive search over all subsets of entries of $\boldsymbol{h}_k$. In lieu of the ℓ_0-norm, an approximation, e.g., the ℓ_1-norm, can be used with $0 < q \leq 1$. While smaller q implies better approximation of the ℓ_0-norm, $q = 1$ is often used because minimization of the ℓ_1-norm is a convex problem, and it can be efficiently solved by standard algorithms. Thus, assuming that the transmitted signal, and hence the matrix $\boldsymbol{S}$, are known, the CIR estimation can be formulated as an ℓ_1-regularization problem [43],

$$\underset{\boldsymbol{h}_k}{\text{minimize}} \quad \|\boldsymbol{r}_k - \boldsymbol{S}\boldsymbol{h}_k\|_2^2 + \lambda_k \|\boldsymbol{h}_k\|_1, \tag{2.4}$$

where $\|\boldsymbol{v}\|_q = \sqrt[q]{\sum_i |v_i|^q}$ denotes the q-norm of vector $\boldsymbol{v}$.

The estimate of the CIR can be used to find the TOA as the timing of the earliest peak of the CIR. We now seek to formulate the problem of TDOA estimation. The TDOA has to be determined from a sufficient statistic involving signals received at two sensors. A common such statistic is cross-correlation of the received signals, implying that the TDOA has to be estimated from the cross-correlation of the CIR of two channels, e.g., from $h_{kl}(t)$. For a single channel, the TOA is determined as the time of the first path of the estimated channel. However, when cross-correlating two CIR's, the time of the first path in the cross-correlation does not necessarily correspond to the TDOA. Assuming that for each of the channels, the line-of-sight path is the strongest, the TDOA

can be found from the time of the strongest component of the cross-correlation. Here, to simplify the situation, it is assumed that one of the sensors does not experience multipath, and use this sensor as reference for TDOA estimation. In this case, the TDOA is given by the delay of the first time component of $h_{kl}(t)$. Cross correlating the signal received at sensor k with the reference sensor l, and dropping the noise term for simplicity,

$$\widetilde{\boldsymbol{y}}_{kl} = \boldsymbol{\Gamma}_S \boldsymbol{h}_{kl}, \tag{2.5}$$

where $\widetilde{\boldsymbol{y}}_{kl} = \boldsymbol{F}\boldsymbol{y}_{kl}$, $\boldsymbol{F}$ is the unitary discrete Fourier transform (DFT) matrix, and $\boldsymbol{y}_{kl}$ is the cross-correlation sequence of the received signal vectors $\boldsymbol{r}_k$ and $\boldsymbol{r}_l$. Let $N = 2Q + 2L - 3$ be the number of elements of the vector $\boldsymbol{y}_{kl}$. The matrix $\boldsymbol{\Gamma}_S$ is a $N \times N$ transformation matrix relating the frequency domain cross-correlations of the received signals, $\widetilde{\boldsymbol{y}}_{kl}$, to the time-domain cross-correlations of the channels, $\boldsymbol{h}_{kl}$. It can be verified that $\boldsymbol{\Gamma}_S = \mathrm{diag}\{\widetilde{\boldsymbol{u}}_S\}\,\boldsymbol{F}$, where $\widetilde{\boldsymbol{u}}_S$ is the power spectral density of the transmitted signal padded with $L - 1$ zeros.

The problem of TDOA estimation can be formulated as an ℓ_1-regularization problem:

$$\underset{\boldsymbol{h}_{kl}}{\text{minimize}} \;\; \|\widetilde{\boldsymbol{y}}_{kl} - \boldsymbol{\Gamma}_S \boldsymbol{h}_{kl}\|_2^2 + \lambda_{kl}\|\boldsymbol{h}_{kl}\|_1, \tag{2.6}$$

which may be efficiently solved with conventional convex optimization algorithms, [52]. Note the presence of the auto-correlation of the transmitted signal within the cost function. The proposed TDOA method utilizes auto-correlation information (for uncorrelated symbols, pulse shape information is sufficient), but the method is blind in the sense that it does not require knowledge of the transmitted symbols.

Formulating (2.3) with a denser sampled channel has the potential of a higher resolution TDOA estimate, but increases the complexity of the optimization algorithms. An iterative grid refinement approach is adopted to keep the complexity of the optimization algorithms in check. Initially, (2.6) is solved for the samples corresponding to a desired range of delays. A refined grid is obtained by taking a second set of samples focusing on a range of delays that are indicated by the first iteration to contain multipath. This corresponds to a higher sampling rate of the smaller area of interest. Samples of the second set are obtained by interpolating the original samples. The transformation matrix $\boldsymbol{\Gamma}_S$ is also recalculated to match the refined sample support of the correlation sequences. With the refined grid, (2.6) is solved again and a new TDOA estimate, of higher resolution, is obtained. The grid refinement procedure can be repeated until a desired resolution is attained.

Discussion

The cost function to be minimized in ℓ_1-regularization problems, e.g., (2.4) and (2.6), has two terms: the first term is a measurement fidelity (or reconstruction error); the second term is a regularization (or penalization) term, that imposes sparsity on the estimate by using its ℓ_1-norm. The factor λ is a regularization parameter. The sparsity of the solution is governed by the choice of λ, which balances the fit of the solution to the measurements versus sparsity, [102]. A small regularization parameter corresponds to a good fit to the measurements, while too much regularization (over-penalization through a large λ) produces sparser results, but may fail to explain the measurements well. A number of methods have been studied in the literature for automated choice of λ (see [103] and the references therein). However, in practice an optimal value of λ is difficult

to select by any of these methods, and usually the choice of λ resorts to semi-empirical means, [102].

It is known that super-resolution methods, such as root-MUSIC, have the capability of asymptotically achieving optimal performance. However, in practice, with limited number of samples, or with highly correlated signal components, the accuracy performance often degrades away from the theoretical lower bounds, due to resolution limitations, [39]. In recent works, [43, 104], it was found that the ℓ_1-regularization method may offer higher resolution than the super-resolution methods. Moreover, the sparse regularization has the advantage of producing good accuracy even at low signal-to-noise ratios (SNR), i.e., it exhibits good robustness to noise, as it has been noted in [104]. In fact, it has been proved (see [105] and the references therein) that there is a fundamental connection between robustness and sparsity. Specifically, if some disturbance is allowed into the transformation matrix $\boldsymbol{\Gamma}_S$ or the measurements vector $\boldsymbol{y}_{kl}$, finding the optimal solution in the worst case sense is equivalent to solving the problem in the ℓ_1-regularization formulation, which imposes sparse solutions.

The ℓ_1-regularization continuously shrinks the estimate elements toward 0 as λ increases, leading to sparse solutions. However, the ℓ_1-regularization shrinkage results in a small bias in the non-zero elements of the estimate, since the estimation of these elements is based on the measurement fidelity term, [106]. Thus, solving the problem of estimating $\boldsymbol{h}_{kl}$ from the measurements $\boldsymbol{y}_{kl}$, (2.5), by employing an ℓ_1-regularization formulation, (2.6), may lead to a sub-optimal solution for the non-zero elements of the estimate. However, despite this downside, with a reasonable choice of λ, the ℓ_1-regularization method still produces better TDOA estimation (and hence source

localization) accuracy than conventional techniques, especially at low SNR, as demonstrated by the results presented in Section 2.3. Moreover, the proposed method doesn't necessary require knowledge of the number of the multipath components, as root-MUSIC does.

When the power spectral density of the transmitted signal is flat across the frequencies of interest, $\boldsymbol{\Gamma}_S$ in (2.5) has the form of a DFT matrix. In this case, the sparse estimate can be found with fewer equations than in (2.6), reducing the required computational effort. A procedure for selecting a subset of equations among those in (2.6) and the sufficient number of equations in the subset to ensure that the solution is not altered, can be found in [107].

2.2 Hyperbolic Source Localization

2.2.1 Methods for Hyperbolic Localization

The hyperbolic localization term is used herein to denote the second of the two stages of the source localization via TDOA estimation. This section offers an overview of the existing hyperbolic localization algorithms.

With hyperbolic localization, the estimated TDOAs are transformed, by multiplication with the known signal propagation speed, into range difference information for constructing a set of hyperbolic curves. Efficient algorithms are needed then to produce an accurate solution to the non-linear system of equations defining the hyperbolic curves, relying on the knowledge of the sensors locations. The solution provided by these equations is the estimated location of the source, but since the system of equations is generally non-linear, solving for it is not a trivial operation.

In the literature, there are mainly two traditional approaches to solve the hyperbolic localization problem. The first approach is based on the nonlinear least squares (NLS) framework [108] and implies finding the global minimum of a NLS objective function. Under the standard assumption that the TDOA estimates have Gaussian distribution, the global minimum of the objective function corresponds to a maximum likelihood (ML) location estimate, enjoying asymptotic optimality properties, [109]. Although optimum estimation performance can be attained, the algorithm converges to the correct solution only if it is initialized sufficiently close to the final solution. Otherwise, the estimate may be a local minimum, since the objective function may have multimodal features, i.e., the problem is non-convex. This is illustrated in Figure 2.2, where one realization of the multimodal objective function is shown for a case with 4 sensors. A second traditional approach is to transform the set of nonlinear equations into a set of linear equations by squaring them and introducing an intermediate variable, expressed as function of the source location, [53, 110-112]. A representative example of this approach is the two-step weighted least squares (WLS) method proposed in [53]. This method provides an approximation of the ML estimator for source location. However, this approximation holds only when the estimation errors are small, [113].

A third, more recent approach to hyperbolic localization is to relax the non-convex problem to a convex one that can be efficiently solved by standard algorithms, [52]. This can be achieved by applying a semi-definite relaxation (SDR) method, [114]. While this approach doesn't guarantee optimality, the solution is generally close enough to the optimal, to at least serve as initialization for a gradient algorithm solving. Moreover, the SDR approach has been found to be more robust to TDOA estimation

errors than traditional approaches. In the literature, various SDR methods, each with its own advantages and drawbacks, were proposed to solve different variations of the hyperbolic localization problem, [109, 113, 115, 116].

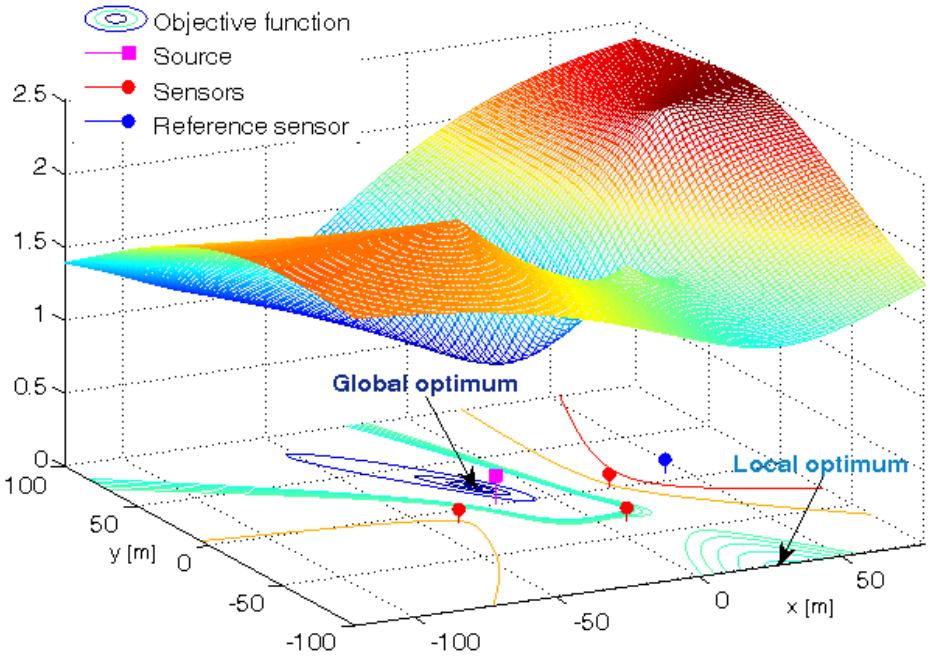

Figure 2.2 Non-convex realization of the localization objective function. The NLS objective function is built on three TDOAs estimated from signals received at four sensors.

In this chapter, three different methods are proposed to solve the nonlinear system of equations defining the hyperbolic localization problem. The proposed methods improve over existing methods in different scenarios, with different computational costs. The first method is an alternative to the WLS solution by formulating the hyperbolic localization problem as a constrained minimization and relaxing the quadratic relation between the intermediate variables introduced and the source location. The second method is to seek a biased estimate instead of the conventional unbiased estimate produced by the WLS method. This method is developed in a more general biased estimation context discussed in [117] and is also formulated as a constrained

minimization problem. Finally, the third method is to introduce a grid over the surveillance area and formulate an objective function related to the likelihood of the source to occupy a certain point on the grid. Exploiting the sparsity of the sources, the problem is formulated as an ℓ_1-regularization, solvable by standard convex optimization algorithms, [52].

2.2.2 System Model

With the hyperbolic localization problem, the unknown location, $\xi_0 = [x_0, y_0]^{\mathrm{T}}$, of a signal source has to be estimated based on $M-1$ TDOAs estimated by a number M of sensors, $M \geq 3$. The sensors are assumed dispersed within a surveillance area, at arbitrary but precisely known locations, $\xi_k = [x_k, y_k]^{\mathrm{T}}$. Perfect time synchronization is assumed across sensors. One of the sensors, say the first, is used as reference. The estimates express the TDOA with respect to the reference sensor. It is further assumed that the TDOA estimates, τ_{k1}, are available at a fusion center, where the location estimation is performed. The location of the source is estimated by converting the TDOA estimates into range differences, i.e., $d_{k1} = c\tau_{k1}$, for $k = 2, \dots, M$, where c is the speed of light. Denoting the true distance (noise free) value of d by d^{g}, the range differences are commonly modeled, [53],

$$d_{k1} = d_{k1}^{\mathrm{g}}(\xi_0) + n_{k1}, \text{ for } k = 2, \dots, M, \tag{2.7}$$

where $d_{k1}^{\mathrm{g}} = \|\xi_k - \xi_0\|_2 - \|\xi_1 - \xi_0\|_2$, with $\|\xi_k - \xi_0\|_2 = \sqrt{(x_k - x_0)^2 + (y_k - y_0)^2}$ denoting the Euclidean distance between the source and sensor k. The noise term n_{k1} is usually modeled as a zero mean Gaussian random process. The covariance of $\boldsymbol{n} = [n_{k2}, \dots, n_{kM}]^{\mathrm{T}}$ is denoted by $\boldsymbol{Q}_n = \mathbb{E}\{\boldsymbol{n}\boldsymbol{n}^{\mathrm{T}}\}$, where $\mathbb{E}$ is the expectation operator; $\boldsymbol{Q}_n$ is

assumed known up to a scalar. Note that because of the common reference, in reality matrix $\boldsymbol{Q}_n$ is not a diagonal matrix. However, it is a common practice in the literature to model the range difference estimation errors as independent across sensor pairs and thus assume $\boldsymbol{Q}_n = \sigma_n^2 \boldsymbol{I}_{M-1}$, where σ_n^2 is the range difference variance of any pair of sensors and $\boldsymbol{I}_{M-1}$ denotes the unity matrix of dimensions $(M-1) \times (M-1)$.

For a number M of sensors, a set of $M(M-1)/2$ TDOA estimated values can be obtained, referred to as the full TDOA set. Instead, by using only one sensor as reference, a set of $M-1$ TDOA estimates is obtained, referred here as the non-redundant TDOA set. It was shown in [118] that if the reference sensor is properly chosen, the non-redundant TDOA set can result in the same localization accuracy as the full set. A procedure for properly choosing the reference sensor can be developed based on the CRB expression, [115, 118]. In this work, the proper choice of the reference sensor is assumed.

2.2.3 An SDR Method for Hyperbolic Localization

In this section, an SDR approach is proposed to solve for the source location ξ_0 estimation from the system of non-linear Equations (2.7). First, both sides of equality (2.7) are squared and the resulting terms rearranged. By introducing three intermediate variables,

$$\rho = \|\xi_1 - \xi_0\|_2, \ \nu = \rho^2, \ \text{and} \ \gamma = \|\xi_0\|_2^2 , \tag{2.8}$$

and denoting the noise term $e_k = n_{k1}(2\|\xi_k - \xi_0\|_2 + n_{k1})$, the following linear equations are obtained for $k = 2, \dots, M$:

$$(d_{k1}^2 + 2d_{k1}\rho + \nu) - \left(\|\xi_k\|_2^2 - 2\xi_k^{\mathrm{T}}\xi_0 + \gamma\right) = e_k . \tag{2.9}$$

By denoting the left hand side of (3) as $\Lambda_k(\xi_0)$, the dependence on ρ, ν, and γ being implicit, and letting $\boldsymbol{\Lambda}(\xi_0) = [\Lambda_2(\xi_0), \dots, \Lambda_M(\xi_0)]^{\mathrm{T}}$, $\boldsymbol{d} = [d_2, \dots, d_M]^{\mathrm{T}}$, and $\boldsymbol{\xi} = [\xi_2, \dots, \xi_M]^{\mathrm{T}}$, it can be verified that

$$\boldsymbol{\Lambda}(\xi_0) = \mathrm{trace}\{\boldsymbol{d}^{\mathrm{T}}\boldsymbol{d} - \boldsymbol{\xi}^{\mathrm{T}}\boldsymbol{\xi} + (\nu - \gamma)\boldsymbol{I}_{M-1}\} + 2(\rho\boldsymbol{d} + \xi_0^{\mathrm{T}}\boldsymbol{\xi}). \tag{2.10}$$

Then the source location ξ_0 can be estimated by formulating the constrained optimization problem

$$\begin{aligned} &\underset{\xi_0,\gamma,\rho,\nu}{\text{minimize}} \ \|\boldsymbol{\Lambda}(\xi_0)\|_{\mathbf{2}}, \\ &\text{subject to (2.8).} \end{aligned} \tag{2.11}$$

The minimization formulation (2.11) is non-convex, but it is amenable to SDR, i.e., the quadratic constraints in (2.8) can be relaxed by SDR, [114]. Thus, instead of (2.8), the following constraints are imposed:

$$\rho = \|\xi_1 - \xi_0\|_2, \ \begin{bmatrix} 1 & \rho \\ \rho & \nu \end{bmatrix} \succcurlyeq 0, \ \begin{bmatrix} \boldsymbol{I}_2 & \xi_0 \\ \xi_0^{\mathrm{T}} & \gamma \end{bmatrix} \succcurlyeq 0, \tag{2.12}$$

where $\boldsymbol{X} \succcurlyeq 0$ denotes positive semidefinite. With this, the localization problem reduces to an semidefinite programming (SDP), i.e., a convex minimization problem, solvable by standard convex optimization algorithms, [52],

$$\begin{aligned} &\underset{\xi_0,\gamma,\rho,\nu}{\text{minimize}} \ \|\boldsymbol{\Lambda}(\xi_0)\|_{\mathbf{2}}, \\ &\text{subject to (2.12).} \end{aligned} \tag{2.13}$$

Note that formulation (2.13) is similar to that in [115], where a minimax formulation was used, i.e., $\|\boldsymbol{\Lambda}(\xi_0)\|_\infty = \max_{k=2,..,M} |\Lambda_k(\xi_0)|$ was minimized to estimate ξ_0, subject to the same constraints. However, minimizing the ℓ_2-norm is equivalent to the LS formulation, which is known to be optimal given the Gaussian distribution of the TDOA

estimates. Indeed, the simulation results in Section 2.3 confirm that the ℓ_2-norm minimization can offer better accuracy than the minimax formulation.

2.2.4 MXTM Method for Hyperbolic Localization

The aim of this section is to improve the localization accuracy over the traditional methods by incorporating the linearized version of the hyperbolic localization problem (traditionally solved by WLS), into a biased estimation framework discussed in [117, 119]. First, the linearized equations and the conventional solution WLS are presented. Then the biased estimation framework is introduced and the proposed integration of the hyperbolic localization problem is presented and discussed.

The non-linear equations (2.7) can be reorganized into a set of linear equations, by squaring and introducing an extra variable expressed as function of the source location, [53, 110-112]. Specifically, (2.7) can be rewritten

$$d_{k1} + \|\xi_1 - \xi_0\|_2 = \|\xi_k - \xi_0\|_2 + n_{k1} \tag{2.14}$$

By squaring both terms of the equality and introducing the new variable $\rho = \|\xi_1 - \xi_0\|_2$, (2.14) becomes

$$(\xi_k - \xi_1)^{\mathrm{T}}\xi_0 + d_{k1}\rho = \frac{1}{2}[(\xi_k - \xi_1)^{\mathrm{T}}(\xi_k + \xi_1) - d_{k1}^2] + e_k\,, \tag{2.15}$$

where $e_k = n_{k1}(\|\xi_k - \xi_0\|_2 + n_{k1}/2)$ is the noise term. Denoting $\theta = [\xi_0^{\mathrm{T}}\ \rho]^{\mathrm{T}}$ and neglecting the second order noise term, (2.15) can be written in a matrix form,

$$\boldsymbol{G}\theta = \boldsymbol{h} + \boldsymbol{e}, \tag{2.16}$$

where $\boldsymbol{G} = \begin{bmatrix} \xi_2^{\mathrm{T}} - \xi_1^{\mathrm{T}} & d_{21} \\ \vdots & \vdots \\ \xi_M^{\mathrm{T}} - \xi_1^{\mathrm{T}} & d_{M1} \end{bmatrix}$, $\boldsymbol{h} = \begin{bmatrix} (\xi_2 - \xi_1)^{\mathrm{T}}(\xi_2 + \xi_1) - d_{21}^2 \\ \vdots \\ (\xi_M - \xi_1)^{\mathrm{T}}(\xi_M + \xi_1) - d_{M1}^2 \end{bmatrix}$, and $\boldsymbol{e} = [n_{21}\|\xi_2 - \xi_0\|_2, \dots, n_{M1}\|\xi_M - \xi_0\|_2]^{\mathrm{T}}$. Problem (2.16) is traditionally solved by minimization of a WLS objective function, as in [53]:

$$\hat{\theta} = \arg\min_{\theta} (\boldsymbol{G}\theta - \boldsymbol{h})^{\mathrm{T}} \boldsymbol{Q}_e^{-1} (\boldsymbol{G}\theta - \boldsymbol{h}), \tag{2.17}$$

where $\boldsymbol{Q}_e$ is an weighting matrix. Usually, the measurement noise n_{k1} is small enough compared to the distances $\|\xi_k - \xi_0\|_2$ such that $n_{k1}^2/2$ can be neglected and the noise term e_k can be modeled as a zero mean Gaussian random process with the covariance matrix $\boldsymbol{Q}_e = \boldsymbol{B}^T \boldsymbol{Q}_n \boldsymbol{B}$, where $\boldsymbol{B} = \mathrm{diag}\{\|\xi_2 - \xi_0\|_2, \dots, \|\xi_M - \xi_0\|_2\}$. Note that $\boldsymbol{B}$ depends on the unknown location ξ_0 and thus the WLS problem (2.17) is first solved with $\boldsymbol{Q}_e = \boldsymbol{Q}_n$ to obtain an estimate of $\boldsymbol{B}$ and then with $\boldsymbol{Q}_e = \widehat{\boldsymbol{B}}^T \boldsymbol{Q}_n \widehat{\boldsymbol{B}}$ to actually estimate θ. This method provides an approximation of the ML estimator for source location. However, this approximation holds only when the errors in the TDOA estimates are small enough.

It was shown in [117, 120] that for linear systems such as (2.16) there exist biased estimates, which can provide better accuracy then the LS solution. The LS solution for linear systems is based on minimizing the ℓ_2-norm of the data error, $\widehat{\boldsymbol{h}} - \boldsymbol{h}$, where $\widehat{\boldsymbol{h}} = \boldsymbol{G}\hat{\theta}$, rather than minimizing the size of the estimation error, $\hat{\theta} - \theta$. To develop an estimation method that is based directly on the estimation error, an estimator $\hat{\theta}$ that minimizes the mean squared error (MSE) is desired. The MSE of an estimate $\hat{\theta}$ of θ is defined, [117],

$$\mathrm{MSE}(\hat{\theta}) = \mathbb{E}\left\{\left\|\hat{\theta} - \theta\right\|_2^2\right\} = \mathrm{var}\{\hat{\theta}\} + \left\|\mathrm{b}\{\hat{\theta}\}\right\|_2^2, \tag{2.18}$$

where $\mathrm{var}\{\hat{\theta}\} = \mathbb{E}\left\{\|\hat{\theta}\|_2^2\right\} - \left(\mathbb{E}\{\hat{\theta}\}\right)^2$ is the variance of the estimate and $\mathrm{b}\{\hat{\theta}\} = \mathbb{E}\{\hat{\theta}\} - \theta$ is the bias of the estimate. Since the bias generally depends on the unknown parameter θ, an estimator cannot be chosen to directly minimize the MSE. A common approach is to restrict the estimator to be linear and unbiased and seek an estimator of this form that minimizes the variance $\mathrm{var}\{\hat{\theta}\}$. It is well known that the LS estimator minimizes the variance of the estimate $\hat{\theta}$ among all unbiased linear estimates. However, this does not imply that the LS estimator has the smallest MSE. This motivates the approach of attempting to reduce the MSE by allowing some nonzero bias. Since the bias depends on the unknown θ, one solution is to exploit some a priori information on θ. For the localization problem, such information can consist in the limits of the surveillance area. With this, a biased estimation approach, denoted minimax total MSE (MXTM) in [117], can be employed to solve the hyperbolic localization problem. Assuming that the estimator is of form $\hat{\theta} = \boldsymbol{\Gamma} h$, for some $3 \times (M-1)$ matrix $\boldsymbol{\Gamma}$, and using it together with (2.16) in (2.18) it can be shown that the MSE of $\hat{\theta}$ is

$$\mathrm{MSE}(\boldsymbol{\Gamma}) = \mathrm{trace}(\boldsymbol{\Gamma} \boldsymbol{Q}_e \boldsymbol{\Gamma}^{\mathrm{T}}) + \theta^{\mathrm{T}} (\boldsymbol{I}_3 - \boldsymbol{\Gamma} \boldsymbol{G})^{\mathrm{T}} (\boldsymbol{I}_3 - \boldsymbol{\Gamma} \boldsymbol{G}) \theta. \tag{2.19}$$

Exploiting the information that *limiting the surveillance* area places a bound on $\|\theta\|_2$, e.g., $\|\theta\|_2 < L$, the estimator can be expressed $\hat{\theta} = \hat{\boldsymbol{\Gamma}} h$, where

$$\hat{\boldsymbol{\Gamma}} = \arg\min_{\boldsymbol{\Gamma}} \max_{\|\boldsymbol{\Gamma} h\|_2 < L} \mathrm{MSE}(\boldsymbol{\Gamma}). \tag{2.20}$$

Problem (2.20) seeks to minimize the worst-case MSE across all possible estimators of θ, of the form $\boldsymbol{\Gamma} h$, with the ℓ_2-norm bounded by L. To solve the problem, the worst-case MSE is first determined. By algebraic manipulations, it can be shown that

the worst-case MSE is $\text{trace}(\boldsymbol{\Gamma Q}_e\boldsymbol{\Gamma}^{\text{T}}) + L^2\lambda_{\max}$, where $\lambda_{\max}$ is the maximum eigenvalue of $(\boldsymbol{I}_3 - \boldsymbol{\Gamma G})^{\text{T}}(\boldsymbol{I}_3 - \boldsymbol{\Gamma G})$. It is known, [114], that $\lambda_{\max}$ can be obtained by

$$\text{minimize } \lambda, \tag{2.21}$$

$$\text{subject to } \lambda\boldsymbol{I}_3 - (\boldsymbol{I}_3 - \boldsymbol{\Gamma G})^{\text{T}}(\boldsymbol{I}_3 - \boldsymbol{\Gamma G}) \succcurlyeq 0. \tag{2.22}$$

By introducing (2.21) in (2.20), $\boldsymbol{\Gamma}$ can be estimated by

$$\text{minimize } \text{trace}(\boldsymbol{\Gamma Q}_e\boldsymbol{\Gamma}^{\text{T}}) + L^2\lambda_{\max}, \tag{2.23}$$

$$\text{subject to (2.22),}$$

with variables $\boldsymbol{\Gamma}$ and λ. The constrained minimization (2.23) is a standard quadratic constrained quadratic problem, [114], that can be relaxed to an SDP,

$$\text{minimize } \beta, \tag{2.24}$$

$$\text{subject to}$$

$$\begin{bmatrix} \beta - L^2\lambda & \boldsymbol{g}^T \\ \boldsymbol{g} & \boldsymbol{I}_3 \end{bmatrix} \succcurlyeq 0, \tag{2.25}$$

$$\begin{bmatrix} \lambda\boldsymbol{I}_3 & (\boldsymbol{I}_3 - \boldsymbol{\Gamma G})^{\text{T}} \\ \boldsymbol{I}_3 - \boldsymbol{\Gamma G} & \boldsymbol{I}_3 \end{bmatrix} \succcurlyeq 0, \tag{2.26}$$

with variables $\beta, \boldsymbol{\Gamma}$, and λ, where $\boldsymbol{g} = \text{vec}\{\boldsymbol{\Gamma Q}_e^{1/2}\}$ denotes the vector obtained by stacking the columns of $\boldsymbol{\Gamma Q}_e^{1/2}$.

Solving for (2.24)-(2.26) provides an estimate of $\theta = [\xi_0^{\text{T}}\ \rho]^{\text{T}}$. However, ρ was introduced into the hyperbolic localization problem as an intermediate variable that depends on ξ_0 through $\rho = \|\xi_1 - \xi_0\|_2$. This needs to be used into the minimization problem as an additional constraint. Introducing a new variable $\boldsymbol{\Theta} = \theta^{\text{T}}\theta$, using $\hat{\theta} = \boldsymbol{\Gamma}h$, and employing SDR, it can be shown that the following two constraints can be introduced

into the minimization (2.24)-(2.26) to account for the relation between ρ and ξ_0 and keep the problem convex at the same time:

$$\mathrm{trace}(\boldsymbol{P\Theta}) + \xi_1^{\mathrm{T}}\xi_1 - 2\xi_1^{\mathrm{T}}\boldsymbol{R\Gamma}h = 0, \tag{2.27}$$

$$\begin{bmatrix} \boldsymbol{\Theta} & \boldsymbol{\Gamma}h \\ (\boldsymbol{\Gamma}h)^T & 1 \end{bmatrix} \succcurlyeq 0, \tag{2.28}$$

where $\boldsymbol{P} = \mathrm{diag}\{1, 1, -1\}$, and $\boldsymbol{R} = \begin{bmatrix} 1 & 0 & 0 \\ 0 & 1 & 0 \end{bmatrix}$.

Thus, the location estimate of ξ_0 is $\boldsymbol{R}\widehat{\boldsymbol{\Gamma}}h$, where $\widehat{\boldsymbol{\Gamma}}$ is obtained by solving the convex optimization problem

$$\begin{aligned} &\text{minimize } \beta, \\ &\text{subject to (2.25), (2.26), (2.27), and (2.28),} \end{aligned} \tag{2.29}$$

with variables β, $\boldsymbol{\Gamma}$, and λ.

The simulation results in Section 2.3 show that the MXTM method offers location estimates of higher accuracy than the previous estimation approach, particularly for the case when the source is placed outside the convex hull of the sensors.

2.2.5 ℓ_1-norm Regularization Method for Hyperbolic Localization

The methods presented in the previous two sections offer high localization accuracy, as demonstrated by the simulation results shown in Section 2.3. However, they solve a linear approximation of the hyperbolic localization problem and are suboptimal. In this section a new approach that may offer even higher accuracy is proposed. This new approach exploits the source sparsity, i.e., the spatial sparsity. The localization problem is converted to a sparse framework by solving the system $\mathbf{1} = \boldsymbol{Az}$, where $\mathbf{1}$ is a unity vector whose length equals the number $M - 1$ of TDOA estimates, τ_{k1}, for $k = 2, \ldots M$, and $\boldsymbol{z}$ is

a vector whose elements are associated with grid points, such that $\boldsymbol{z}_j \neq 0$ if a source is present at the grid. The elements $\boldsymbol{A}_{ij}$ are values of a function f chosen such that $f\left(\left|\tau_{k1}^{(j)} - \tau_{k1}\right|\right) = 1$, when the estimated TDOA associated with sensor k, τ_{k1}, equals the true TDOA, $\tau_{k1}^{(j)}$, calculated for sensor k and grid point j. Function f is chosen as a measure of the likelihood that the source is located at the grid point j. Thus, for grid points j for which $\tau_{k1}^{(j)} \neq \tau_{k1}$, function f takes values smaller than 1, such that $f\left(\left|\tau_{k1}^{(j)} - \tau_{k1}\right|\right)\Big|_{\tau_{k1}^{(j)} \neq \tau_{k1}}$ is monotonic decreasing. Estimation of $\boldsymbol{z}$ yields then the source location. Solving the system $\mathbf{1} = \boldsymbol{A}\boldsymbol{z}$ by traditional LS produces poor estimates since the number of unknowns, which equals the number of grid points, is usually much larger than the number equations, $M - 1$, and thus matrix $\boldsymbol{A}$ is a fat matrix. The problem can be addressed by exploiting the source sparsity, which means that the size of the support of vector $\boldsymbol{z}$, or otherwise number of non-zero elements, is small relative to the length of $\boldsymbol{z}$.

Thus, the localization problem is formulated as an ℓ_1-regularization problem, i.e., the ℓ_1-norm is used to impose a sparsity constraint on vector $\boldsymbol{z}$, whose support indicates the source location:

$$\underset{\mathbf{z}}{\text{minimize}} \ \ \|\mathbf{1} - \boldsymbol{A}\boldsymbol{z}\|_2^2 + \lambda\|\boldsymbol{z}\|_1 \ , \tag{2.30}$$

where λ is a regularization parameter, balancing the fit of the solution $\boldsymbol{z}$ to the estimates τ_{k1} versus sparsity. This formulation is a convex optimization problem that can be efficiently solved by standard algorithms, [52].

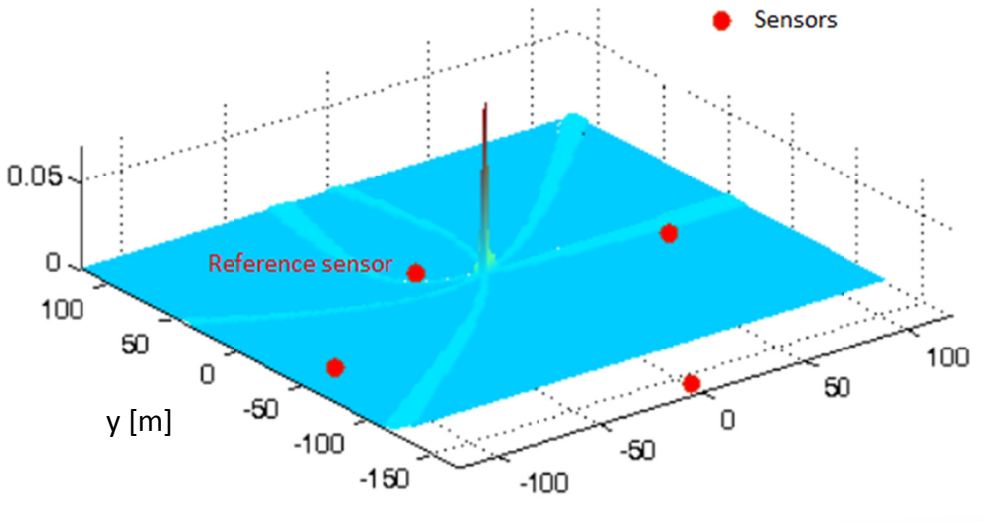

Figure 2.3 Hyperbolic localization. The source is localized by the intersection of a set of hyperbolas given by the TDOA estimates. The sensor closest to the source is used as reference. The peak of the objective function obtained by ℓ_1-regularization gives the location of the source.

Ideally, the sparsity of $\boldsymbol{z}$ is enforced by its ℓ_0-norm, i.e., the number of non-zero elements. However, the minimization problem with the ℓ_0-norm constraint is a NP-hard non-convex optimization problem. By using the ℓ_1-norm as an approximation of the ℓ_0-norm, [105], the problem becomes convex. In Figure 2.3 the estimated values of $\boldsymbol{z}$, acting as a localization objective function, are plotted at the corresponding space grid points, for a case with four sensors. The peak, which gives the location of the source, corresponds to the intersection of the hyperbolas associated with the three TDOA measurements available in this case.

A number of methods have been studied in the literature for automated choice of the regularization parameter λ (see [103] and the references therein). However, in practice, an optimal value of λ is difficult to select by any of these methods, and usually the choice of λ resorts to semi-empirical means, [102].

Formulating (2.30) with a denser sampled space has the potential of a higher resolution location estimate, but increases the complexity of the optimization algorithms. An iterative grid refinement approach is adopted to keep the complexity of the optimization algorithms in check. Initially, (2.30) is solved for the samples corresponding to a desired range of locations. A refined grid is obtained by taking a second set of samples focusing on an area that are indicated by the first iteration to include the source location. This corresponds to a higher sampling rate of the smaller area of interest. The transformation matrix $\boldsymbol{A}$ is also recalculated to match the refined sample support of the correlation sequences. With the refined grid, (2.30) is solved again and a new source location estimate, of higher resolution, is obtained. The grid refinement procedure can be repeated to improve the localization resolution. However, decreasing the grid spacing effects in high inter-column correlation in matrix $\boldsymbol{A}$. It is known, [121, 122], that as the inter-column correlation increases, the ℓ_1-regularization solution may become suboptimal, i.e., it does not coincides with the solution of the minimization with the ℓ_0-norm constraint. This sets an empirical lower bound on the localization resolution.

As demonstrated by the results in the Section 2.3, the ℓ_1-regularization method has the potential of higher accuracy than the other two hyperbolic localization methods proposed. However, its performance depends on the choice of the regularization parameter. Also, a couple of iterations may be needed for grid refinement. Additionally, the localization resolution is limited by the grid spacing.

2.3 Numerical Results

In this section, some simulation results are presented to demonstrate the performance of the proposed localization methods. For a typical setup, significant improvement in localization accuracy is shown, compared to conventional methods, such as cross-correlation and root-MUSIC.

The first simulation scenario

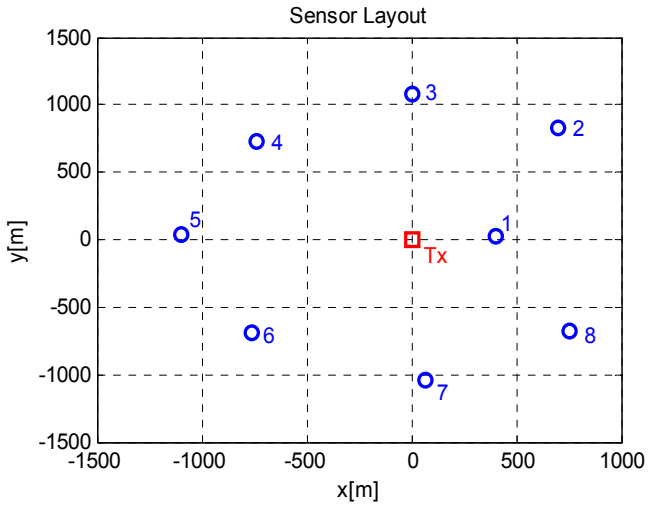

Figure 2.4 Sensors layout. Sensor 1 is used as reference.

The first set of simulations regards the TDOA estimation in some typical setup. The same setup is further used to determine source location by employing as hyperbolic localization method the ℓ_2-norm version of the SDR approach, proposed in Section 2.2.3.

A system in which a number $M = 8$ of sensors are approximately uniformly distributed around the source, on an approximately circular shape of radius 1 km, as in Figure 2.4, is considered. The source, which location is to be estimated, transmits a Gaussian Minimum Shift Keying (GMSK) modulated signal of bandwidth $B = 200$ kHz that is received by the M sensors through different multipath channels. For each sensor $k = 2, \dots M$, the TDOAs are measured relative to the chosen reference sensor, $l = 1$. The

pulse shape is known at the sensors side and used to generate the auto-correlation of the transmitted signal. The wireless channels between the source and each of the sensors are modeled as (2.2). Specifically, a three-paths model is used, as in [40]. The first two paths are spaced well below the bandwidth resolution, while the separation between the second and the third path is higher, as it can be seen in Figure 2.5. The only exception is the reference sensor assumed to be an AWGN channel, i.e., no multipath. The simulation scenario also employs the same noise level across sensors. For ℓ_1-regularization, the regularization parameter λ is chosen according to the noise level, as discussed in Section 2.1.3. Originally, when solving problem (2.6), the sampling rate is 8 times the Nyquist rate. An oversampling factor of $\times 50$ is used for grid refinement as previously explained in Section 2.1.3.

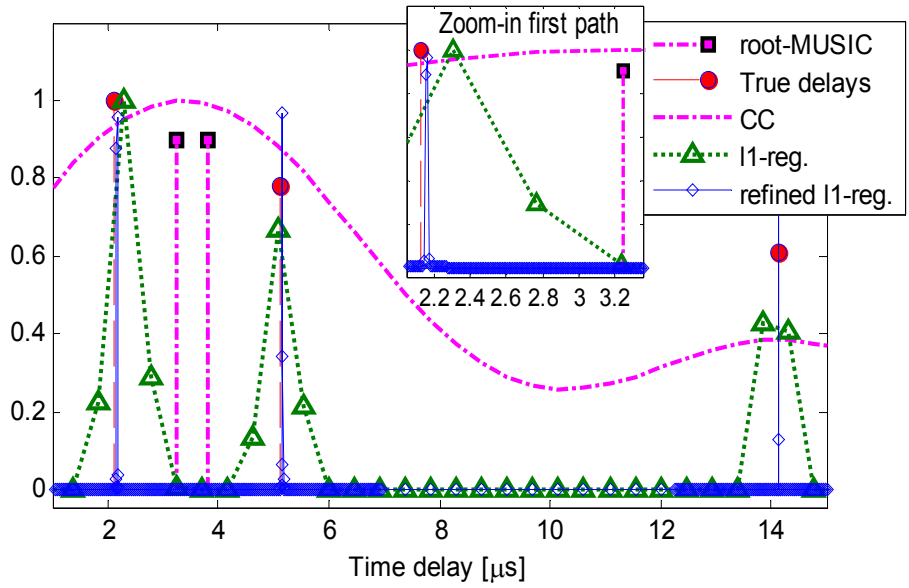

Figure 2.5 True and estimated multipath components. The ℓ_1-regularization with grid refinement estimated components are the closest to the true ones.

Figure 2.5 shows the time-delays of the multipath components and their estimates at one of the sensors, for a received SNR of 15 dB per sample. The TDOA is given by the

earliest of these components. The estimate by the ℓ_1-regularization approach with grid refinement is the closest to the true delays, when compared to the other methods considered. The result of the ℓ_1-regularization without grid refinement is visibly biased due to the limited sampling rate. The CC and the root-MUSIC estimates show significantly larger errors particularly for the two close paths.

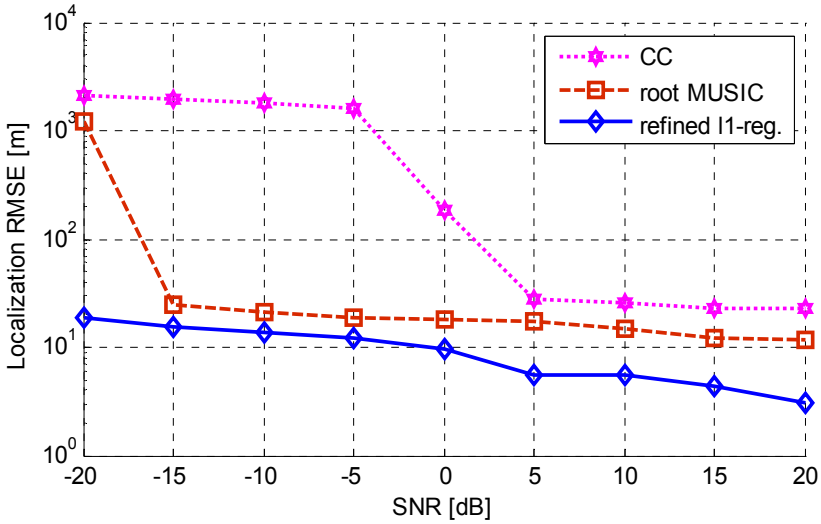

Figure 2.6 Source localization accuracy in noise. The result obtained by the ℓ_1-regularization is more accurate than the conventional methods.

Figure 2.6 illustrates the two-stage overall localization performance, in terms of root mean square error (RMSE) against SNR, of the proposed methods in the aforementioned scenario. The technique used for the second stage is the ℓ_2-norm version of the SDR approach, as described in Section 2.2.3. The RMSE is obtained from Monte Carlo simulations with 100 runs per SNR value. The plot shows better accuracy of the proposed method over CC and root-MUSIC, at both high and low SNR. At high SNR, given the low separation between the first two multipaths, both CC and root-MUSIC provide biased estimates due to their limited resolution capabilities, though root-MUSIC

is better. The reason for the better accuracy at low SNR is that ℓ_1-regularization is robust to noise, as discussed in Section 2.1.3.

The second simulation scenario

The second set of simulations regards the hyperbolic localization alone. The three methods proposed in Section 2.2, SDR based, MXTM, and ℓ_1-regularization, have been applied to source localization based on TDOA measurements. Monte Carlo computer simulations were carried out for a number $M = 8$ sensors placed in the plane according to the layout in Figure 2.7. Two cases were considered: one when the source is located inside the convex hull of the sensors and another one when the source is placed outside. The TDOA estimation errors were drawn from a zero-mean Gaussian distribution, with standard deviation σ_τ, where σ_τ was varied between 0 and 200 ns, i.e., the variance σ_n of the range differences varied between 0 and 60 m. For each value of σ_τ considered, 100 runs were performed. A zero-mean Gaussian function,

$$f\left(\left|\tau_{k1}^{(j)} - \tau_{k1}\right|\right) = \exp\left\{-\left|\tau_{k1}^{(j)} - \tau_{k1}\right|^2 / 2\sigma^2\right\}, \tag{2.31}$$

was used for simulations of (2.30), with $\sigma = 500$ ns. The plots in Figure 2.8 and Figure 2.9 show the root mean squared error (RMSE) of the methods proposed in this paper for a source placed with inside or outside of the convex hull of the sensors. The RMSE is plotted against the standard deviation of the TDOA estimation error.

The first remark is that all the three methods proposed in this paper outperform, for the cases simulated, the minimax approach from [115], known to be already more robust to errors in the TDOA estimates than conventional NLS and WLS methods for hyperbolic localization. The SDR method presented in Section 2.2.3 and MXTM presented in Section 2.2.4 show similar accuracies when the source is placed inside the

convex hull of the sensors, while MXTM performs better when the source is outside the convex hull. Both methods solve a linearized approximation of the hyperbolic localization problem. Finally, the ℓ_1-regularization outperforms for the simulated cases both the SDR and MXTM methods. In simulations, optimal choice of the regularization parameter was used. However, in practice a good choice of λ is difficult. A grid refinement procedure is needed if high resolution is desired, e.g., a number of five iterations were used in the simulations for a surveillance area of 1000 m by 1000 m, stopping at a grid resolution of 0.1 m.

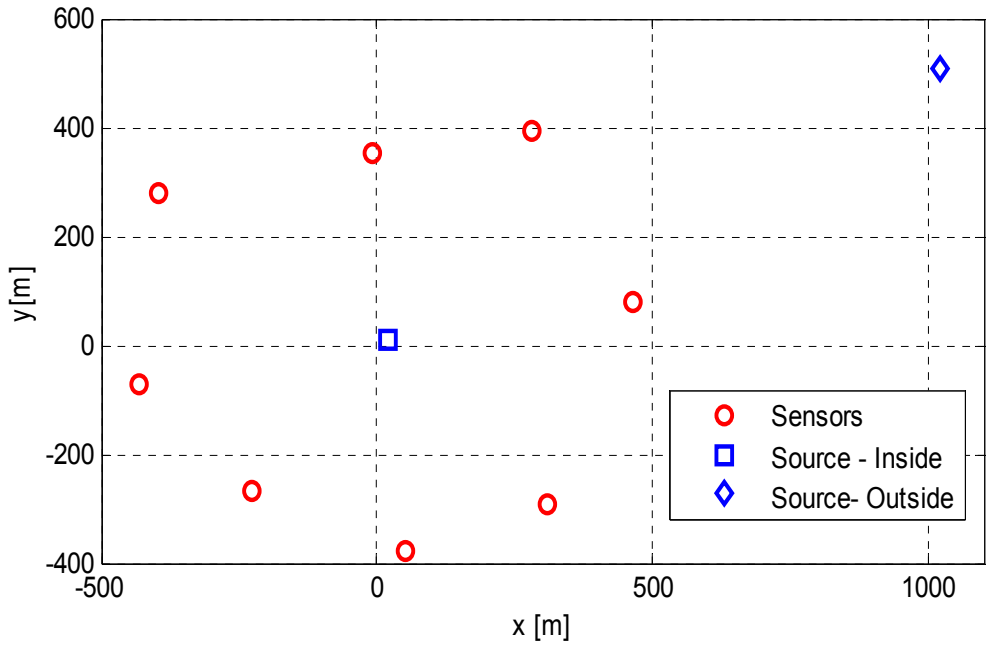

Figure 2.7 Sensors layout. The source may be located inside or outside the sensors footprint.

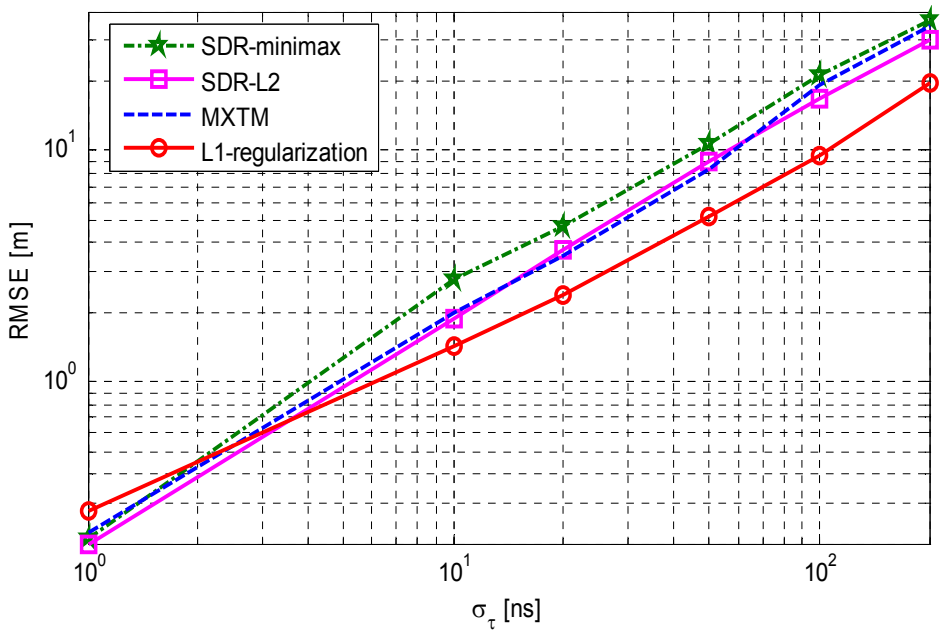

Figure 2.8 Hyperbolic source localization for the case when the source is located inside the footprint of the sensors.

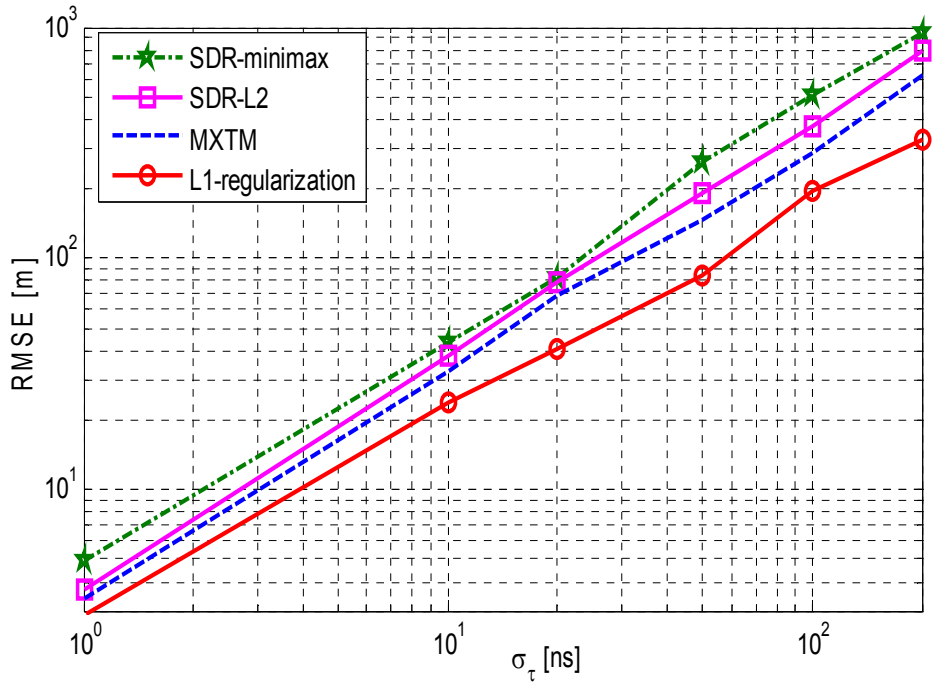

Figure 2.9 Hyperbolic source localization for the case when the source is located outside the footprint of the sensors.

2.4 Concluding Remarks

A two-stage approach for source localization via TDOA estimation in multipath environments was developed. First, the sparsity of the channels is exploited and a grid refinement procedure was formulated to improve the resolution of the TDOA estimation. Second, the hyperbolic localization was addressed. Three methods for hyperbolic localization were proposed to offer high accuracy at different computational costs. All of them are computationally efficient and show better accuracy when compared to other existing techniques.

The proposed overall two-stage localization approach compares favorably to the conventional cross-correlation and root-MUSIC techniques, in terms of TDOA and source location accuracy estimation. For dense multipath environments the proposed TDOA approach may succeed where conventional methods fail to resolve closely separated components. Therefore it is suitable for applications like source localization in multipath. Moreover, simulation results confirmed the noise robustness of the methods proposed within the approach.

CHAPTER 3

SINGLE-STAGE COHERENT LOCALIZATION

3.1 Signal Model

With the single-stage approach to source localization, coherent processing, i.e., utilizing the relative carrier phases of the received signals among pairs of sensors, in addition to TDOAs, is possible when the sensors are synchronized in both time and frequency. The coherent localization is accomplished by formulating a localization metric which is a joint statistic that incorporates the phase information contained in the received signals as if transmitted from various points of the source location space, as illustrated in Figure 3.1.

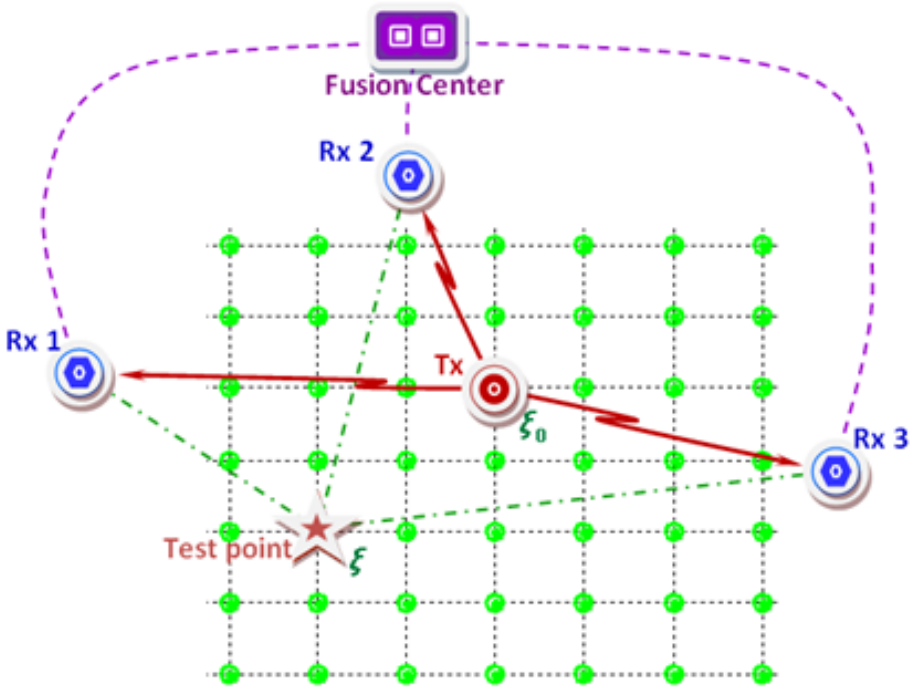

Figure 3.1 Single-stage localization system layout. The fusion center estimates the location of the source by maximizing a localization metric over the source location space.

In this section the coherent (single-stage) source localization in the general framework described in the Chapter 1 is studied. In order to construct a maximum likelihood (ML) estimator and derive the CRB for source localization, a multipath free environment is considered. The signal model for this case is given by equations (1.2) and (1.3).

For localization metric derivation, it is useful to model the system in the frequency domain. The received signal at the k^{th} sensor, can be written in frequency by applying the Fourier transform on (1.2):

$$R_k(\omega) = \Gamma_k(\omega)S_0(\omega) + W_k(\omega), \tag{3.1}$$

where $\Gamma_k(\omega) = g_k e^{-j\omega\tau_k(\xi_0)} e^{-j\omega_c\tau_k(\xi_0)}$ and $W_k(\omega)$ is the frequency domain correspondent of the AWGN noise. Putting together the spatial samples from all the M sensors into one frequency domain snapshot, a vectorial form of (3.1) can be written for each frequency bin of interest ω, as

$$\boldsymbol{R}(\omega) = \boldsymbol{\Gamma}(\omega)S_0(\omega) + \boldsymbol{W}(\omega), \tag{3.2}$$

with $\boldsymbol{R}(\omega) = [R_1(\omega), \dots, R_M(\omega)]^T$, $\boldsymbol{\Gamma}(\omega) = [\Gamma_1(\omega), \dots, \Gamma_M(\omega)]^T$, and $\boldsymbol{W}(\omega) = [W_1(\omega), \dots, W_M(\omega)]^T$.

3.2 ML Coherent Estimator

Coherent processing of the collected signals for source location direct estimation involves a two-dimensional search for the maximum of a localization metric among all the possible plane locations of the source. Such a metric can be obtained based on the ML procedure. Due to the phase term in the received signal model (3.1), the derivation can be more conveniently carried in frequency domain. Joint probability density function (pdf) of the noise across the sensors, at frequency ω

$$f_{\omega}\big(\boldsymbol{W}(\omega)\big) = \frac{1}{\pi^{M}\det(\boldsymbol{K}_{W}(\omega))}\exp\{-\boldsymbol{W}^{H}(\omega)\boldsymbol{K}_{W}^{-1}(\omega)\boldsymbol{W}(\omega)\}, \tag{3.3}$$

where $\boldsymbol{K}_{W}(\omega)$ is the covariance matrix of the noise across the sensors, defined as $\mathbb{E}\{\boldsymbol{W}(\omega)\boldsymbol{W}^{H}(\omega)\} = \sigma^{2}\boldsymbol{I}_{M}$, $\boldsymbol{I}_{M}$ being the M-dimensional identity matrix. The signal transmitted by source is deterministic and unknown, i.e., no statistical model is assumed for it. A discussion on the deterministic versus statistic ML estimation is included in [28].The signal model (3.2) is used in (3.3) to express the joint pdf of the received signals across sensors, for all frequencies ω within the set B_0 of interest, given any source location ξ and source signal $S_0(\omega)$:

$$f(\boldsymbol{R}|\xi,\boldsymbol{S}_{0}) = \prod_{\omega\in B_{0}} f_{\omega}\big(\boldsymbol{R}(\omega)\big|\xi,S_{0}(\omega)\big), \tag{3.4}$$

where it was considered that the received signal has independent distributions over frequencies of interest.

The ML estimation of the source location is given by the following optimization:

$$\hat{\xi}_{0} = \arg\max_{\xi} \Lambda(\xi). \tag{3.5}$$

Here $\Lambda(\xi)$ is the log-likelihood function obtained by taking $\ln f(\boldsymbol{R}|\xi,\boldsymbol{S}_{0})$ and dropping source location invariant terms: $\Lambda(\xi) = -\sum_{\omega\in B_{0}} L(\xi,\omega)$, where

$$L(\xi,\omega) = [\boldsymbol{R}(\omega) - \boldsymbol{\Gamma}(\omega)S_{0}(\omega)]^{H}[\boldsymbol{R}(\omega) - \boldsymbol{\Gamma}(\omega)S_{0}(\omega)]. \tag{3.6}$$

The maximization (3.5) of $\Lambda(\xi)$ is equivalent to the minimization of $L(\xi,\omega)$ over the space of source locations and signal, for all ω bins. The minima of $L(\xi,\omega)$ with respect to the source signal $S_0(\omega)$ must satisfy $(\partial L/\partial S_{0}^{*})(\omega) = 0$. Hence the estimate of the source signal that yields to the minimum residue at any source location is given by

$\hat{S}_0(\omega) = [\boldsymbol{\Gamma}^H(\omega)\boldsymbol{\Gamma}(\omega)]^{-1}\boldsymbol{\Gamma}^H(\omega)\boldsymbol{R}(\omega)$. After substituting the estimate of $S_0(\omega)$ in (3.6) and dropping location independent terms, the source location can be estimated by maximizing the log-likelihood

$$\Lambda(\xi) = \sum_{\omega\in B_0} \boldsymbol{R}^H(\omega)\boldsymbol{\Gamma}(\omega)\boldsymbol{\Gamma}^H(\omega)\boldsymbol{R}(\omega)d\omega = \sum_{\omega\in B_0} \left|\sum_{l=1}^{M} \alpha_l^* R_l(\omega)e^{-j\omega\tau_l(\xi)}\right|^2 d\omega \qquad (3.7)$$

After expanding (3.7) and again keeping only the terms dependent on the source location, the log-likelihood to be maximized becomes

$$\Lambda(\xi) = \sum_{k=1}^{M}\sum_{l=k+1}^{M}\sum_{\omega\in B_0} \mathrm{Re}\left\{\alpha_l^*\alpha_k R_l(\omega)R_k^*(\omega)e^{-j\omega\Delta\tau_{kl}(\xi)}\right\} d\omega, \qquad (3.8)$$

where Re{·} denotes the real part. One may note that $R_l^*(\omega)R_k(\omega)$ represents the discrete Fourier transform of the cross-correlation of signals $r_l(t)$ and $r_k(t)$, denoted $x_{lk}(\tau)$. With this, a localization metric for coherent processing is formulated in time domain as

$$\Lambda(\xi) = \sum_{k=1}^{M}\sum_{l=k+1}^{M} \mathrm{Re}\left\{g_l g_k x_{lk}^*\left(\Delta\tau_{kl}(\xi)\right)e^{-j\omega_c\Delta\tau_{kl}(\xi)}\right\}. \qquad (3.9)$$

A scheme for implementing Equation (3.9) is plotted in Figure 3.2 , assuming the channel attenuation, g_k, a priori known.

Equation (3.9) accounts for both the envelope and carrier phase of the collected signals. A non-coherent system instead processes only the received envelopes. As such, for a non-coherent system the channel gain is real-valued, i.e., $\alpha_k = g_k$. Consequently, a non-coherent localization metric is expressed

$$\Lambda^{(nc)}(\xi) = \sum_{k=1}^{M}\sum_{l=k+1}^{M} \mathrm{Re}\left\{g_l g_k x_{lk}^*\left(\Delta\tau_{kl}(\xi)\right)\right\}. \qquad (3.10)$$

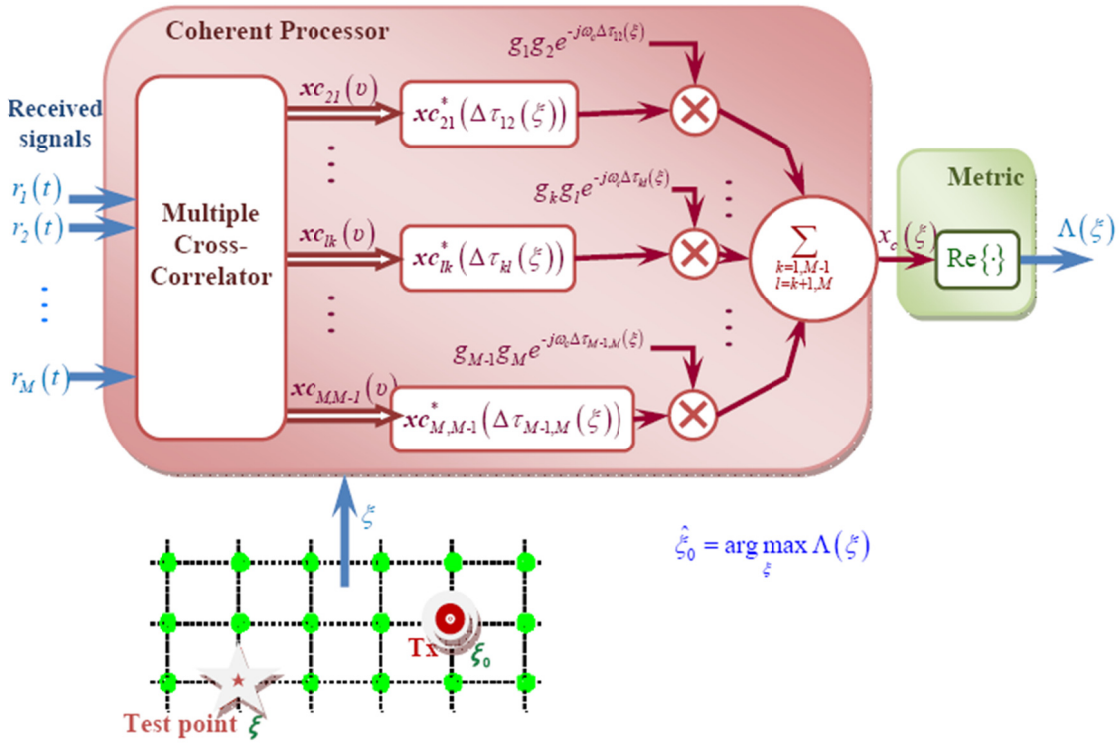

Figure 3.2 Scheme for single-stage coherent location estimator implementation.

The coherent localization metric (3.9) is similar to the non-coherent localization metric (3.10), except for the term $e^{-j\omega_c \Delta\tau_{kl}(\xi)}$, which aims to compensate for the carrier phase difference at each pair of sensors. This term sets the premise to the high accuracy localization capabilities of the coherent processing over the non-coherent. This is also graphically illustrated in Figure 3.3 for a ratio $\omega_c/B_0 \approx 5000$ and a received average SNR $= 10$ dB, where the coherent and non-coherent localization metrics were plotted for $M = 16$ sensors uniformly placed on a virtual circle of radius 500 m around the source. By comparing the two plots it becomes evident how coherent processing enhances the localization accuracy by substantially narrowing the main lobe of the localization metric. Similar enhancement was shown for the case of target active localization in [63].

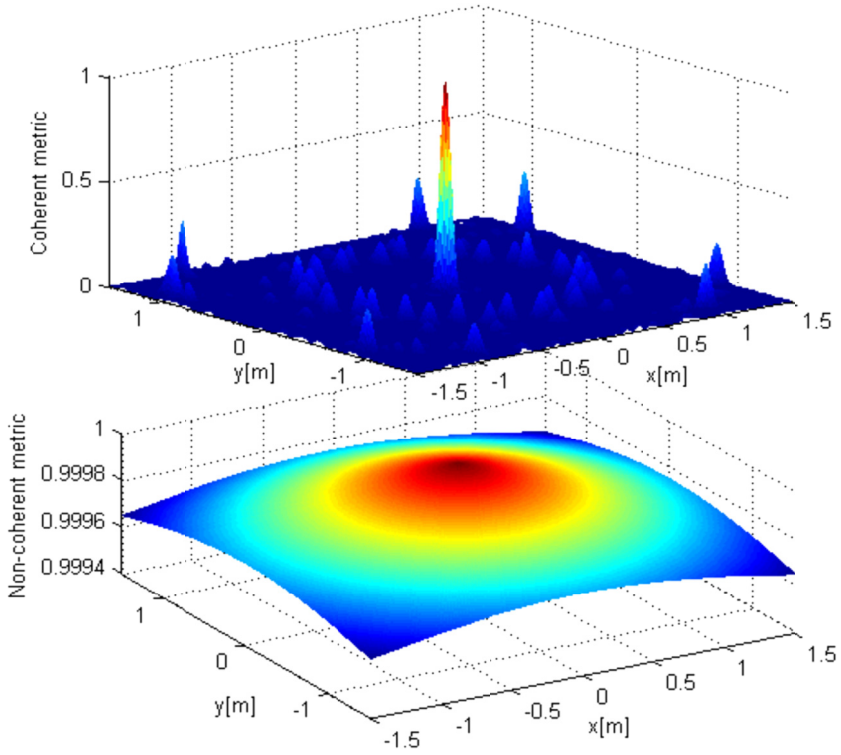

Figure 3.3 Coherent processing resolution capabilities improvement over non-coherent processing.

3.3 CRB for Coherent Localization

The common measure of the performance of a localization algorithm is the square root of the MSE (root-MSE). Since to obtain a MSE figure of merit extended computer simulations are required, finding a lower bound for it is extremely useful. The CRB for a parameter vector $\boldsymbol{\xi}^E$ to be estimated, which parameterizes the observation signal array $\boldsymbol{R}(\omega)$, is given by

$$\mathbb{E}\left\{\left(\hat{\boldsymbol{\xi}}^E - \boldsymbol{\xi}^E\right)\left(\hat{\boldsymbol{\xi}}^E - \boldsymbol{\xi}^E\right)^H\right\} \geq \boldsymbol{C}_{CRLB}(\boldsymbol{\xi}^E) = \boldsymbol{J}^{-1}(\boldsymbol{\xi}^E), \tag{3.11}$$

where $\mathbb{E}\{\cdot\}$ denotes the mean over all the observation snapshots. CRB provides a lower bound for the MSE of any unbiased estimator for the unknown parameters ξ_i^E. This is expressed by, [91]:

$$\mathrm{var}\{\hat{\xi}_i^E\} \geq [\boldsymbol{C}_{CRLB}(\boldsymbol{\xi}^E)]_{i,i}. \tag{3.12}$$

The parameter vector $\boldsymbol{\xi}^E$ contains here the source location ξ_0, which is the parameter of interest, but includes also the real and imaginary parts of the signal emitted by the source, as nuisance, i.e., $\boldsymbol{\xi}^E = \left[x_0, y_0, S_{01}^R, \dots, S_{0N_F}^R, S_{01}^I, \dots, S_{0N_F}^I\right]^T$. The signal parameter set includes N_F frequency bins to account for the whole signal bandwidth B_0. In (3.11), $\boldsymbol{J}(\boldsymbol{\xi}^E)$ refers to the Fisher Information matrix (FIM) which can be easier calculated by introducing an alternative parameter vector, $\boldsymbol{\theta} = \left[\tau_1, \dots, \tau_M, S_{01}^R, \dots, S_{0N_F}^R, S_{01}^I, \dots, S_{0N_F}^I\right]^T$. Using the chain rule, $\boldsymbol{H}(\boldsymbol{\xi}^E) = \boldsymbol{H}\boldsymbol{J}(\boldsymbol{\theta})\boldsymbol{H}^T$, where the relation between τ_k and ξ_0 is described by (1.1) and the transformation matrix $\boldsymbol{H}$ is

$$\boldsymbol{H} = \nabla_{\boldsymbol{\xi}^E}\boldsymbol{\theta}^T = -\frac{1}{c}\left[\begin{array}{c|c} \boldsymbol{H}_{2\mathrm{x}M} & \boldsymbol{O}_{2\mathrm{x}2N_F} \\ \hline \boldsymbol{O}_{2N_F\mathrm{x}M} & \boldsymbol{I}_{2N_F\mathrm{x}2N_F} \end{array}\right], \tag{3.13}$$

with $\nabla_{\boldsymbol{\xi}^E}\boldsymbol{\theta}^T$ denoting the gradient of $\boldsymbol{\theta}^T$ with respect to $\boldsymbol{\xi}^E$, $\boldsymbol{I}_{2N_F\times 2N_F}$ being the $2N_F$ by $2N_F$ identity matrix, $\boldsymbol{O}$ the all-zero matrix and $\boldsymbol{H}$ given by $\boldsymbol{H} = [\boldsymbol{\nu}_1, \dots, \boldsymbol{\nu}_M]$. The pair $[\cos\varphi_k, \sin\varphi_k]^T$, denoted by $\boldsymbol{\nu}_k$ and defined as $(\xi_k - \xi_0)/d_k(\xi_0)$, is a unit vector indicating the direction from the source to the k^{th} sensor. Individually, the components of this unit vector, $\cos\varphi_k$ and $\sin\varphi_k$, can be expressed as $(x_k - x_0)/d_k(\xi_0)$ and $(y_k - y_0)/d_k(\xi_0)$, respectively.

With these, the FIM matrix can be written as of form

$$\boldsymbol{J}(\boldsymbol{\xi}^E) = \frac{1}{c^2}\left[\begin{array}{c|c} \left[\boldsymbol{H}\,\boldsymbol{J}_{\tau\tau}(\boldsymbol{\theta})\boldsymbol{H}^T\right]_{2\mathrm{x}2} & \left[\boldsymbol{H}\,\boldsymbol{J}_{S_0\tau}^T(\boldsymbol{\theta})\right]_{2\mathrm{x}2N_F} \\ \hline \left[\boldsymbol{J}_{S_0\tau}(\boldsymbol{\theta})\boldsymbol{H}^T\right]_{2N_F\mathrm{x}2} & \left[\boldsymbol{J}_{S_0S_0}(\boldsymbol{\theta})\right]_{2N_F\mathrm{x}2N_F} \end{array}\right], \tag{3.14}$$

where $\boldsymbol{J}_{\tau\tau}(\boldsymbol{\theta})$, $\boldsymbol{J}_{S_0\tau}(\boldsymbol{\theta})$ and $\boldsymbol{J}_{S_0S_0}(\boldsymbol{\theta})$ are sub-matrices of $\boldsymbol{J}(\boldsymbol{\theta})$. Given that within the parameter set $\boldsymbol{\xi}^E$ only the source location coordinates ξ_0 are of interest, let $\boldsymbol{C}_{CRB}(\xi_0)$ be the matrix formed by the first two rows and two columns of $\boldsymbol{C}_{CRB}(\boldsymbol{\xi}^E)$. Using the matrix theory, [123], based on (3.14), it can be shown that

$$\boldsymbol{C}_{CRB}(\xi_0) = c^2\left[\boldsymbol{H}\,\boldsymbol{J}_{\tau\tau}(\boldsymbol{\theta})\boldsymbol{H}^T - \boldsymbol{H}\,\boldsymbol{J}_{S_0\tau}^T(\boldsymbol{\theta})\,\boldsymbol{J}_{S_0S_0}^{-1}(\boldsymbol{\theta})\,\boldsymbol{J}_{S_0\tau}(\boldsymbol{\theta})\,\boldsymbol{H}^T\right]^{-1}. \tag{3.15}$$

Following a procedure in frequency domain similar to that in [124], the elements of the sub-matrices $\boldsymbol{J}_{\tau\tau}(\boldsymbol{\theta})$, $\boldsymbol{J}_{S_0\tau}(\boldsymbol{\theta})$ and $\boldsymbol{J}_{S_0S_0}(\boldsymbol{\theta})$ can be determined in closed form expression. For this the AWGN noise and deterministic signal source assumptions are exploited. Also, equation (15.52) from [91] is used as

$$[\boldsymbol{J}(\omega,\boldsymbol{\theta})]_{i,j} = 2\mathrm{Re}\left\{\sum_{k=1}^{M} \frac{1}{\sigma^2}\frac{\partial S_{R_k}^*}{\partial\theta_i}(\omega,\boldsymbol{\theta})\frac{\partial S_{R_k}}{\partial\theta_j}(\omega,\boldsymbol{\theta})\right\}, \tag{3.16}$$

where $S_{R_k}(\omega,\boldsymbol{\theta}) = \Gamma_k(\omega)S_0(\omega) = g_kS_0(\omega)e^{-j(\omega+\omega_c)\tau_k}$. Thus, the expressions for the elements of the sub-matrices $\boldsymbol{J}_{\tau\tau}(\boldsymbol{\theta})$, $\boldsymbol{J}_{S_0\tau}(\boldsymbol{\theta})$ and $\boldsymbol{J}_{S_0S_0}(\boldsymbol{\theta})$ are given in Appendix A.

For simplicity of the expressions, let the following two terms be defined: $\beta_{\omega_c} = 1 + \beta_0^2/\omega_c^2$ and $SNR_k = \mathcal{P}_{S_0}g_k^2/\sigma^2$, where β_0 is the effective bandwidth defined as $\beta_0^2 = \int_{B_0}\omega^2|S_0(\omega)|^2d\omega/\int_{B_0}|S_0(\omega)|^2d\omega$, [125], and $\mathcal{P}_{S_0}$ is the transmitted power defined as $\mathcal{P}_{S_0} = (1/2\pi)\int_{B_0}|S_0(\omega)|^2d\omega$. One may note that with the narrow-band signal assumption $\beta_{\omega_c} \approx 1$ and that SNR_k stands for the received signal-to-noise ratio at the k^{th} sensor. With these, expression (3.15) for $\boldsymbol{C}_{CRB}(\xi_0)$ can be alternatively written as

$$\boldsymbol{C}_{CRB}(\xi_0) = \eta_R\left[Z_{\xi_0} - Z_{S_0}\right]^{-1}, \tag{3.17}$$

where $\eta_R = c^2/2\omega_c^2\beta_{\omega_c}$, $Z_{S_0} = (\sum_{k=1}^{M} SNR_k \boldsymbol{\nu}_k)(\sum_{l=1}^{M} SNR_l \boldsymbol{\nu}_l^T)/\sum_{k'=1}^{M} SNR_{k'}$, and $Z_{\xi_0} = \sum_{k=1}^{M} SNR_k \boldsymbol{\nu}_k \boldsymbol{\nu}_k^T$.

Using (3.17), it follows that the MSE of the source location estimation is lower bounded by

$$\mathbb{E}\left\{\left\|\hat{\xi}_0 - \xi_0\right\|^2\right\} = \mathrm{var}\left\{\hat{\xi}_0\right\} = \mathrm{var}\left\{x_0\right\} + \mathrm{var}\left\{y_0\right\} \geq \eta_R \rho_L , \tag{3.18}$$

where $\rho_L = \left(q_x + q_y\right)/\left(q_x q_y - p_{xy}^2\right)$, given that

$$\boldsymbol{C}_{CRB}\left(\xi_0\right) = \frac{\eta_R}{q_x q_y - p_{xy}^2}\begin{bmatrix} q_x & p_{xy} \\ p_{xy} & q_y \end{bmatrix}, \tag{3.19}$$

with

$$q_x = \sum_{k=1}^{M} SNR_k \sin^2\varphi_k - \frac{1}{\sum_{k'=1}^{M} SNR_{k'}}\left(\sum_{k=1}^{M} SNR_k \sin\varphi_k\right)^2, \tag{3.20}$$

$$q_y = \sum_{k=1}^{M} SNR_k \cos^2\varphi_k - \frac{1}{\sum_{k'=1}^{M} SNR_{k'}}\left(\sum_{k=1}^{M} SNR_k \cos\varphi_k\right)^2, \tag{3.21}$$

$$\begin{aligned} p_{xy} = &-\sum_{k=1}^{M} SNR_k \sin\varphi_k \cos\varphi_k + \\ &+\frac{1}{\sum_{k'=1}^{M} SNR_{k'}}\left(\sum_{k=1}^{M} SNR_k \sin\varphi_k\right)\left(\sum_{k=1}^{M} SNR_k \cos\varphi_k\right). \end{aligned} \tag{3.22}$$

As discussed in [55] for the non-coherent case, equation (3.17) shows that also for the coherent localization the CRB with unknown source signal is always larger than that with known source signal. This is because it can be shown that the Z_{S_0} matrix, which is the average of weighted $\boldsymbol{\nu}_k$ vectors, is non-negative definite and it acts as a penalty term.

The lower bound on the source localization MSE given by (3.18) contains essentially two factors. The first one, η_R, shows the effect of the signal bandwidth and carrier frequency, which is similar to the case of high resolution MIMO radar, [65]. For narrow-band signals, i.e., $\beta_{\omega_c} \approx 1$, the effect of the signal bandwidth is negligible. Instead, the inverse proportionality with ω_c leads to the conclusion that the coherent processing offers much higher accuracy capabilities than the non-coherent processing. However, this conclusion is based on the CRB, which is known as being a tight bound at high SNR only and being a bound of small errors, [65]. As such, it ignores effects that could lead to large errors, like those determined by the high sidelobes that are characteristic to the coherent processing, [69], [72].

The second factor in (3.18), ρ_L, shows the effect of the geometric relations between the source and the sensors, impacted by the number of sensors and the *SNR* at these sensors. This effect is similar to the non-coherent processing case, as discussed in [55]: the estimation variance is larger when the source is far away, since the $\boldsymbol{\nu}_k$ vectors are similar in directions to generate a larger penalty matrix, i.e., the $\boldsymbol{\nu}_k$ vectors add up. When the source is inside the convex hull of the sensor array, the estimation variance is smaller since Z_{S_0} approaches the zero matrix, i.e., the $\boldsymbol{\nu}_k$ vectors cancel each other.

Beside lower bounding the MSE, another common measure for the attainable localization accuracy by the localization systems, for a given sensor layout, is the geometric dilution of precision (GDOP) metric, [126]:

$$\mathrm{GDOP} = \sqrt{\mathrm{var}\{\hat{\xi}_0\} \Big/ \frac{1}{M}\sum_{k=1}^{M} \mathrm{var}\{\hat{\tau}_k\}}. \tag{3.23}$$

Using the fact that $\sum_{k=1}^{M} \mathrm{var}\{\hat{\tau}_k\}$ can be written as $\mathrm{tr}\{\boldsymbol{J}_{\tau\tau}^{-1}(\boldsymbol{\theta})\}$, where $\mathrm{tr}\{\cdot\}$ stands for the trace of a matrix, it can be easily shown based on (3.18) and the expression of $\boldsymbol{J}_{\tau\tau}(\boldsymbol{\theta})$, that the GDOP for the non-cooperative source localization (non-coherent or coherent processing) is given by

$$\mathrm{GDOP} = \sqrt{M\rho_L \Big/ \sum_{k=1}^{M} \frac{1}{SNR_k}}, \tag{3.24}$$

which becomes identical to the expression in [65] by fixing the sensors' locations on a virtual circle around the source location.

3.4 Numerical Examples

While the best achievable performance of the estimation is indicated by the CRB, the MSE of the ML estimate is close to the CRB only at high SNR, [91]. A threshold effect was observed in location estimation systems, meaning essentially that there is a threshold value of the SNR, above which is the asymptotic region, where the estimation errors are small and the MSE is close to the CRB, [75], [77]. Otherwise, in the non-asymptotic region, the MSE rises quickly and deviates significantly from the CRB. This behavior can be observed in Figure 3.4, where a system of $M = 8$ sensors has been employed to localize a GSM source (the transmitted signal is GMSK and has a bandwidth of 200 kHz, while the carrier frequency is $f_c = 980$ MHz) situated within a known area of 50 m by 50 m. The sensors have been randomly placed within a virtual circle with radius of 500 m around the source location. While the continuous line indicates the root-MSE, the dots denote the error for each of the 100 simulations performed for each of the SNR values considered. The threshold effect can be observed at $\mathrm{SNR} = -3$ dB. Below the threshold,

the root-MSE increases up to some value close to the limitation imposed by the a priori known area within which the source is placed.

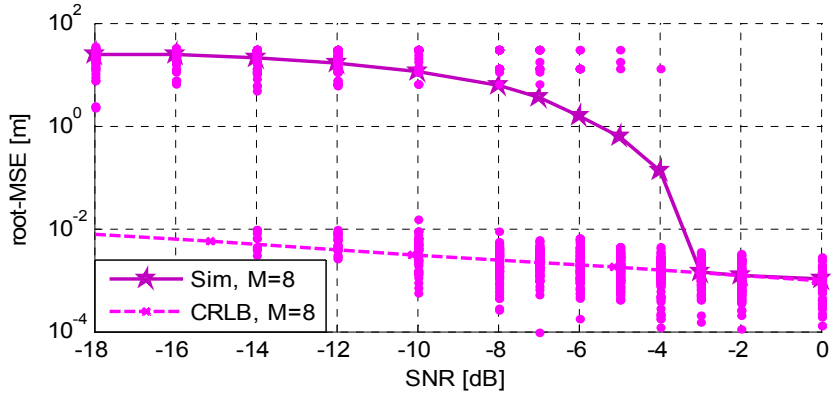

Figure 3.4 Localization accuracy for an array of 8 sensors. Sensors are randomly placed within the surveillance area.

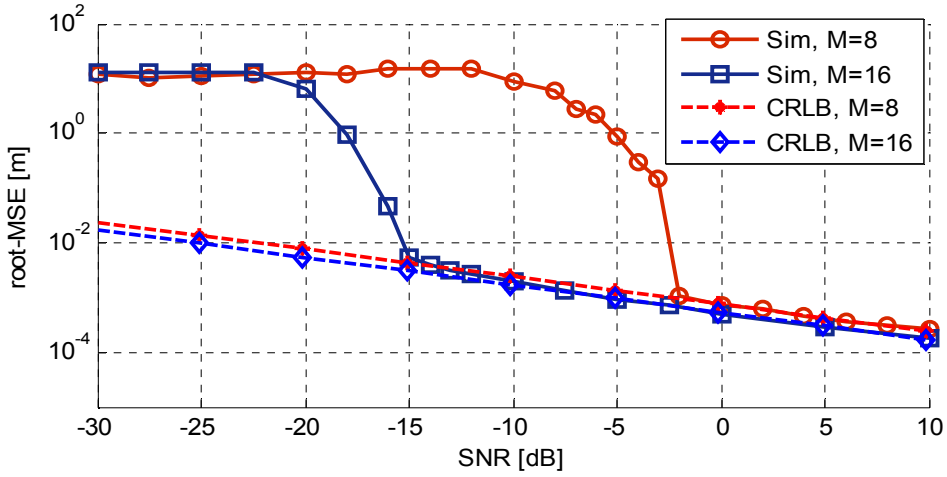

Figure 3.5 Localization accuracy for an array of 8 and 16 sensors, respectively. Sensors are uniformly placed on a virtual circle around the source.

The root-MSE increasing as the SNR decreases below the threshold means that the large localization errors take the place of the small ones (see the vertical distribution of the dots in Figure 3.4 for different SNR values; each dot has the meaning of the localization error for an individual simulation, while the line is the average of 100 such simulations). As expected, above the threshold, the root-MSE follows closely the CRB

and one may note that these values are below 1 m, while for the non-coherent systems the best achievable performance is tens of meters, [24].

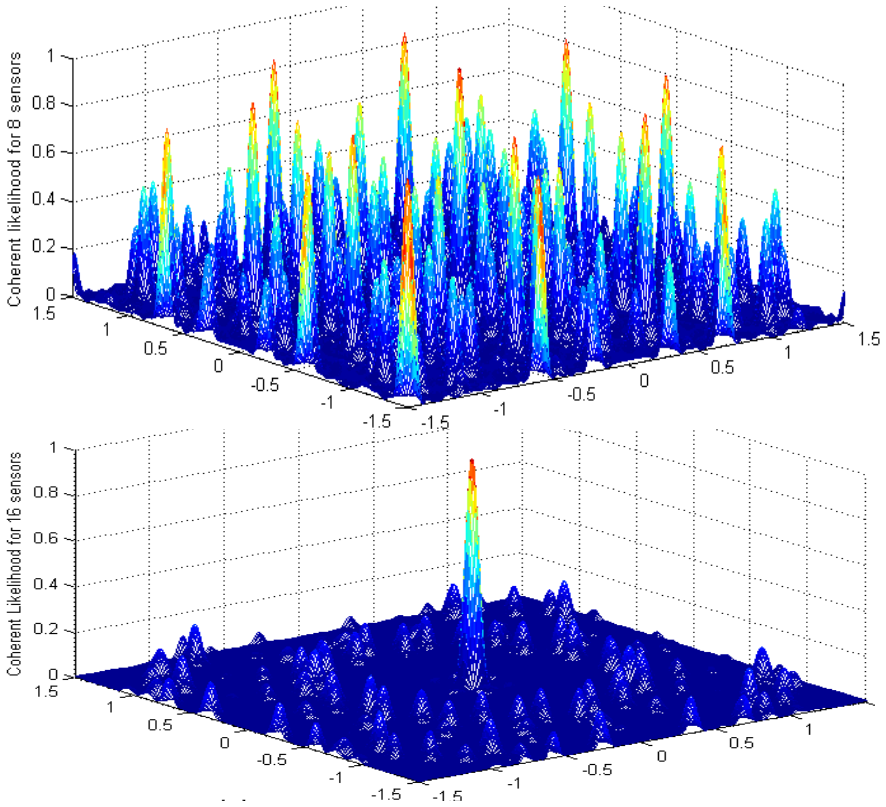

Figure 3.6 The localization metric for an array of 8 and 16 sensors, respectively. Sensors are uniformly placed on a virtual circle around the source.

While from the close form expression of the CRB (3.18) it may not be evident, *by* numerical evaluation, it can be shown that increasing the number of sensors improves the performance of the system. In Figure 3.5 it is shown that an increase from 8 to 16 in the number of sensors, under the systemic set-up aforementioned (except this time the sensors have been uniformly placed on a virtual circle with radius of 500 m around the source location), can bring, according to the CRB, a performance improvement of about 3 dB in terms of MSE. The MSE also shows that the SNR threshold moved from -2 dB to -15 dB by increasing the number of sensors from 8 to 16. This is sustained also by Figure

3.6, which shows that the sidelobes have been substantially lowered by increasing the number of sensors from 8 to 16, at SNR=5 dB.

The spatial advantage, ρ_L, is illustrated by Figure 3.7 and Figure 3.8, where the CRB is plotted for various sensor layouts. As such, it can be noticed that at high SNR, distributing sensors randomly within the surveillance area, (b), as well as clustering the sensors, (c), is not as good as having the sensors distributed uniformly on a circle around the source, (a). However, it has been shown in [77] that at moderate SNR the localization accuracy it is better when placing the sensors randomly, (b), rather than uniformly, (a). Layout (d) shows that the accuracy can be improved by increasing the number of sensors although they are grouped, as long as a reasonable separation is maintained.

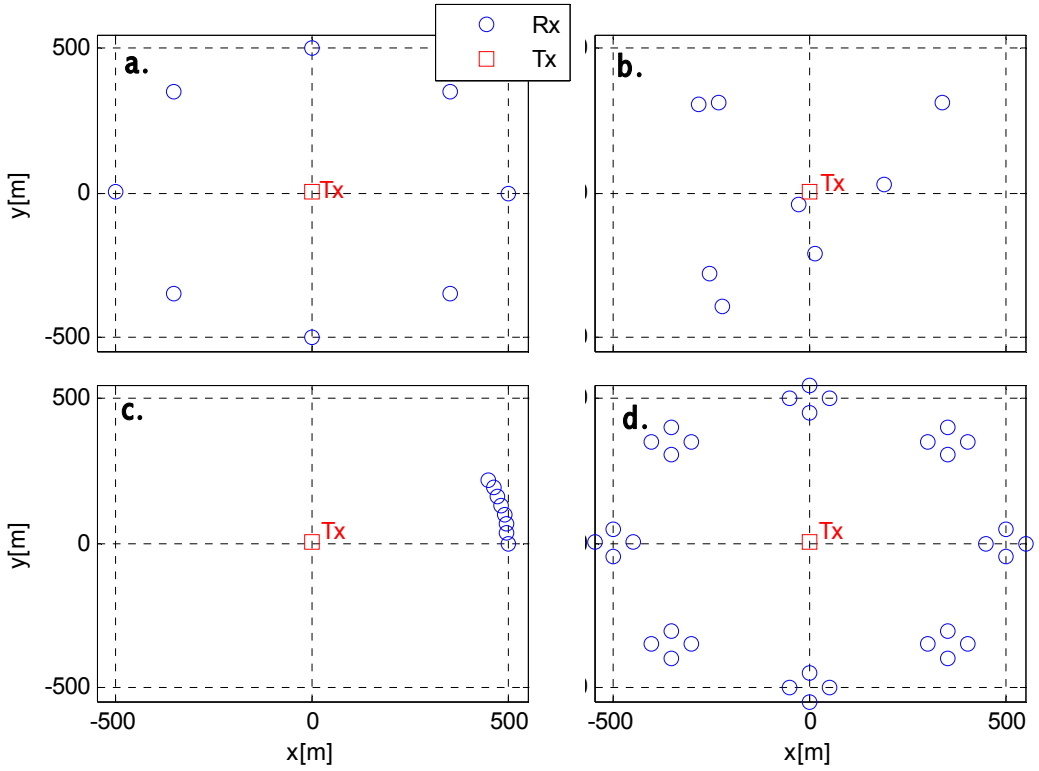

Figure 3.7 Different sensors layouts. a. Sensors are uniformly distributed on a virtual circle around the source. b. The sensors are randomly distributed around the source. c. The sensors are placed on a virtual arc around the source. d. The sensors are placed in groups on a virtual circle around the source.

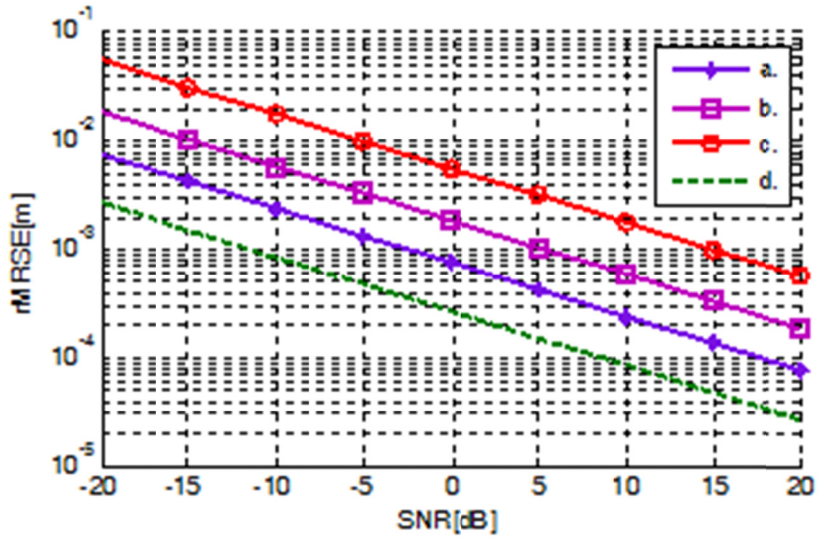

Figure 3.8 The CRB for the sensor layouts presented in Figure 3.7.

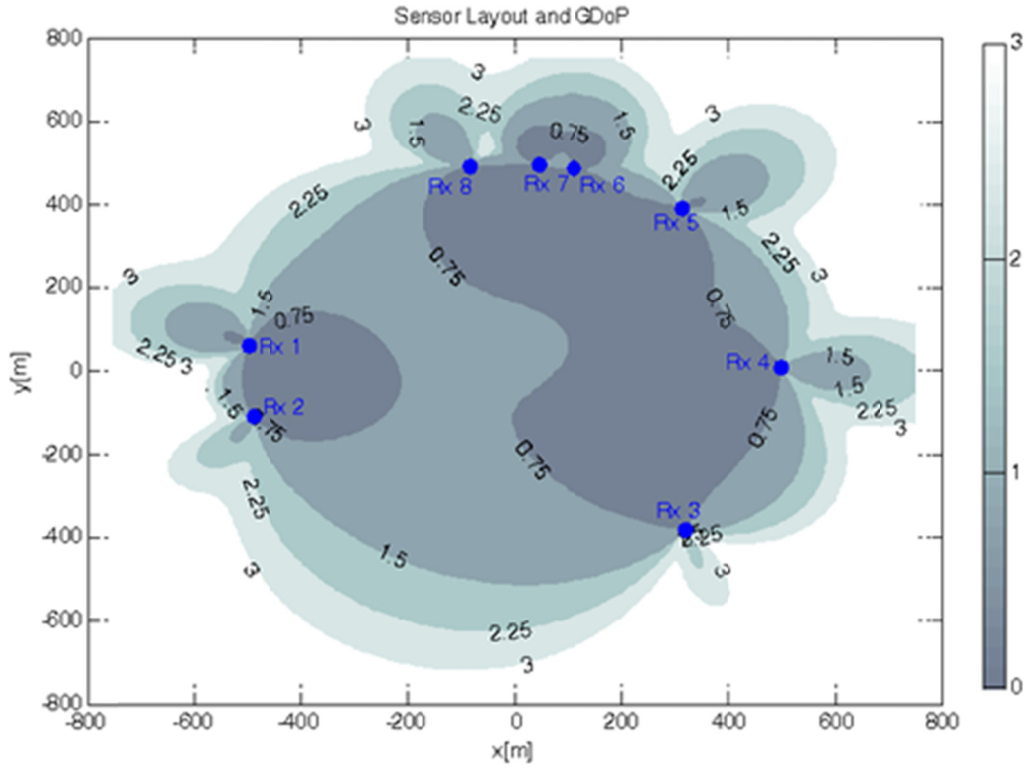

Figure 3.9 GDOP for coherent source localization with a distributed array of eight sensors randomly placed on virtual circle. The darker shade areas denote higher localization accuracy of sources placed within those areas.

The spatial advantage, ρ_L, can be studied also by the GDOP measure. In Figure 3.9 some GDOP contours are plotted for the case of 8 sensors randomly placed on a circle. The values marked on the contours are the values of the GDOP metric. Lower values of GDOP mean a higher precision of localization. It is noted that the localization precision is highest within the footprint of the sensors.

3.5 Location Estimation with Multi-Antenna Sensors

It has been observed in Section 3.4 that the level of the peak sidelobes in the localization metric can be lowered by increasing the number of receiving sensors. But increasing the number of sensors is often impractical.

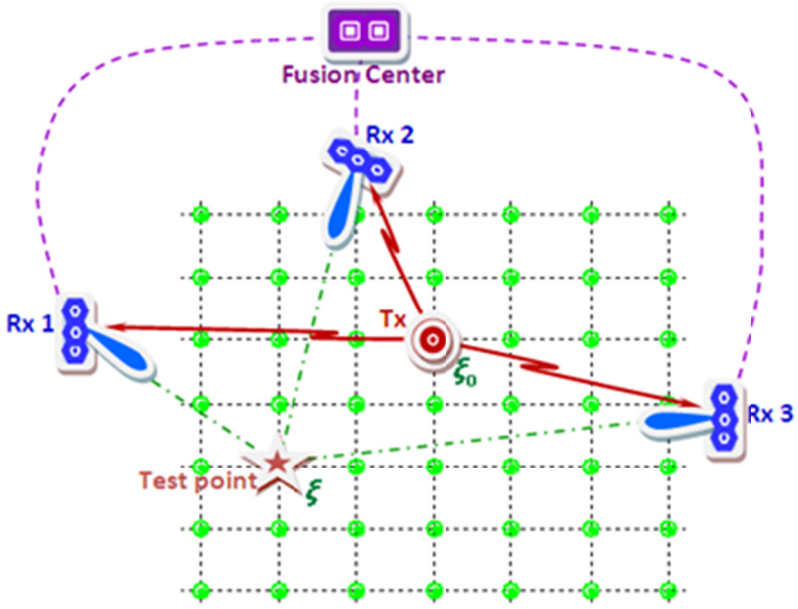

Figure 3.10 Multi-antenna sensors system layout for source localization. Before relaying the measured signal to the fusion sensor, each sensor performs some signal pre-processing, i.e., beamforming.

It may be easier in practice to have some sensors grouped in clusters, e.g., a cluster would be formed by more sensors mounted on a vehicle. But by clustering the sensors, the spatial diversity advantage diminishes considerably (see Figure 3.7 and Figure 3.8). To overcome this issue, instead of increasing the number of sensors and simply clustering them, the same number of sensors can be used but employing small antenna-arrays at each sensor and performing some signal pre-processing, e.g., optimal beamforming, locally at each sensor. Such a system layout is illustrated in Figure 3.10.

Assuming a small uniform linear array (ULA) of M_a antennas at each of the M sensors, the signal received at the m^{th} antenna of the k^{th} sensor is modeled in a multipath free environment by modifying the signal model (1.2):

$$\tilde{r}_{k,m}(t) = a_{k,m}\big(\theta_k(\xi)\big)\alpha_k s_0\big(t - \tau_k(\xi_0)\big) + w_{k,m}(t)\,, \tag{3.25}$$

where $a_{k,m}\big(\theta_k(\xi)\big) = e^{-j2\pi f_c(m-1)\frac{d_\Delta}{c}\cos\theta_k(\xi)}$ are the elements of the steering vector $\boldsymbol{a}_k$, [92], $\theta_k(\xi)$ is the bearing angle of the of the k^{th} sensor to the location ξ tested for source presence, and d_Δ is the spacing of the antennas at a sensor; d_Δ is considered herein half the value of the carrier wavelength.

The received signals at any sensor k can be expressed in a compact form:

$$\tilde{\boldsymbol{r}}_k(t) = \boldsymbol{a}_k\alpha_k s_0\big(t - \tau_k(\xi_0)\big) + \boldsymbol{w}_k(t)\,, \tag{3.26}$$

with $\tilde{\boldsymbol{r}}_k(t) = \big[\tilde{r}_{k,1}(t), \dots, \tilde{r}_{k,M_a}(t)\big]^T$, $\boldsymbol{a}_k = \big[a_{k,1}\big(\theta_k(\xi)\big), \dots, a_{k,M_a}\big(\theta_k(\xi)\big)\big]^T$, and $\boldsymbol{w}_k(t) = \big[w_{k,1}(t), \dots, w_{k,M_a}(t)\big]^T$. Employing the minimum power distortionless response (MPDR) beamformer, [92], at each sensor, let the output of the beamformer be

$$r_k(t,\xi) = \mathbf{v}_k^H(\xi)\,\tilde{\boldsymbol{r}}_k(t)\,, \tag{3.27}$$

for every test location ξ. The MPDR weights are chosen such that to minimize the overall received power $\mathbf{v}_k^H(\xi)\boldsymbol{C}_{r_k}\mathbf{v}_k(\xi)$, while keeping unit gain in the direction of steering (the direction of the test location ξ):

$$\mathbf{v}_k(\xi) = \text{argmin}_{\mathbf{v}}\, \mathbf{v}_k^H(\xi)\boldsymbol{C}_{r_k}\mathbf{v}_k(\xi), \text{ subject to } \text{Re}\{\mathbf{v}_k^H(\xi)\boldsymbol{a}_k(\xi)\} = 1\,, \qquad (3.28)$$

where $\boldsymbol{C}_{r_k}$ denotes the sample correlation matrix at the k^{th} sensor, [92]. The weights satisfying (3.28) are given by

$$\mathbf{v}_k(\xi) = \frac{\boldsymbol{C}_{r_k}^{-1}\boldsymbol{a}_k(\xi)}{\boldsymbol{a}_k^H(\xi)\boldsymbol{C}_{r_k}^{-1}\boldsymbol{a}_k(\xi)}\,. \qquad (3.29)$$

With these, the localization metric $\Lambda(\xi)$ used for source localization is the same as in (3.9), except that this time $x_{lk}(\tau)$ represents the cross-correlation of signals $r_l(t,\xi)$ and $r_k(t,\xi)$, which are the result of the beamformers at sensors l and k, (3.27).

With multi-antenna sensors, simulation results show improved performance. For example, in Figure 3.11 it can be observed that the peak sidelobes located further away from the source are considerably smaller with multi-antenna sensors compared to single-antenna sensors. In Figure 3.12 accuracy curves of localization in noise are plotted. The threshold effect is seen to be lowered by about 18 dB by using 5-antenna instead of single-antenna sensors. This means the system is more robust to noise when using multi-antenna sensors. The accuracy versus average SNR when utilizing eigth 5-antenna sensors uniformly distributed on a circle around the source is observed to be about the same with the accuracy obtained by employing 24 single-antenna sensors uniformly distributed on a circle around the source.

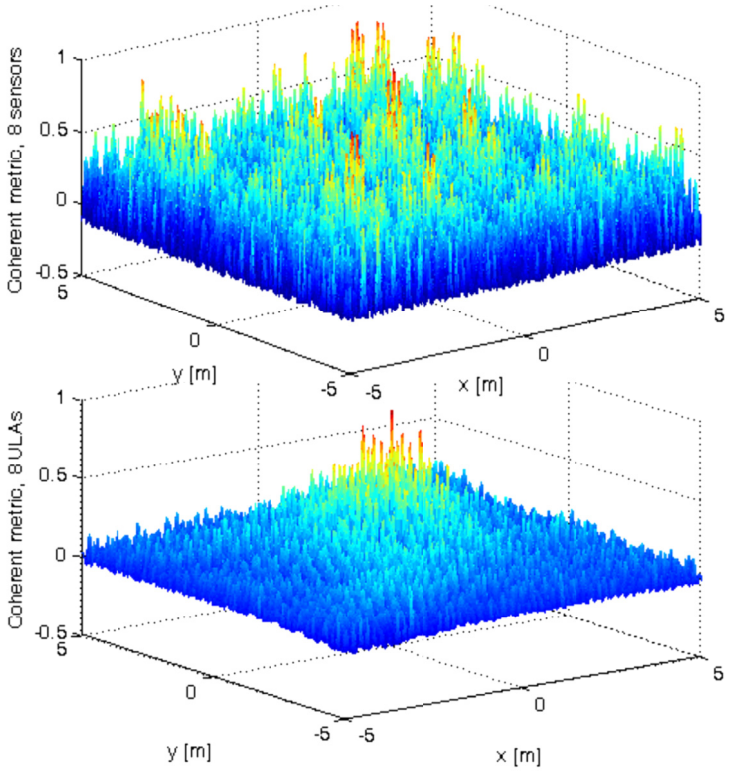

Figure 3.11 The localization metric for the case using single-antenna sensors versus the case of using 5-antenna sensors. It can be observed that the peak sidelobes located further away from the source are considerably smaller with multi-antenna sensors.

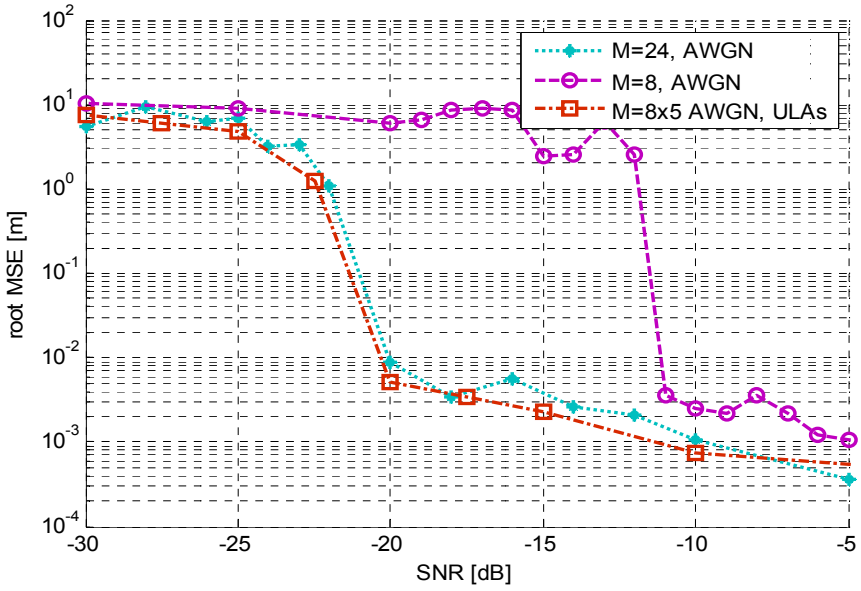

Figure 3.12 Coherent localization accuracy in noise for single-antenna and multi-antenna sensors.

3.6 Concluding Remarks

This section has discussed a coherent processing technique for the planar localization of an unknown radio source in the near field of a widely distributed passive sensor array. A coherent localization metric for deterministic unknown signal source is proposed. The CRB for the MSE is also derived. The expression obtained is consistent with the results presented in literature for non-coherent processing using passive sensor arrays and for coherent processing using active arrays. As such, the accuracy of the localization is strongly dependent on the carrier frequency and the sensor layout. The numerical examples of CRB are in accordance with the computer simulations for the root-MSE. At low SNR, the performance is dominated by noise, with false peaks popping up in the localization metric anywhere in the a priori parameter space of the source location. At high SNR, the performance is ambiguity free and the CRB tightly bounds the MSE. Increasing the number of sensors increase the accuracy at high SNR and also expands the ambiguity free region. The same effect is obtained by employing receiving sensors with a small number of antennas instead of single-antenna sensors.

CHAPTER 4

SIGNAL PARAMETERS ESTIMATION FROM LOW RATE SAMPLES

4.1 Motivation

As described in Section 1.4, in many localization applications the received signals have finite rate of innovation (FRI), e.g., as it the case of streams of short pulses of known shape, and thus they can be sampled at rates lower than the conventional Nyquist rate. This section considers the sampling of FRI signals as presented in [84]. But rather than recovering the signal itself, the interest is on estimating specific signal parameters, i.e., on time delay estimation (TDE) and amplitudes estimation (AE). This is motivated by the fact that source localization can be performed based on these parameters. With the low rate (LR) sampling scheme proposed in [84], the signal recovery is equivalent to estimating all the unknowns parameterizing the signal, e.g., time delays and corresponding attenuations. By contrast, estimation of individual parameters may be performed independently, e.g., TDE does not require the estimation of amplitudes and thus its performance with system parameters may vary differently from that of signal recovery.

As mentioned in Section 1.4, it was found in [86] that the performance of the signal recovery from LR samples can deteriorate in the presence of noise substantially more than the recovery from samples taken at the Nyquist rate would deteriorate. The first goal of this chapter is to determine if the performance of signal parameters estimation (SPE) from samples taken at LR also deteriorates in noise more than if samples taken at the Nyquist rate would be available and if sampling higher than rate of

innovation (ROI) helps. The second goal is to analytically quantify the performance of SPE from LR samples and to identify the influence on the SPE performance of system parameters, e.g, the sampling rate and the inter-path separation. Finally, the third goal is to compare the SPE performance for different types of received signals. Specifically, let a periodic stream of pulses be transmitted through a multipath channel. Let us consider that the time delays are invariant with respect to the beginning of each period. The received signal is periodic if the amplitude of each path does not vary from period to period or is said to be semi-periodic if the amplitudes vary. Since these situations may be encountered in practice, it is of interest to compare the SPE performance in the two cases. To achieve the three goals enumerated, a Cramér-Rao bound (CRB) is developed for SPE from LR samples in a general setup. This can be used to numerically evaluate the performance of SPE from LR samples as the CRB developed in [86] was used for signal recovery performance evaluation. However, we go further and develop closed form CRB expressions for SPE from LR samples in a specific setup and particularize it for $K = 1$ and $K = 2$, i.e., for the cases when there is no multipath and for the case when the signal propagates through two paths, respectively.

With $K = 1$, the first finding is that the performance of SPE from LR samples in noise is lower than if samples taken at the Nyquist rate would be available. This is similar to the results found in [86] for signal recovery. Additionally, if the sampling rate is increased by a factor P over ROI, the TDE performance in terms of mean squared error (MSE) improves, i.e., it decreases, with a factor of P^{-3} until it reaches the performance obtained with the same number of samples as if sampling at the Nyquist rate. By contrast, the AE performance improves only with P^{-1}. The SPE CRB for the case of taking with

the scheme from [84] the same number of samples as if sampling at the Nyquist rate can be compared with the sampling scheme used in [83]. Thus, by considering the sampling filter in [83] as being equivalent to the filter that shapes the pulses in [84], the CRB expressions for the two cases become equivalent. At the same time, the CRB expression found herein for $K = 1$, although in a different context, is similar to the results shown in [39] for parameter estimation, e.g., angle of arrival, by jointly processing the signals received with an array of sensors. This allows drawing parallels between the problems of TDE estimation from LR samples and angle of arrival estimation. Comparing the derived CRB expressions for periodic and semi-periodic received signals, it is found that the TDE performance does not change, while the AE performance worsens in the semi-periodic case.

With $K = 2$, the effect of time separation between the multipath components on the TDE resolution is found by numerical simulations to be similar to that on signal recovery in [86]. However, the analytical expression developed shows not only that the resolution increases with the time separation between the signal components, as in [86], but this improvement depends on the sampling rate. Thus, sampling in noise at rates higher than ROI also effects in better resolution of closely separated signal components.

4.2 FRI Signals

The FRI concept is characteristic to signals that support parametric modeling. A stream of pulses is such a parametric signal, uniquely defined by the time-delays of the pulses and their amplitudes. Let a pulse stream of finite-duration T consist of K pulses, whose time delays $\{\tau_k\}$ are known to be located within the $[0, T)$ interval. For a known pulse $g(t)$, the stream can be expressed as

$$x_R(t) = \sum_{k=1}^{K} a_k g(t - \tau_k). \tag{4.1}$$

This signal is characterized by the K unknown time delays $\{\tau_k\}$ and K amplitudes $\{a_k\}$. The total number of parameters determining the signal is thus $2K$, leading to a ROI given by $2K/T$. The signal is then FRI.

The finite-duration stream (4.1) can be extended to infinite-length. One particular extension is that of periodic FRI signals. With the assumption that there are K different time delays $\{\tau_k\}$ and K amplitudes $\{a_k\}$ that are repeated every T,

$$x_R(t) = \sum_{n\in\mathbb{Z}} \sum_{k=1}^{K} a_k g(t - \tau_k - nT). \tag{4.2}$$

For this case, the whole signal, as well as any of its segments of length T, can be uniquely defined by only $2K$ parameters. Thus ROI of the full length signal is again $2K/T$, being the same as the local ROI for every T.

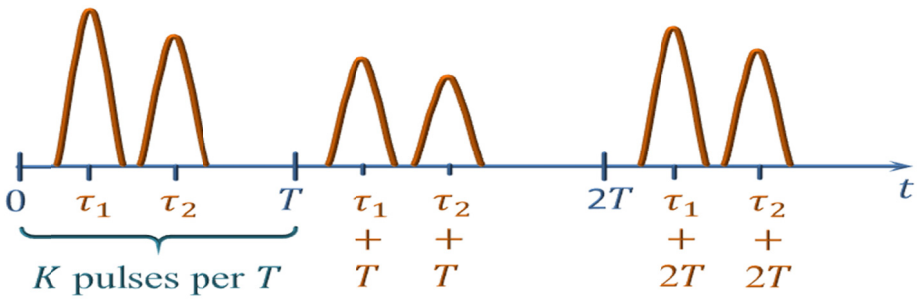

Figure 4.1 Semi-periodic stream of pulses, $x_R(t)$.

Another class of stream of pulses of practical interest is formed by the semi-periodic signals defined as

$$x_R(t) = \sum_{n\in\mathbb{Z}} \sum_{k=1}^{K} a_k[n] g(t - \tau_k - nT). \tag{4.3}$$

These are similar to the periodic signals defined by (4.2), except that the amplitudes vary from period to period. Signals from this class can be used to describe the propagation of a pulse with known shape $g(t)$ which is transmitted at a constant rate $1/T$ through an environment consisting of K paths. Each path has a constant delay τ_k and a time-varying gain $a_k[n]$, as illustrated in Figure 4.1. In this case, the signal is defined by K time delays $\{\tau_k\}$ and by an infinite number of amplitudes $\{a_k[n]\}$. However, any segment of length T is defined by K time delays and K amplitudes. Thus the local ROI is again finite, i.e., $2K/T$.

The signals (4.1)-(4.3) can be thought of as belonging to a union of subspaces, where the delays $\{\tau_k\}$ determine an K-dimensional subspace and the amplitudes $\{a_k\}$ describe the position within the subspace, [84, 127, 128]. The union of subspaces is infinite since there are infinitely many values that the parameters $\tau_1, \dots, \tau_K$ can take. The subspaces are shift invariant since the time delays do not vary with respect to the beginning of each segment of length T. For signals of forms (4.1) and (4.2), the subspaces are finite-dimensional since the number of amplitudes is limited to K. By contrast, for (4.3), each subspace is infinite-dimensional, as it is determined by an infinite number of amplitudes. Thus, once the subspace is selected (the delays are estimated) for (4.3) it is more difficult to identify the point within the subspace (to estimate the amplitudes) than for (4.2). Thus, performance of SPE is of interest to be evaluated in order to confirm this observation. When comparing the non-periodic (and finite-duration) stream (4.1) and the periodic stream (4.2), they are similar from the point of view of identifying the subspace and a point within the subspace, [86]. Performance differences between the two are however expected to occur in noise because of the different signal

energy. For example, if the signal segment of length T is repeated N times, where N is large to fit model (4.2), the signal energy is increased by N compared to (4.1).

To measure and compare the best performance that can be attained for estimation of signal parameters from LR samples for different cases as those described above, i.e., non-periodic, periodic, and respectively semi-periodic streams of pulses, CRB expressions for SPE are developed in Section 4.4. But before that, the low rate sampling scheme adopted is described in the next section.

4.3 Filter-bank LR Sampling of FRI Signals

Sampling of FRI signals at low rates was first addressed by uniform sampling of the signal convolved with a sampling kernel $s(t)$. For example, in [82] and [83] a stream of Diracs repeated periodically every T seconds is sampled using a Diricklet kernel of bandwidth $\mathcal{B}_s$, $s(t) = \frac{1}{\mathcal{B}_s T}\frac{\sin(\pi \mathcal{B}_s t)}{\sin(\pi t/T)}$, which is equivalent to a sinc function for $\mathcal{B}_s T \gg 1$. The result of the convolution is sampled at a rate $\mathcal{B}_s$. This sampling scheme relies on the observation that the time delays and amplitudes can be recovered from a set of signal's Fourier series coefficients. This follows from the fact that in the frequency domain, the problem translates into estimating the frequencies and amplitudes of a sum of complex sinusoids, a problem that can be addressed by super-resolution parameter estimation methods, [35, 37, 39, 92, 129, 130]. The sampling scheme is such designed to determine the Fourier coefficients. While this works for periodic streams, for sampling non-periodic streams, compact sampling kernels, i.e., with finite time support, are desirable. A family of such sampling kernels was introduced in [131], defined as sum of sincs. Another class of compact support kernels that can be used to sample FRI signals is given by the family

of exponential reproducing kernels, presented in [132] and [133]. While these sampling techniques are simple, improved performance and lower sampling rates can be achieved at the cost of slightly more complex hardware. In particular, a filter-bank sampling scheme in which the signal $x_R(t)$ is convolved with P different sampling kernels, $s_1^*(-t),\ldots, s_P^*(-t)$, and the output of each channel is sampled at a rate of $1/T$ is presented in [84, 85, 134]. The system is said to have a total sampling rate of P/T. An alternative multichannel structure can be obtained in which the filter is replaced by a multiplier followed by an integrator, [135]. This alternative follows a similar path to the single channel method from [82] in the sense that the signal parameters are retrieved from a set of Fourier coefficients of the signal. The Fourier coefficients are obtained by the multichannel designed LR sampling scheme. This scheme can be used to treat all cases of FRI signals, non-periodic, periodic, semi-periodic, under the assumption that the pulse $g(t)$ is compactly supported. In contrast, the filter-bank approach from [84] can accommodate arbitrary pulse shapes $g(t)$, including infinite-length functions. This means that it is particularly beneficial for signals for which one can no longer speak of Fourier series, as is the case of signals that are not periodic and cannot be divided into distinct intervals.

The filter-bank sampling scheme is presented in the followings for a semi-periodic stream of pulses for which the pulse shape is not necessarily compact supported and thus pulses from different repetition intervals of length T may overlap. For practical illustration, let us consider the case of transmitting a stream of amplitude modulated pulses through a multipath channel and sampling the received stream at LR. Such a transmitted stream is defined by a known pulse shape, $g(t)$, pulse repetition interval, T,

and symbols $x[n]$ taken from a finite alphabet: $x_T(t) = \sum_{n\in\mathbb{Z}} x[n]g(t-nT)$. For a noiseless multipath channel, $h(\tau,t) = \sum_{k=1}^{K} \alpha_k \delta(t-\tau_k)$, where α_k are the complex valued gains and $\tau_k < T$, the received signal $x_R(t)$ is modeled as a semi-periodic stream of pulses, (4.3), where $a_k[n] = \alpha_k x[n]$.

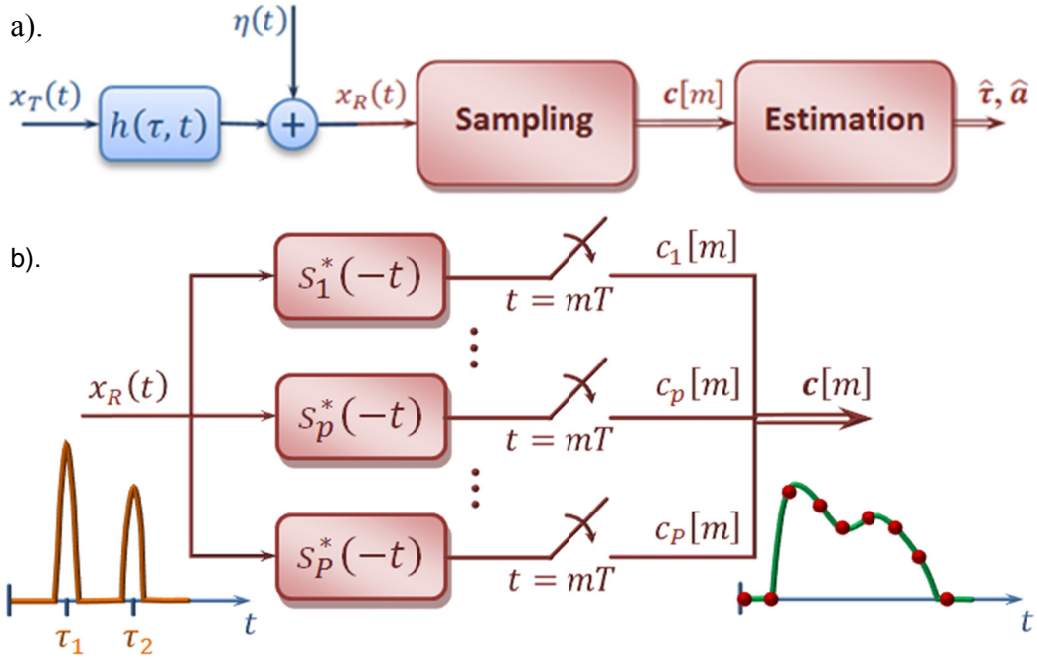

Figure 4.2 a) System model; b) Filter-bank sampling block.

The channel is considered time invariant, i.e., α_k does not vary from one interval T to another. The signal is shift invariant in the sense that the time delays τ_k are the same from one interval T to another, with respect to the beginning of each interval. Note that if the sequence $x[n]$ is not known, the signal $x_R(t)$ is a semi-periodic stream of pulses and the parameters to be estimated are the time delays $\{\tau_k\}$ and amplitudes $\{a_k[n]\}$. If the sequence $x[n]$ is known, the parameters to be estimated are the time delays $\{\tau_k\}$ and multipath gains $\{\alpha_k\}$. Particularly, for $x[n] = 1$, for any $n \in \mathbb{Z}$, signal $x_R(t)$ reduces to the periodic stream of pulses (4.2). However, in both cases, $x_R(t)$ has local ROI of

$2K/T$. For signals with this feature, it was shown that in the absence of noise a filter-bank LR sampling scheme allows perfect recovery of the received signal $x_R(t)$ as long as the number of samples P per interval T is in general at least $2K$, [84], but not higher than $2T\mathcal{B}_g$, where $\mathcal{B}_g$ is the single side bandwidth of the pulse shape (if band-limited), [136]. Combined, these lead to condition $2K \leq P \leq 2T\mathcal{B}_g$. Additional conditions for perfect recovery will be given later in this section.

A system model for the case when the transmitted signal is affected by complex valued additive white Gaussian noise (AWGN), $\eta(t)$, of PSD $\bar{\Phi}_\eta$ is illustrated in Figure 4.2.a. For later use, let $\sigma_\eta^2 = \bar{\Phi}_\eta/T$ denote the power of the noise after passing through an ideal low pass filter of cut-off frequency $1/2T$. The sampling filter bank, detailed in Figure 4.2.b, and the estimation procedure are sequentially presented in the followings.

The DTFT of the p-th sampling sequence corresponding to the p-th branch in Figure 4.2.b is

$$C_p\left(e^{j\omega T}\right) = \frac{1}{T}\sum_{m\in\square} S_p^*\left(\omega - \frac{2\pi}{T}m\right) X_R\left(\omega - \frac{2\pi}{T}m\right) + \\ + \frac{1}{T}\sum_{m\in\square} S_p^*\left(\omega - \frac{2\pi}{T}m\right) \mathcal{N}\left(\omega - \frac{2\pi}{T}m\right), \tag{4.4}$$

where $S_p(\omega)$, $X_R(\omega)$, and $\mathcal{N}(\omega)$ denote the Fourier transform of $s_p(t)$, $x_R(t)$, and $\eta(t)$ respectively. Taking the Fourier transform of (4.3),

$$X_R(\omega) = \sum_{k=1}^{K} A_k\left(e^{j\omega T}\right) G(\omega) e^{-j\omega\tau_k}, \tag{4.5}$$

where $A_k\left(e^{j\omega T}\right)$ denotes the DTFT of the sequence $a_k[n]$, and $G(\omega)$ denotes the Fourier transform of $g(t)$. Substituting (4.5) into (4.4),

$$C_p\left(e^{j\omega T}\right) = \sum_{k=1}^{K} A_k\left(e^{j\omega T}\right) e^{-j\omega\tau_k} \frac{1}{T} \sum_{m\in\square} S_p^*\left(\omega - \frac{2\pi}{T}m\right) \cdot$$

$$\cdot G\left(\omega - \frac{2\pi}{T}m\right) e^{j\frac{2\pi}{T}m\tau_k} + \frac{1}{T} \sum_{m\in\square} S_p^*\left(\omega - \frac{2\pi}{T}m\right) \mathcal{N}\left(\omega - \frac{2\pi}{T}m\right). \quad (4.6)$$

Focusing, as proposed in [84], on sampling filters $s^*(-t)$ with finite support in the frequency domain, e.g., contained in the range $\mathcal{F} = [-P\pi/T\,,\ P\pi/T]$, (4.6) becomes

$$C_p\left(e^{j\omega T}\right) = \sum_{k=1}^{K} A_k\left(e^{j\omega T}\right) e^{-j\omega\tau_k} \frac{1}{T} \sum_{q=1}^{P} S_p^*(\omega + \omega_q) \cdot$$

$$\cdot G(\omega + \omega_q) e^{-j\omega_q\tau_k} + \frac{1}{T} \sum_{q=1}^{P} S_p^*(\omega + \omega_p) \mathcal{N}(\omega + \omega_p), \quad (4.7)$$

where $\omega_q = 2\pi(q - 1 - P/2)/T$. Note that all the expressions in the DTFT domain are $2\pi/T$ periodic and ω is restricted to the interval $[0, 2\pi/T)$. Let $\boldsymbol{c}\left(e^{j\omega T}\right)$ denote the length P column vector whose p-th element is $C_p\left(e^{j\omega T}\right)$, $\boldsymbol{W}\left(e^{j\omega T}\right)$ the $P \times P$ matrix whose pq-th element is $W_{pq}\left(e^{j\omega T}\right) = \frac{1}{T} S_p^*(\omega + \omega_q) G(\omega + \omega_q)$, $\boldsymbol{\mu}\left(e^{j\omega T}\right)$ the length P column vector whose q-th element is $\mu_q\left(e^{j\omega T}\right) = \sum_{k=1}^{K} A_k\left(e^{j\omega T}\right) e^{-j(\omega+\omega_q)\tau_k}$, and $\boldsymbol{\varepsilon}\left(e^{j\omega T}\right)$ the length P column vector whose p-th element is $\varepsilon_p\left(e^{j\omega T}\right) = \frac{1}{T} S_p^*(\omega + \omega_p)$ $\mathcal{N}(\omega + \omega_p)$. With these, (4.7) can be written in matrix form as

$$\boldsymbol{c}\left(e^{j\omega T}\right) = \boldsymbol{W}\left(e^{j\omega T}\right) \boldsymbol{\mu}\left(e^{j\omega T}\right) + \boldsymbol{\varepsilon}\left(e^{j\omega T}\right). \quad (4.8)$$

Further, $\boldsymbol{\mu}\left(e^{j\omega T}\right)$ can be written

$$\boldsymbol{\mu}\left(e^{j\omega T}\right) = \boldsymbol{N}(\boldsymbol{\tau}) \boldsymbol{D}\left(e^{j\omega T}, \boldsymbol{\tau}\right) \boldsymbol{a}\left(e^{j\omega T}\right), \quad (4.9)$$

where $\boldsymbol{\tau} = [\tau_1, \dots, \tau_K]^{\mathrm{T}}$, $\boldsymbol{N}(\boldsymbol{\tau})$ is a $P \times K$ matrix with elements $N_{qk}(\boldsymbol{\tau}) = e^{-j\omega_q \tau_k}$, $\boldsymbol{D}\left(e^{j\omega T}, \boldsymbol{\tau}\right) = \mathrm{diag}\left\{\left[e^{-j\omega\tau_1}, \dots, e^{-j\omega\tau_K}\right]\right\}$, and $\boldsymbol{a}\left(e^{j\omega T}\right) = \left[A_1\left(e^{j\omega T}\right), \dots, A_K\left(e^{j\omega T}\right)\right]^{\mathrm{T}}$. By denoting the K dimensional vector $\boldsymbol{b}\left(e^{j\omega T}\right) = \boldsymbol{D}\left(e^{j\omega T}, \boldsymbol{\tau}\right)\boldsymbol{a}\left(e^{j\omega T}\right)$, (4.9) becomes in the time domain

$$\boldsymbol{\mu}[n] = \boldsymbol{N}(\boldsymbol{\tau})\boldsymbol{b}[n], \forall\, n \in \mathbb{Z}. \tag{4.10}$$

One may note that $\boldsymbol{N}(\boldsymbol{\tau})$ has a Vandermonde structure and thus super-resolution techniques, e.g., MUSIC, [35, 37], or ESPRIT, [129, 130], traditionally used in frequency and direction of arrival (DOA) estimation, can be employed with (4.10) to estimate the time delays $\boldsymbol{\tau}$, where the number of multipaths K is a priori known, [84]. Disregarding the noise, the values of $\boldsymbol{\mu}[n]$ are obtained from (4.8) by taking $\boldsymbol{W}^{-1}\left(e^{j\omega T}\right)\boldsymbol{c}\left(e^{j\omega T}\right)$. Thus, the matrix $\boldsymbol{W}\left(e^{j\omega T}\right)$ needs to be stable invertible, leading to the recovery conditions (i) that $g(t)$ needs to satisfy $0 < a \leq |G(\omega)| \leq b < \infty$, almost everywhere $\omega \in \mathcal{F}$, and (ii) that the filters $s^*(-t)$ should be chosen in such a way that they form a stable invertible $P \times P$ matrix $\boldsymbol{S}\left(e^{j\omega T}\right)$, with elements $S_{pq}\left(e^{j\omega T}\right) = \frac{1}{T}S_p^*\left(\omega + \omega_q\right)$. One example of filters satisfying this condition and which is adopted throughout this work is

$$S_p(\omega) = \begin{cases} T, \text{for } \omega \in \left[\omega_p,\ \omega_p + \dfrac{2\pi}{T}\right] \\ 0, \text{otherwise.} \end{cases} \tag{4.11}$$

4.4 Performance Lower Bound

The accuracy of an estimate $\widehat{\boldsymbol{\theta}}$ of a column vector parameter $\boldsymbol{\theta}$ is typically measured by its mean squared error (MSE), defined as $\mathrm{MSE}\{\widehat{\boldsymbol{\theta}}\} = \mathbb{E}\left\{\left\|\boldsymbol{\theta} - \widehat{\boldsymbol{\theta}}\right\|^2\right\}$, where $\mathbb{E}$ denotes the expectation taken with respect to the probability density function (pdf) of $\boldsymbol{c}$ parameterized by $\boldsymbol{\theta}$, i.e., $\mathbb{E}\left\{\left\|\boldsymbol{\theta} - \widehat{\boldsymbol{\theta}}\right\|^2\right\} = \int \left\|\boldsymbol{\theta} - \widehat{\boldsymbol{\theta}}\right\|^2 f(\boldsymbol{c};\boldsymbol{\theta})\mathrm{d}\boldsymbol{c}$, and $\left\|\boldsymbol{\theta} - \widehat{\boldsymbol{\theta}}\right\|^2 = \left(\boldsymbol{\theta} - \widehat{\boldsymbol{\theta}}\right)^H\left(\boldsymbol{\theta} - \widehat{\boldsymbol{\theta}}\right)$, [137].

To assess the performance of any estimation method, it is useful to find theoretical limits on this performance. For this purpose, CRB for a vector $\boldsymbol{\theta}$ that parameterizes the samples $\boldsymbol{c}[m]$, $m \in \mathbb{Z}$, is a matrix, say $\boldsymbol{C}(\boldsymbol{\theta})$, that provides a lower bound on the covariance of any unbiased estimate $\widehat{\boldsymbol{\theta}}$, i.e., $\mathbb{E}\left\{\left(\mathbb{E}\{\widehat{\boldsymbol{\theta}}\} - \widehat{\boldsymbol{\theta}}\right)\left(\mathbb{E}\{\widehat{\boldsymbol{\theta}}\} - \widehat{\boldsymbol{\theta}}\right)^{\mathrm{H}}\right\} \geq \boldsymbol{C}(\boldsymbol{\theta})$, where "$\geq$" is here an element-wise operator. An unbiased estimate is an estimate for which $\mathbb{E}\{\widehat{\boldsymbol{\theta}}\} = \boldsymbol{\theta}$ and thus its MSE equals its variance. Thus, the MSE of any unbiased estimate $\widehat{\boldsymbol{\theta}}$ is lower bounded by the trace of $\boldsymbol{C}(\boldsymbol{\theta})$ and the MSE of any element i of $\widehat{\boldsymbol{\theta}}$, $\hat{\theta}_i$, is lower bounded by the i-i element of matrix $\boldsymbol{C}(\boldsymbol{\theta})$, i.e., $\mathrm{CRB}(\theta_i) = [\boldsymbol{C}(\boldsymbol{\theta})]_{i,i}$.

By definition, the CRB matrix can be determined as the inverse of the Fisher Information Matrix (FIM), $\boldsymbol{C}(\boldsymbol{\theta}) = \boldsymbol{J}^{-1}(\boldsymbol{\theta})$, whose elements are given [138], by

$$[\boldsymbol{J}(\boldsymbol{\theta})]_{i,j} = \mathbb{E}\left\{\frac{\partial^2 \ln f(\boldsymbol{c};\boldsymbol{\theta})}{\partial\theta_i\,\partial\theta_j}\right\}. \tag{4.12}$$

A CRB for the signal reconstruction from LR samples was discussed in [86]. Here a CRB in closed form expression for SPE from LR samples is presented and discussed. This is given in a general form by Theorem 1. To bring some analytical insight on the SPE performance variation with system parameters, the CRB for TDE and AE in a particular setting, given in Theorem 2, is developed.

Theorem 1. Let $x_R(t)$ be a semi-periodic stream of short-length pulses of form (4.3), received by a sensor in the presence of complex valued AWGN noise $\eta(t)$. The observation interval is limited to N intervals of length T. The power of the noise passing through an ideal low pass filter with cut-off frequency $1/2T$ is σ_η^2. Let $\boldsymbol{c}(e^{j\omega T})$ be the DTFT domain samples of $x_R(t)$ obtained according to the sampling scheme illustrated in Figure 4.2 and described by (4.8). Let $\boldsymbol{\theta}$ be a deterministic unknown vector that parameterizes the signal $x_R(t)$ and its samples $\boldsymbol{c}(e^{j\omega T})$. Then, the FIM for estimating $\boldsymbol{\theta}$ from $\boldsymbol{c}(e^{j\omega T})$ is given for large N by

$$\boldsymbol{J}(\boldsymbol{\theta}) = \frac{T}{\pi} \int_{-\pi/T}^{\pi/T} \mathrm{Re}\left\{\boldsymbol{\Gamma}^{\mathrm{H}}(e^{j\omega T})\boldsymbol{K}_\varepsilon^{-1}(e^{j\omega T})\boldsymbol{\Gamma}(e^{j\omega T})\right\}\mathrm{d}\omega, \tag{4.13}$$

where $\boldsymbol{\Gamma}(e^{j\omega T})$ is a matrix with lines i defined as $\partial \boldsymbol{c}(e^{j\omega T})/\partial\theta_i$ and $\boldsymbol{K}_\varepsilon(e^{j\omega T}) = \boldsymbol{S}^{\mathrm{H}}(e^{j\omega T})\boldsymbol{K}_\eta(e^{j\omega T})\boldsymbol{S}(e^{j\omega T})$. The elements p-q of matrix $\boldsymbol{S}(e^{j\omega T})$ are determined by the sampling filters $S_p(\omega + \omega_q)$ and $\boldsymbol{K}_\eta(e^{j\omega T})$ is the noise covariance matrix $\sigma_\eta^2 \mathbb{I}_P$, with $\mathbb{I}_P$ denoting the $P \times P$ identity matrix.

Proof: See Appendix B for the proof.

Corollary 1. In the signal model (4.8), $\boldsymbol{\varepsilon}(e^{j\omega T})$ refers to the continuous-time transmission noise $\eta(t)$, filtered by the sampling filters $s_p^*(-t)$. Usually the noise term $\boldsymbol{\varepsilon}(e^{j\omega T})$ has to account also for the discrete-time quantization noise that appears during the sampling process. If this is the case, then $\boldsymbol{K}_\varepsilon(e^{j\omega T})$ becomes $\boldsymbol{S}^{\mathrm{H}}(e^{j\omega T})\boldsymbol{K}_\eta(e^{j\omega T})\boldsymbol{S}(e^{j\omega T}) + \boldsymbol{K}_d(e^{j\omega T})$, where $\boldsymbol{K}_d(e^{j\omega T})$ is the covariance matrix of the discrete-time sampling noise. However, the sampling noise can be in general

mitigated by increasing the gain of the sampling filters, resulting in a signal-to-sampling-noise-ratio improvement. Thus, the transmission noise is of more interest for the SPE performance analysis.

Corollary 2. Under the settings of Theorem 1, let the amplitudes sequence be of form $a_k[n] = \alpha_k x[n]$, where $\{x[n]\}$ is an arbitrary known sequence. The vector of unknown parameters of the received signal is then $\boldsymbol{\theta} = [\tau_1, \dots, \tau_K, \alpha_1^{\mathrm{R}}, \dots, \alpha_K^{\mathrm{R}}, \alpha_1^{\mathrm{I}}, \dots, \alpha_K^{\mathrm{I}}]^{\mathrm{T}}$, where $\alpha_i^{\mathrm{R}} = \mathrm{Re}\{\alpha_i\}$ is the real part of α_i and α_i^{I} is the imaginary part of α_i. With this, a compact form expression can be written for matrix $\boldsymbol{\Gamma}\left(e^{j\omega T}\right)$, which is of size $P \times 3K$, i.e., $\boldsymbol{\Gamma}\left(e^{j\omega T}\right) = \left[\boldsymbol{\Gamma}_{\tau}\left(e^{j\omega T}\right)\ \boldsymbol{\Gamma}_{\alpha^{\mathrm{R}}}\left(e^{j\omega T}\right)\ j\boldsymbol{\Gamma}_{\alpha^{\mathrm{R}}}\left(e^{j\omega T}\right)\right]$, where

$$\boldsymbol{\Gamma}_{\tau}\left(e^{j\omega T}\right) = x\left(e^{j\omega T}\right)\left[\boldsymbol{W}_{\omega}\left(e^{j\omega T}\right) \odot \boldsymbol{W}\left(e^{j\omega T}\right)\right]\boldsymbol{N}(\boldsymbol{\tau})\boldsymbol{D}\left(e^{j\omega T}, \boldsymbol{\tau}\right)\boldsymbol{D}_{\alpha},$$

$$\boldsymbol{\Gamma}_{\alpha^{\mathrm{R}}}\left(e^{j\omega T}\right) = x\left(e^{j\omega T}\right)\boldsymbol{W}\left(e^{j\omega T}\right)\boldsymbol{N}(\boldsymbol{\tau})\boldsymbol{D}\left(e^{j\omega T}, \boldsymbol{\tau}\right), \tag{4.14}$$

where $\odot$ denotes the element wise product of two matrices, $\boldsymbol{D}_{\alpha} = \mathrm{diag}\{\alpha_1, \dots, \alpha_K\}$ and the elements of the $P \times P$ matrix $\boldsymbol{W}_{\omega}$ are $[\boldsymbol{W}_{\omega}]_{pq} = -j\left(\omega + \omega_q\right)$. Note that $x\left(e^{j\omega T}\right)$ is a scalar.

Proof: The proof of (4.14) is straightforward by taking the derivatives of $\boldsymbol{c}\left(e^{j\omega T}\right)$ as expressed by (4.8), with respect to τ_i, α_i^{R}, and α_i^{I}, respectively, and then grouping them to get a matrix form expression.

Discussion. A generic expression of the FIM for estimating $\boldsymbol{\theta}$ was also given in [86]. While similar to (4.13), the latter is expressed in the frequency domain which is advantageous for taking it further and particularize it for certain sampling filters, e.g., of form (4.11). Closed form expressions of the FIM for different parameters estimation were

also presented in other works, e.g., in [20, 27, 39, 139-141]. However, those considered a different signal model, not dealing with LR sampled signals. By using (4.14) in the general expression (4.13), the FIM for SPE can be numerically computed for any choice of the sampling filters $S_p(\omega)$, any pulse shape $g(t)$, any known sequence $\{x[n]\}$, and any noise model with known covariance matrix $\boldsymbol{K}_\varepsilon\left(e^{j\omega T}\right)$. An expression similar to (4.14) can be easily determined for the case of unknown sequence $\{x[n]\}$. However, the aim is to get more analytical insight on the influence of the system parameters on the SPE performance. For this the is focus on a specific setting.

Theorem 2. Let $\boldsymbol{c}\left(e^{j\omega T}\right)$ be the samples taken in the context of Theorem 1 from a signal $x_R(t)$ of form (4.3). Furthermore, let a particular setting be defined by the following assumptions. Let the pulse shape $g(t)$ be ideal, in the sense that $G(\omega) = 1$ for $\omega \in \left[-2\pi\mathcal{B}_g,\ 2\pi\mathcal{B}_g\right]$ and $G(\omega) = 0$ everywhere else. Let the amplitudes be of form $a_k[n] = \alpha_k x[n]$, where $\{x[n]\}$ is an arbitrary known sequence. Let $\Phi_x(\omega) = \left|x\left(e^{j\omega T}\right)\right|^2$, where $x\left(e^{j\omega T}\right)$ is the DTFT of the sequence $\{x[n]\}$, and let us assume $\Phi_x(\omega)$ is constant within the frequency range of interest. Furthermore, for a long bipolar sequence $\{x[n]\}_{n=1}^{N}$, where the $+1$ and -1 symbols are equiprobable, $\Phi_x = N$, [142]. Let the propagation environment be multipath free, i.e., $K = 1$. Then, with the choice (4.11) of sampling filters, the CRBs for TDE and AE from samples $\boldsymbol{c}\left(e^{j\omega T}\right)$ are:

$$\mathrm{CRB}(\tau_1) = \frac{3}{2\pi^2}\frac{\sigma_\eta^2}{\Phi_x|\alpha_1|^2}\frac{T^2}{P^3}, \tag{4.15}$$

$$\mathrm{CRB}(\alpha_1) = \frac{\sigma_\eta^2}{\Phi_x}\frac{1}{P}. \tag{4.16}$$

Proof: See Appendix B for the proof.

Discussion. The CRB expression (4.15) shows that the performance of TDE improves with the signal to noise ratio (SNR), i.e., it improves as the signal power or the observation interval increases and it decreases with higher noise power. The same observation stands for the CRB expression (4.16) for AE. The best TDE MSE is relative to the repetition interval T, i.e., the MSE of estimating τ_1/T is constant with T. Finally, the CRB on TDE improves with the cube of the number of sampling filters, i.e., it varies with P^{-3}. This means that increasing the number of sampling filters quickly improves the performance of TDE. By contrast, the CRB on AE improves only with P^{-1}.

Relation to DOA estimation. The CRB expressions (4.15) and (4.16) can be further validated by comparison with other CRB expressions existing in the literature for other systems. For instance, the bound developed in [39] for estimating the angle of arrival of a plane waveform impinging on a linear uniform narrow-band array of P sensors is $6/P^3N$ SNR. This is very similar to (4.15) with the observation that SNR is equivalent to $1/\sigma_\eta^2$ while the number of symbols N is embedded into Φ_x. A $(T/2\pi)^2$ factor accounts for the angle-to-time transformation. Obtaining similar performance on parameter estimation with the two systems makes sense since they have strong similarities. As such, in [39] the signal is received by P sensors, each of them takes samples at a rate $1/T$, and then all the samples are jointly processed for signal's parameter estimation. On the other side, expression (4.15) is for the case when the signal received at one sensor is filtered by P filters each followed by sampling at a rate $1/T$. The samples are then also jointly processed. However, the difference is that in the first case the signal is a conventional stream of modulated pulses of bandwidth $1/T$ with a

symbol interval T, while for the later case, the signal is a train of short pulses, e.g., of bandwidth $\mathcal{B}_g \ll T$, separated by an interval equal to T. The gain T of the sampling filters (4.11) does not affect the comparison since it affects both the noise and signal the same way.

Relation to LR sampling of a stream of Diracs. In [83] a T-periodic stream of Diracs is sampled at low rates by using a single Dirichlet sampling filter of total bandwidth $\mathcal{B}_s$ (equivalent to a sinc filter for large $T\mathcal{B}_s$). The gain of the filter is $1/T\mathcal{B}_s$ for frequencies inside the bandwidth and 0 outside. For this system, a CRB expression for TDE is given in [83]. Scaling the noise variance in [83] by $1/(T\mathcal{B}_s)^2$ to match the signal model where the noise was generated before the sampling filter, their CRB expression becomes $(3/\pi^2)(\sigma^2/T\mathcal{B}_s)(T^2/T\mathcal{B}_s(T^2\mathcal{B}_s^2-1))$. Compared to (4.15), firstly the $1/2$ factor is missing because the received signal is real in [83] versus complex in this case, [138]. Then $\sigma^2/T\mathcal{B}_s = \sigma_\eta^2$ because the ratio between the bandwidths of the filters filtering the noise in the two cases is $T\mathcal{B}_s$. Finally, for $T\mathcal{B}_s \gg 1$, $T^2/T\mathcal{B}_s(T^2\mathcal{B}_s^2-1) \cong T^2/T^3\mathcal{B}_s^3$. The Φ_x term is missing in [83] because the observation interval is restricted to $[0,T)$, rather than $[0,NT)$, and thus $\Phi_x = 1$. With these, for $P = T\mathcal{B}_s$ the CRB expression presented in [83] is equivalent to (4.15). With the same observations as for TDE, it can be shown that CRB expression on AE given in [83] is $\sigma_\eta^2/T\mathcal{B}_s$, where the amplitudes are real valued. Thus, it is equivalent to (4.16) for $P = T\mathcal{B}_s$.

Relation to sampling at Nyquist rate. The signal model in [83] is similar to (4.3) by considering instead of the stream of Diracs in [83] a stream of pulses $g(t)$ of same bandwidth with the Dirichlet filter. However, the sampling scheme from [83] applied to

this modified signal model would not be low rate anymore, but Nyquist rate equivalent. The two sampling schemes differ in the sense that in [83] a single sampling filter is used and the sampling rate is $\mathcal{B}_s$, whereas herein P sampling filters are used, each followed by a sampling operation at rate $1/T$. The advantage of the sampling scheme with multiple sampling filters is that it can perform sampling of the signals at rates lower than $\mathcal{B}_s$, i.e., using a number of sampling filters $P < T\mathcal{B}_s$. However, our result shows that its performance is lower than in the Nyquist equivalent rate case, unless $P = T\mathcal{B}_s$, as shown later in Figure 4.5 and Figure 4.6.

Periodic vs. semi-periodic stream of pulses. The CRB expressions (4.15) and (4.16) were determined for the signal model described by Equation (4.3), with $a_k[n] = \alpha_k x[n]$, where $\{x[n]\}$ is an arbitrary known sequence and $\Phi_x(\omega)$ is constant across the frequency. At limit, $x[n]$ can be the all-ones sequence and thus the signal model (4.3) reduces to that of a periodic stream of pulses, as described by (4.2). For this case, it can be easily shown that Φ_x is N in (4.15) and (4.16). Thus, the SPE performance shows explicit dependence on the number of repetition intervals, improving with N^{-1}.

It is of interest to compare the SPE performance for LR sampling of the periodic stream versus the semi-periodic one, (4.3), where the unknown parameters to be estimated are the time delays $\{\tau_k\}$ and amplitudes $\{a_k[n]\}$ (both the $\{\tau_k\}$ and $\{x[n]\}$ are unknown and cannot be separated). One may find a direct comparison between the periodic and semi-periodic streams unfair because the number of degrees of freedom and thus the ROI is different. That is, while the periodic stream has K time delays and K amplitudes to be estimated, for the semi-periodic stream there are K time delays and NK amplitudes to be determined (where the observed time was limited to NT). In [86], to

make the comparison fair from this consideration, an effort was made to equalize the ROI for the two cases, before comparing the signal recovery performance. To this end, while the overall unknown parameter number was the same, the semi-periodic signal was described by less time delays and more amplitudes than the periodic signal. The finding was a lower bound on signal recovery from LR samples in the case of the semi-periodic signal, outlying the idea that estimating the time delays is more challenging than estimating amplitudes.

For the SPE, comparing a periodic stream with a semi-periodic one for the same number of time delays, same length and repetition interval T, although they have different ROI is preferred, because the interest is in the performance of estimating individual parameters, rather than recovering the signal. For simplicity of expressions, the two cases for $K = 1$ are compared. Repeating the steps in Appendix C, for the semi-periodic signal with unknown $= \left[\tau_1, a_1^{\mathrm{R}}[m], \dots, a_1^{\mathrm{R}}[m], a_1^{\mathrm{I}}[m], \dots, a_1^{\mathrm{I}}[m]\right]^{\mathrm{T}}$, the CRB can be determined as

$$\mathrm{CRB}(\tau_1) = \frac{3}{2\pi^2}\frac{\sigma_\eta^2}{N|\alpha_1|^2}\frac{T^2}{P^3}, \tag{4.17}$$

$$\mathrm{CRB}(a_1[n]) = \sigma_\eta^2\frac{1}{P}, \forall\, n \in \mathbb{Z}. \tag{4.18}$$

By comparing (4.17) with (4.15) and (4.18) with (4.16), one may note that the performance bound on TDE is the same (with $\Phi_x = N$), while the bound on estimating one amplitude in the periodic case is N times lower than estimating one amplitude in the semi-periodic case. Thus, for TDE it does not matter if the signal is periodic or semi-

periodic, while for AE, the periodic one would be preferred. The result is in accordance with the explanation from [86] that TDE is equivalent to identifying a subspace and AE to determining a point within the subspace. Identifying the subspace is equally difficult for the two signals since it is determined by the same number of time delays. Determining a point within the subspace is more difficult in the semi-periodic case since the point is determined by N times more amplitudes than in the periodic case.

4.5 Numerical Results

Behavior with SNR. In general, the CRB for SPE can be numerically evaluated based on the expression (4.13) for the FIM matrix. For the multipath free case and with the simplifying assumptions of Theorem 2, the CRB for SPE can be evaluated based on (4.15) and (4.16). For this case, the linear variation of TDE accuracy expressed by the MSE with the SNR, defined as $1/\sigma_\eta^2$ can be observed in Figure 4.3 for $N = 100$ symbols, $P = 10$ sampling channels, $\Phi_x = N$, $\alpha_1 = 1$, and $T = 10\mu s$. It may also be noticed that for high SNR, the MSE obtained by averaging over 1000 runs asymptotically approaches the CRB confirming that the CRB as given by (4.15) is a tight lower bound for the TDE case considered. At low SNR, the TDE experiences a threshold effect, i.e., the simulated MSE departs from the linearity of CRB.

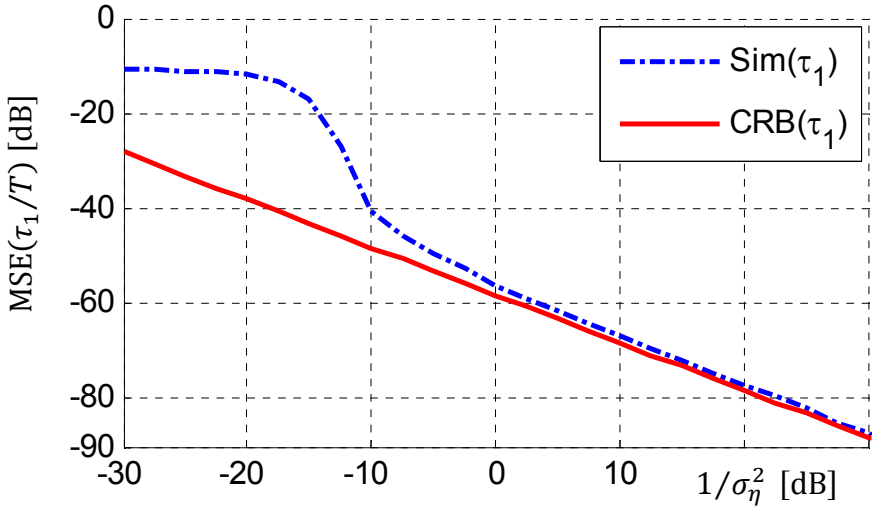

Figure 4.3 Accuracy of TDE from noisy LR samples.

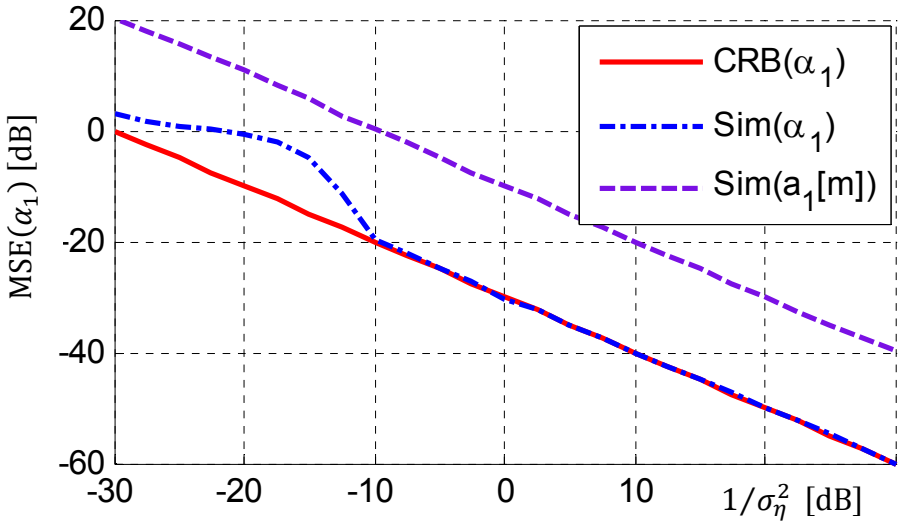

Figure 4.4 Accuracy of AE from noisy LR samples.

This is because, as the SNR decreases, the estimation enters a so called "large-errors" region, where the time delay estimates are subject to ambiguities resulting from the oscillatory nature of the signal sample correlation, [74]. For the given TDE problem the time delay values are however bounded by T and thus a plateau region occurs at very low

SNR. The CRB is a local or "small-errors" bound in the sense that it cannot predict this estimation behavior at low SNR and is realizable only at high SNR. For low SNR there are other bounds that are realizable, such as Weiss-Weinstein, [75], or Ziv-Zakai, [67, 77].

The linear variation of AE accuracy expressed by the MSE with the SNR can be observed in Figure 4.4 for the same setup as for TDE. Both the periodic and semi-periodic cases are represented. It can be observed that $\mathrm{CRB}(\alpha_1)$ is N times (the periodic case) lower than $\mathrm{CRB}(a_1[n])$ (the semi-periodic case). From the simulated MSE it can also be observed that the threshold effect characteristic to TDE appears in the AE only in the periodic case. For the semi-periodic signal, the AE errors are already too high to reflect the threshold effect manifested in TDE. In other words, an erroneous choice of the subspace does not introduce AE errors higher than those made when the subspace would be exactly chosen.

Number of sampling filters. Based on (4.15) and (4.16), the performance of TDE improves with P^{-3} when P varies from $2K$ to $2TB_g$, while the AE performance improves only with P^{-1}. When $P = 2TB_g$, the estimation performance of the multiple sampling filters scheme equals the one of the single filter scheme described in [83] sampling the signal model (4.3) at a Nyquist equivalent rate, i.e., taking the same number of samples as with a conventional Nyquist sampling scheme. This can be observed in Figure 4.5, and Figure 4.6, where for LR sampling the simulated MSE and CRB are plotted against the number of sampling filters P. The CRB for Nyquist equivalent rate is marked for $TB_g = 10$, being the same as the CRB for LR sampling with $P = 20$.

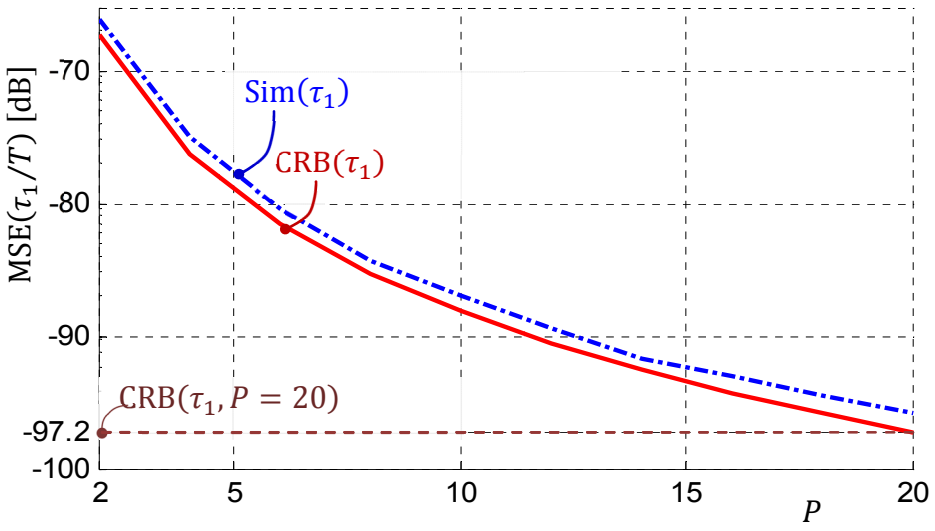

Figure 4.5 TDE accuracy with number of sampling filters.

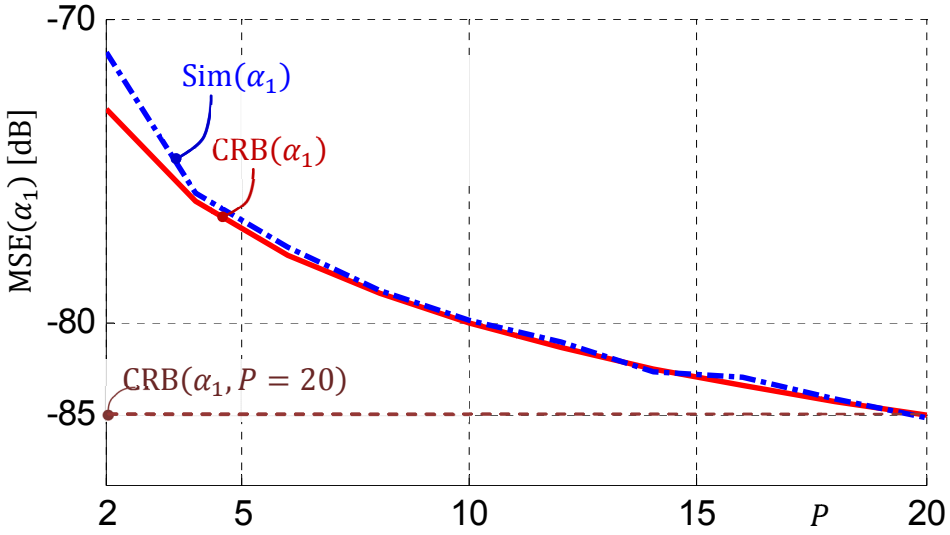

Figure 4.6 AE accuracy with number of sampling filters.

Inter-path separation. The case of $K = 2$ allows an analysis of the SPE performance dependence on the separation between paths. This can be performed numerically by employing the expression (4.13) or by developing a closed form expression as is in Appendix C (C.22)-(C.24) for TDE.

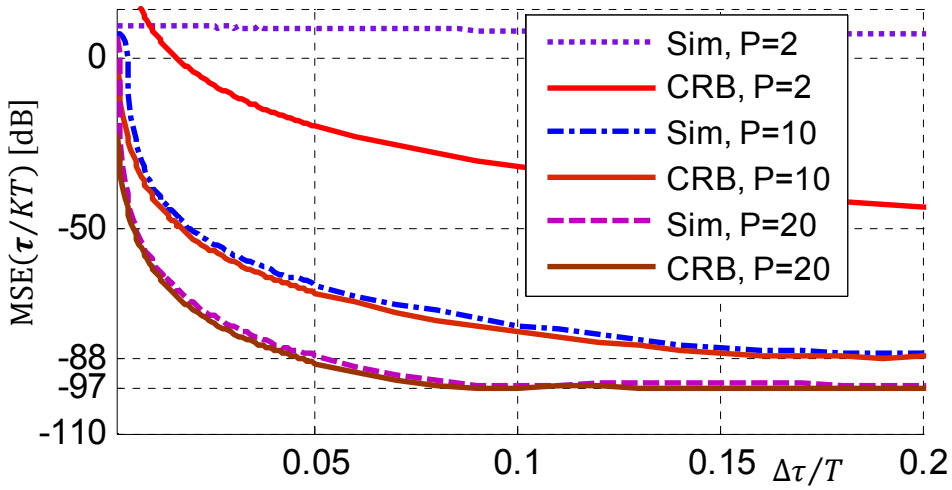

Figure 4.7 TDE accuracy with inter-path separation.

Compared to the multipath free case, the estimation is penalized by two categories of cross-terms: one describing the $\boldsymbol{\tau}$-$\boldsymbol{\alpha}$ interactions and a second one describing the τ_1-τ_2 interaction. The later is expressed essentially a term (ρ_τ in (C.22)) which shows the explicit dependence of the performance penalty with the paths separation $\Delta\tau_{12}$. Thus, as the separation increases, i.e., $\Delta\tau_{12} \to \infty$, $\rho_\tau \to 0$ and the penalty terms can be neglected. However, the argument of the trigonometric functions defining ρ_τ (C.12) depends not only on $\Delta\tau_{12}$, but also on P. Thus, the rate at which the penalty terms tend to vanish when increasing the inter-path separation depends on the number of sampling filters, i.e., the greater P is, the faster the rate is. This behavior can be observed in Figure 4.7, where simulated MSE and CRB are plotted for $P = 10$ and $P = 20$, varying $\Delta\tau_{12}$.

At the other extreme, when the inter-path separation is very small, i.e., $\Delta\tau_{12} \to 0$, the two paths are inseparable and thus a system model with $K = 1$ would be better than the model with $K = 2$ considered. Due to this inaccurate modeling, both the CRB and the employed ESPRIT estimation technique indicate very high error rates. For $\Delta\tau_{12} \to 0$, $\rho_\tau \to \beta^2/3$ which for $\alpha_2 = 1$ leads to a rank 1 non-invertible matrix $\boldsymbol{J}_\tau(\boldsymbol{\theta})$. In practice,

for $\Delta\tau_{12}$ lower than a certain threshold the model should be modified from $K = 2$ to $K = 1$ and with this the performance would attain (4.15) as $\Delta\tau_{12} \to 0$, rather than increasing to arbitrary high values. A similar analysis can be carried out for AE, with similar conclusions. In [136] a radar system based on LR samples is presented and the resolution reported for target localization (which is based on TDE) is better than when using traditional match-filtering techniques with Nyquist sampling. By contrast, the results in Figure 4.7 show that sampling at lower rates, i.e., with small P, effects in resolution loss. Thus, the best resolution that can be attained is for Nyquist equivalent sampling, i.e., $P = 2TB_g$. However, it is known that the match-filtering techniques have resolution capabilities limited by the bandwidth of the pulse, [88]. Thus, the good results reported in [136] are motivated by the use of a super-resolution technique, rather than by the use of a LR sampling scheme.

Too low sampling rate. It has been shown in [84] that perfect signal recovery is possible even when sampling at rates lower than $2K/T$. Specifically, if the received signal is uncorrelated from one repetition interval T to another, then super-resolution estimation techniques can be applied directly and the minimum sampling rate needed is $(K + 1)/T$. This is similar to the findings in source localization, where the maximum number of sources that can be uniquely localized is at best equal to the number of receiving sensors, [143, 144]. For received signals with high correlation, smoothing techniques, are required, [145, 146], and at least $2K$ samples are needed every T, [84]. Thus, with LR sampling at a rate P/T, with $P < K + 1$, unique parameter identification is not possible from the samples, irrespective to the correlation of the signal. This is shown for $K = 2$ and $P = 2$ in Figure 4.7 where the simulated MSE for TDE has very

high values (limited only by T as the maximum possible value for time delays). Note that the CRB does not accurately reflect this effect because the CRB assumes there exists a unique solution to the estimation problem, which is not the case for $P < K + 1$.

4.6 Concluding Remarks

In this section, the performance of SPE from LR samples of FRI signals has been addressed. In particular, a CRB expression for the case of using multiple parallel sampling filters was developed. With some simplifying assumptions, closed form expressions were determined for one and two multipath signal components. The estimation performance was shown to significantly deteriorate in noise, unless the number of sampling filters is increased from the one indicated by the rate of innovation to moderate this deterioration. However, depending on the performance requirements, an acceptable performance may be attained by a small increase in the number of sampling filters. The inter-component separation was also found to impact the estimation performance, but weighted by the number of sampling filters.

CHAPTER 5

CONCLUSIONS

This dissertation has addressed the topic of passive source localization in plane of wireless non-cooperative sources. To this end, localization methods based on TDOA estimates have been studied.

A two-stage localization has been discussed in Chapter 2. With the first stage, the TDOA at pairs of sensors are estimated, while during the second stage, the actual source location is estimated based on the TDOA values previously determined. Accurate TDOA estimation is especially challenging in multipath propagation environments, where resolving the multipath components is needed. A new method exploring the sparse structure of the channel was introduced. Simulation results have showed higher resolution capabilities compared to conventional existing methods.

With the second stage, three new methods have been proposed for hyperbolic localization, i.e., for estimating the source location based on TDOA measurements. The first method is based on an SDR approach, the second method, MXTM, seeks a biased estimate through a linearized formulation of the localization problem, and the third method formulates the localization problem as an ℓ_1-regularization, by exploiting the sparsity of the source location. The proposed methods compare favorably with other existing methods, each of them having its own advantages. The SDR method has the advantage of simplicity and low computational cost. The MXTM may perform better than the SDR approach in some situations, but at the price of higher computational cost. The ℓ_1-regularization may outperform the first two methods, but is sensitive to the choice of the regularization parameter.

In Chapter 3, the source localization has followed a direct approach. That is, rather than intermediately estimating the TDOAs, a localization metric that implicitly includes the TDOAs has been constructed. Specifically, a ML approach was taken to derive such a localization metric. The approach is coherent in the sense that beside the time delays, the phase of the received signal is also considered. For performance benchmarking, a *CRB expression* has been also developed. A coherence gain due to inclusion of the carrier phase in the metric and a spatial gain due to proper sensors placement over the surveillance field, have been demonstrated. A cause of potential accuracy deterioration, especially at low SNR, has been identified in the false peaks popping up in the localization metric anywhere within the surveillance area. These high sidelobes far away from the actual source location are particularly encountered with the coherent processing. One solution to lower the level of the sidelobes is to increase the number of receiving sensors or to employ at each sensor a small multi-antenna array.

Chapter 4 departs from the localization approaches in the previous chapters in the sense that rather than using signals sampled at or above the Nyquist rate, a technique for time delay estimation from samples taken at lower rates has been explored. Specifically, it was shown in [84] and [86] that for FRI signals, the original signal can be perfectly recovered from LR samples while in the presence of noise, the signal recovery may deteriorate more than it would deteriorate if the samples would be taken at the Nyquist rate. In Chapter 4 it has been shown that also the performance of time delay and amplitude individual estimation from LR samples deteriorates in noise significantly more compared to the estimation from samples taken at the Nyquist rate. However, depending on the performance requirements, an acceptable performance level may be attained by a

small increase in the sampling rate, especially for TDE. That is because according to the CRB expression developed, with TDE, the estimation accuracy varies exponentially with the number of samples per time interval. For multipath environments, the inter-component separation has been also found to impact the estimation performance, but weighted by the sampling rate.

This dissertation aimed at filling some gaps in the source localization field. However, naturally, with the new methods proposed also more questions have arisen that can be subject of future research. In Chapter 2, exploiting the channel and source space sparsity has been shown to have high resolution potential. However, one drawback, characteristic to sparse techniques is lack of good methods for automated choice of some parameters such as the regularization parameter. Another topic of future research is the accuracy and resolution limits of sparse methods relative to the choice of the grid points involved in solving a sparse problem.

Chapter 3 has been proved the high accuracy capabilities of the coherent processing approach. However, this approach has to contend with the high sidelobes popping up in the localization metric anywhere within the surveillance area. Moreover, the technique is very sensitive to synchronization errors. Thus calibration techniques are necessary for accurate coherent localization.

Sampling at LR is a promising approach to lower the communication and potentially computational burden of the localization methods. The performance of other LR sampling schemes than that discussed in Chapter 4 and their application to other classes of signals is another possible avenue of future research.

APPENDIX A

DERIVATION OF THE FIM ELEMENTS FOR COHERENT LOCALIZATION

The sub-matrices $\boldsymbol{J}_{\tau\tau}(\boldsymbol{\theta})$, $\boldsymbol{J}_{S_0\tau}(\boldsymbol{\theta})$ and $\boldsymbol{J}_{S_0S_0}(\boldsymbol{\theta})$ needed to determine the FIM matrix (3.14) are calculated in the followings.

A.1. Calculation of $\left[\boldsymbol{J}_{\tau\tau}(\boldsymbol{\theta})\right]_{MxM}$

Using the general form (3.16) for $\left[\boldsymbol{J}(\omega,\boldsymbol{\theta})\right]_{i,j}$, the elements of $\boldsymbol{J}_{\tau\tau}(\omega,\boldsymbol{\theta})$ can be written

$$\left[\boldsymbol{J}_{\tau\tau}(\omega,\boldsymbol{\theta})\right]_{i,j}=\begin{cases}2\,\mathrm{Re}\left\{\dfrac{1}{\sigma_i^2}\dfrac{\partial S_{Ri}^*}{\partial\tau_i}(\omega,\boldsymbol{\theta})\dfrac{\partial S_{Ri}}{\partial\tau_i}(\omega,\boldsymbol{\theta})\right\}, & \text{for } j=i\\ 0, & \text{for } j\neq i.\end{cases} \tag{A.1}$$

Employing equation (3.1) in (A.1), the non-diagonal elements of $\boldsymbol{J}_{\tau\tau}(\boldsymbol{\theta})$ result all zero, while the diagonal elements are calculated in the sequel:

$$\begin{aligned}\left[\boldsymbol{J}_{\tau\tau}(\omega,\boldsymbol{\theta})\right]_{k,k}&=\frac{1}{2\pi}\int_{-\pi}^{\pi}\left[\boldsymbol{J}_{\tau\tau}(\omega,\boldsymbol{\theta})\right]_{k,k}d\omega=\\&=\frac{1}{\sigma_k^2}2\,\mathrm{Re}\left\{\frac{1}{2\pi}\int_{-\pi}^{\pi}\frac{\partial S_{Rk}^*}{\partial\tau_k}(\omega,\boldsymbol{\theta})\frac{\partial S_{Rk}}{\partial\tau_k}(\omega,\boldsymbol{\theta})d\omega\right\}=\\&=\frac{1}{\sigma_k^2}2\,\mathrm{Re}\left\{\frac{1}{2\pi}\int_{-\pi}^{\pi}(\omega+\omega_c)^2\left|S_0(\omega)\right|^2 g_k^2\,d\omega\right\}=\\&=8\pi^2\frac{g_k^2}{\sigma_k^2}\left[\int_{-\infty}^{\infty}f^2\left|S_0(f)\right|^2 df+f_c^2\int_{-\infty}^{\infty}\left|S_0(f)\right|^2 df\right]=\\&=8\pi^2 f_c^2\left(1+\frac{\beta_0^2}{f_c^2}\right)\int_{-\infty}^{\infty}\left|S_0(f)\right|^2 df\,\frac{g_k^2}{\sigma_k^2}=\\&=8\pi^2 f_c^2\beta_{f_c}\mathcal{P}_{S_0}SNR_k\ .\end{aligned} \tag{A.2}$$

Note that $\int_{-\pi}^{\pi}\omega\left|S_0(\omega)\right|^2 d\omega=0$ since the quantity under the integral is an odd function.

A.2. Calculation of $\left[\boldsymbol{J}_{S_0S_0}(\boldsymbol{\theta})\right]_{2N_F \text{x} 2N_F}$

The sub-matrix $\boldsymbol{J}_{S_0S_0}(\boldsymbol{\theta})$ at its own is composed by four sub-matrices:

$$\boldsymbol{J}_{S_0S_0}(\boldsymbol{\theta}) = \left[\begin{array}{c|c} \left[\boldsymbol{J}^{RR}_{S_0S_0}(\boldsymbol{\theta})\right]_{N_F \text{x} N_F} & \left[\boldsymbol{J}^{RI}_{S_0S_0}(\boldsymbol{\theta})\right]_{N_F \text{x} N_F} \\ \hline \left[\boldsymbol{J}^{IR}_{S_0S_0}(\boldsymbol{\theta})\right]_{N_F \text{x} N_F} & \left[\boldsymbol{J}^{II}_{S_0S_0}(\boldsymbol{\theta})\right]_{N_F \text{x} N_F} \end{array}\right]_{2N_F \text{x} 2N_F}. \tag{A.3}$$

Using the general form (3.16) for $\left[\boldsymbol{J}(\omega,\boldsymbol{\theta})\right]_{i,j}$, the elements of $\boldsymbol{J}^{RR}_{S_0S_0}(\omega,\boldsymbol{\theta})$ can be determined as

$$\left[\boldsymbol{J}^{RR}_{S_0S_0}(\omega,\boldsymbol{\theta})\right]_{i,j} = \begin{cases} 2\,\text{Re}\left\{\sum_{k=1}^{M} \frac{1}{\sigma_k^2} \frac{\partial S^*_{Rk}}{\partial S^R_{0i}}(\omega,\boldsymbol{\theta}) \frac{\partial S_{Rk}}{\partial S^R_{0i}}(\omega,\boldsymbol{\theta})\right\}, & \text{for } j = i \\ 0, & \text{for } j \neq i. \end{cases} \tag{A.4}$$

Employing equation (3.1) in (A.4), the non-diagonal elements of $\boldsymbol{J}^{RR}_{S_0S_0}(\boldsymbol{\theta})$ are all zero, while the diagonal elements are calculated in the sequel:

$$\begin{aligned} \left[\boldsymbol{J}^{RR}_{S_0S_0}(\omega,\boldsymbol{\theta})\right]_{n_f,n_f} &= \frac{1}{2\pi}\int_{-\pi}^{\pi} \left[\boldsymbol{J}^{RR}_{S_0S_0}(\omega,\boldsymbol{\theta})\right]_{n_f,n_f} d\omega = \\ &= 2\,\text{Re}\left\{\frac{1}{N_F}\sum_{k=1}^{M}\frac{1}{\sigma_k^2}\frac{\partial S^*_{Rk}}{\partial S^R_{0n_f}}\left(\omega_{n_f},\boldsymbol{\theta}\right)\frac{\partial S_{Rk}}{\partial S^R_{0n_f}}\left(\omega_{n_f},\boldsymbol{\theta}\right)\right\} = \\ &= 2\,\text{Re}\left\{\frac{1}{N_F}\sum_{k=1}^{M}\frac{1}{\sigma_k^2}g_k^2\right\} = \frac{2}{N_F}\sum_{k=1}^{M} SNR_k\,. \end{aligned} \tag{A.5}$$

Note that in (A.5) the integral $\frac{1}{2\pi}\int_{-\pi}^{\pi}(\cdot)d\omega$ was approximated with a sum for all frequency bins, and by derivation to $S^R_{0n_f}$ only the terms depending on the n_f-th frequency bin are non-zero.

Similarly to $\boldsymbol{J}^{RR}_{S_0S_0}(\boldsymbol{\theta})$, the non-diagonal terms of $\boldsymbol{J}^{II}_{S_0S_0}(\boldsymbol{\theta})$, $\boldsymbol{J}^{IR}_{S_0S_0}(\boldsymbol{\theta})$ and $\boldsymbol{J}^{RI}_{S_0S_0}(\boldsymbol{\theta})$ are all zeros, while the diagonal elements are calculated in the sequel.

$$\left[\boldsymbol{J}^{II}_{S_0S_0}(\omega,\boldsymbol{\theta})\right]_{n_f,n_f} = \frac{1}{2\pi}\int_{-\pi}^{\pi}\left[\boldsymbol{J}^{II}_{S_0S_0}(\omega,\boldsymbol{\theta})\right]_{n_f,n_f} d\omega =$$

$$= 2\,\mathrm{Re}\left\{\frac{1}{N_F}\sum_{k=1}^{M}\frac{1}{\sigma_k^2}\frac{\partial S^*_{Rk}}{\partial S^I_{0n_f}}\left(\omega_{n_f},\boldsymbol{\theta}\right)\frac{\partial S_{Rk}}{\partial S^I_{0n_f}}\left(\omega_{n_f},\boldsymbol{\theta}\right)\right\} = \tag{A.6}$$

$$= 2\,\mathrm{Re}\left\{\frac{1}{N_F}\sum_{k=1}^{M}\frac{1}{\sigma_k^2}(-j)^2\,g_k^2\right\} = \frac{2}{N_F}\sum_{k=1}^{M}SNR_k\,.$$

$$\left[\boldsymbol{J}^{IR}_{S_0S_0}(\omega,\boldsymbol{\theta})\right]_{n_f,n_f} = \frac{1}{2\pi}\int_{-\pi}^{\pi}\left[\boldsymbol{J}^{IR}_{S_0S_0}(\omega,\boldsymbol{\theta})\right]_{n_f,n_f} d\omega =$$

$$= 2\,\mathrm{Re}\left\{\frac{1}{N_F}\sum_{k=1}^{M}\frac{1}{\sigma_k^2}\frac{\partial S^*_{Rk}}{\partial S^I_{0n_f}}\left(\omega_{n_f},\boldsymbol{\theta}\right)\frac{\partial S_{Rk}}{\partial S^R_{0n_f}}\left(\omega_{n_f},\boldsymbol{\theta}\right)\right\} = \tag{A.7}$$

$$= 2\,\mathrm{Re}\left\{\frac{1}{N_F}\sum_{k=1}^{M}\frac{1}{\sigma_k^2}(-j)\,g_k^2\right\} = 0\,.$$

$$\left[\boldsymbol{J}^{RI}_{S_0S_0}(\omega,\boldsymbol{\theta})\right]_{n_f,n_f} = \frac{1}{2\pi}\int_{-\pi}^{\pi}\left[\boldsymbol{J}^{RI}_{S_0S_0}(\omega,\boldsymbol{\theta})\right]_{n_f,n_f} d\omega =$$

$$= 2\,\mathrm{Re}\left\{\frac{1}{N_F}\sum_{k=1}^{M}\frac{1}{\sigma_k^2}\frac{\partial S^*_{Rk}}{\partial S^R_{0n_f}}\left(\omega_{n_f},\boldsymbol{\theta}\right)\frac{\partial S_{Rk}}{\partial S^I_{0n_f}}\left(\omega_{n_f},\boldsymbol{\theta}\right)\right\} = \tag{A.8}$$

$$= 2\,\mathrm{Re}\left\{\frac{1}{N_F}\sum_{k=1}^{M}\frac{1}{\sigma_k^2}\,j\,g_k^2\right\} = 0\,.$$

From (A.4) and (A.5)-(A.8), it results that

$$\boldsymbol{J}_{S_0S_0}(\boldsymbol{\theta}) = \frac{2}{N_F}\sum_{k=1}^{M}SNR_k\;\boldsymbol{I}_{2N_F\mathrm{x}2N_F}\,. \tag{A.9}$$

A.3. Calculation of $\left[\boldsymbol{J}_{S_0\tau}(\boldsymbol{\theta})\right]_{2N_F\mathrm{x}M}$

The sub-matrix $\boldsymbol{J}_{S_0\tau}(\boldsymbol{\theta})$ at its own is composed by two sub-matrices:

$$\boldsymbol{J}_{S_0\tau}(\boldsymbol{\theta}) = \left[\begin{array}{c}\left[\boldsymbol{J}^{R}_{S_0\tau}(\boldsymbol{\theta})\right]_{N_F\mathrm{x}M}\\ \hdashline \left[\boldsymbol{J}^{I}_{S_0\tau}(\boldsymbol{\theta})\right]_{N_F\mathrm{x}M}\end{array}\right]_{2N_F\mathrm{x}M}\,. \tag{A.10}$$

Using the general form (3.16) for $\left[\boldsymbol{J}(\omega,\boldsymbol{\theta})\right]_{i,j}$, the elements of $\boldsymbol{J}^R_{S_0\tau}(\omega,\boldsymbol{\theta})$ can be determined as

$$\left[\boldsymbol{J}^R_{S_0\tau}(\omega,\boldsymbol{\theta})\right]_{i,j} = 2\,\mathrm{Re}\left\{\sum_{k=1}^{M}\frac{1}{\sigma_k^2}\frac{\partial S^*_{Rk}}{\partial S^R_{0i}}(\omega,\boldsymbol{\theta})\frac{\partial S_{Rk}}{\partial \tau_j}(\omega,\boldsymbol{\theta})\right\}. \tag{A.11}$$

Employing equation (3.1) in (A.11), the non-diagonal elements of $\boldsymbol{J}^R_{S_0\tau}(\boldsymbol{\theta})$ can be calculated as follows:

$$\begin{aligned}\left[\boldsymbol{J}^R_{S_0\tau}(\omega,\boldsymbol{\theta})\right]_{n_f,k} &= \frac{1}{2\pi}\int_{-\pi}^{\pi}\left[\boldsymbol{J}^R_{S_0\tau}(\omega,\boldsymbol{\theta})\right]_{n_f,k}d\omega = \\ &= 2\,\mathrm{Re}\left\{\frac{1}{N_F}\frac{1}{\sigma_k^2}\frac{\partial S^*_{Rk}}{\partial S^R_{0n_f}}\left(\omega_{n_f},\boldsymbol{\theta}\right)\frac{\partial S_{Rk}}{\partial \tau_j}\left(\omega_{n_f},\boldsymbol{\theta}\right)\right\} = \\ &= 2\,\mathrm{Re}\left\{\frac{1}{N_F}\frac{1}{\sigma_k^2}g_k\,e^{j\left(\omega_{n_f}+\omega_c\right)\tau_k}\left(-j\right)\left(\omega_{n_f}+\omega_c\right)g_k S_0\left(\omega_{n_f}\right)e^{-j\left(\omega_{n_f}+\omega_c\right)\tau_k}\right\} = \\ &= \frac{2}{N_F}\left(\omega_{n_f}+\omega_c\right)\mathrm{Im}\left\{S_0\left(\omega_{n_f}\right)\right\}SNR_k\,,\end{aligned} \tag{A.12}$$

where ω_{n_f} denotes the n_f-th angular frequency bin, $\omega_{n_f} = \dfrac{2\pi n_f F_s}{N_F}$, F_s being the sampling frequency and N_F the total number of frequency samples.

Similarly, the elements of $\boldsymbol{J}^I_{S_0\tau}(\boldsymbol{\theta})$ can be determined as

$$\begin{aligned}\left[\boldsymbol{J}^I_{S_0\tau}(\omega,\boldsymbol{\theta})\right]_{n_f,k} &= \frac{1}{2\pi}\int_{-\pi}^{\pi}\left[\boldsymbol{J}^I_{S_0\tau}(\omega,\boldsymbol{\theta})\right]_{n_f,k}d\omega = \\ &= 2\,\mathrm{Re}\left\{\frac{1}{N_F}\frac{1}{\sigma_k^2}\frac{\partial S^*_{Rk}}{\partial S^I_{0n_f}}\left(\omega_{n_f},\boldsymbol{\theta}\right)\frac{\partial S_{Rk}}{\partial \tau_j}\left(\omega_{n_f},\boldsymbol{\theta}\right)\right\} = \\ &= 2\,\mathrm{Re}\left\{\frac{1}{N_F}\frac{1}{\sigma_k^2}\left(-j\right)g_k\,e^{j\left(\omega_{n_f}+\omega_c\right)\tau_k}\left(-j\right)\left(\omega_{n_f}+\omega_c\right)g_k S_0\left(\omega_{n_f}\right)e^{-j\left(\omega_{n_f}+\omega_c\right)\tau_k}\right\} = \\ &= -\frac{2}{N_F}\left(\omega_{n_f}+\omega_c\right)\mathrm{Re}\left\{S_0\left(\omega_{n_f}\right)\right\}SNR_k\,.\end{aligned} \tag{A.13}$$

APPENDIX B

PROOF OF THEOREM 1

The proof of Theorem 1 starts from the definition (4.12) of the FIM and ends with a general expression for calculating the FIM for estimating $\boldsymbol{\theta}$ from samples $\boldsymbol{c}\left(e^{j\omega T}\right)$. Using the time samples domain version of the signal model (4.8),

$$\boldsymbol{c}[n] = \widetilde{\boldsymbol{\mu}}[n] + \boldsymbol{\varepsilon}[n], \tag{B.1}$$

where $\widetilde{\boldsymbol{\mu}}[n]$ is the inverse DTFT of $\boldsymbol{W}\left(e^{j\omega T}\right)\boldsymbol{\mu}\left(e^{j\omega T}\right)$, the pdf $f(\boldsymbol{c};\boldsymbol{\theta})$ used in (4.12) is given by

$$f(\boldsymbol{c};\boldsymbol{\theta}) = \frac{1}{\det\left(\pi \boldsymbol{K}_{\varepsilon_N}\right)} e^{-(\boldsymbol{c}_N - \widetilde{\boldsymbol{\mu}}_N)^{\mathrm{H}} \boldsymbol{K}_{\varepsilon_N}^{-1} (\boldsymbol{c}_N - \widetilde{\boldsymbol{\mu}}_N)}, \tag{B.2}$$

where $\boldsymbol{c}_N^{\mathrm{T}} = [\boldsymbol{c}^{\mathrm{T}}[1], \ldots, \boldsymbol{c}^{\mathrm{T}}[N]\,]$, $\widetilde{\boldsymbol{\mu}}_N^{\mathrm{T}} = [\widetilde{\boldsymbol{\mu}}^{\mathrm{T}}[1], \ldots, \widetilde{\boldsymbol{\mu}}^{\mathrm{T}}[N]\,]$, and the observation interval is limited to $[0, NT)$. The matrix $\boldsymbol{K}_{\varepsilon_N}$ denotes the $NP \times NP$ covariance matrix of the noise vector $\boldsymbol{\varepsilon}_N^{\mathrm{T}} = [\boldsymbol{\varepsilon}^{\mathrm{T}}[1], \ldots, \boldsymbol{\varepsilon}^{\mathrm{T}}[N]\,]$. With (B.2), equation (15.52) from [138] can be applied to reduce (4.12) to

$$[\boldsymbol{J}(\boldsymbol{\theta})]_{i,j} = 2\mathrm{Re}\left\{\frac{\partial \widetilde{\boldsymbol{\mu}}_N^{\mathrm{H}}}{\partial \theta_i} \boldsymbol{K}_{\varepsilon_N}^{-1} \frac{\partial \widetilde{\boldsymbol{\mu}}_N}{\partial \theta_j}\right\} + \mathrm{tr}\left\{\boldsymbol{K}_{\varepsilon_N}^{-1} \frac{\partial \boldsymbol{K}_{\varepsilon_N}}{\partial \theta_i} \boldsymbol{K}_{\varepsilon_N}^{-1} \frac{\partial \boldsymbol{K}_{\varepsilon_N}}{\partial \theta_j}\right\}, \tag{B.3}$$

where tr{·} denotes the trace of a matrix. However, the information in the considered case is in the mean of the received signal, not in its covariance. That is, the data signal $\boldsymbol{c}[n]$ is deterministic rather than bayesian, i.e., there is no prior information on its statistical distribution or otherwise the covariance matrix $\boldsymbol{K}_{\varepsilon_N}$ does not depend on parameter $\boldsymbol{\theta}$. For this case, [26, 28, 130],

$$[\boldsymbol{J}(\boldsymbol{\theta})]_{i,j} = 2\mathrm{Re}\left\{\frac{\partial \widetilde{\boldsymbol{\mu}}_N^{\mathrm{H}}}{\partial \theta_i}\boldsymbol{K}_{\varepsilon_N}^{-1}\frac{\partial \widetilde{\boldsymbol{\mu}}_N}{\partial \theta_j}\right\}. \tag{B.4}$$

The evaluation of (B.4) would be greatly simplified if matrix $\boldsymbol{K}_{\varepsilon_N}$is diagonal (or block diagonal). This can be achieved by replacing the data vector $\boldsymbol{c}_N$ by the vector of its Fourier coefficients (obtained by applying the DTFT to $\boldsymbol{c}_N$, when $N \to \infty$) since the Fourier coefficients are asymptotically uncorrelated, [25, 147]. With these, it was shown in [124] that (B.3) has for large N a simple expression in the discrete Fourier transform (DFT) domain, given by equation (B.2) from [124]. Considering its equivalent in the DTFT domain, (B.4) asymptotically becomes

$$[\boldsymbol{J}(\boldsymbol{\theta})]_{i,j} = \frac{T}{\pi}\int_{-\pi/T}^{\pi/T} \mathrm{Re}\left\{\frac{\partial(\boldsymbol{\mu}^{\mathrm{H}}\boldsymbol{W}^{\mathrm{H}})}{\partial \theta_i}\left(e^{j\omega T}\right)\boldsymbol{K}_{\varepsilon}^{-1}\left(e^{j\omega T}\right)\frac{\partial(\boldsymbol{W}\boldsymbol{\mu})}{\partial \theta_j}\left(e^{j\omega T}\right)\right\}\mathrm{d}\omega, \tag{B.5}$$

where $\boldsymbol{K}_{\varepsilon}\left(e^{j\omega T}\right)$ is a $P \times P$ matrix of elements $\left[K_{\varepsilon}\left(e^{j\omega T}\right)\right]_{p,q}$ given by the DTFT of the cross-correlation of sequences $\left[\varepsilon_p[1], \ldots, \varepsilon_p[N]\right]$ and $\left[\varepsilon_q[1], \ldots, \varepsilon_q[N]\right]$. For simplicity, given that the noise $\boldsymbol{\varepsilon}[n]$ does not depend on the parameter vector $\boldsymbol{\theta}$, equation (B.5) can be written as (4.13), concluding the proof of Theorem 1.

APPENDIX C

CRB DERIVATION FOR SPE FROM LR SAMPLES

While the general expression (4.13) can be used in conjunction with (4.14) to numerically evaluate the FIM and then the CRB, it is of interest to derive simple closed form FIM and CRB expressions for particular cases. Such a case is that defining the setup of Theorem 2. Within this context, in the followings the focus is on determining a CRB in closed form expression for each parameter θ_i, continuing from equation (B.5).

With the choice (4.11) of sampling filters, $\boldsymbol{K}_{\varepsilon}\left(e^{j\omega T}\right)$ becomes $\left(\sigma_{\eta}^2/T^2\right)\text{diag}\{|S_1(\omega+\omega_1)|^2, \ldots |S_P(\omega+\omega_P)|^2\}$. Furthermore, the choice of an ideal pulse shape $g(t)$, in the sense that $G(\omega)=1$ for $\omega \in \left[-\mathcal{B}_g,\ \mathcal{B}_g\right]$ and $G(\omega)=0$ everywhere else, determines matrix $\boldsymbol{W}\left(e^{j\omega T}\right)$ to become a $P \times P$ identity matrix. Thus, (B.5) is further simplified,

$$[\boldsymbol{J}(\boldsymbol{\theta})]_{i,j} = \frac{T}{\pi}\int_{-\pi/T}^{\pi/T}\sum_{p=1}^{P}\frac{1}{\sigma_{\eta}^2}\text{Re}\left\{\frac{\partial \mu_p^*}{\partial \theta_i}\left(e^{j\omega T}\right)\frac{\partial \mu_p}{\partial \theta_j}\left(e^{j\omega T}\right)\right\}\text{d}\omega. \tag{C.1}$$

To determine the elements of the FIM, $\boldsymbol{\theta} = [\tau_1, \ldots, \tau_K, \alpha_1^{\text{R}}, \ldots, \alpha_K^{\text{R}}, \alpha_1^{\text{I}}, \ldots, \alpha_K^{\text{I}}]^{\text{T}}$ and $\mu_p\left(e^{j\omega T}\right) = x\left(e^{j\omega T}\right)\sum_{k=1}^{K}\alpha_k e^{-j(\omega+\omega_p)\tau_k}$ are used. FIM is formed by sub-matrices,

$$\boldsymbol{J}(\boldsymbol{\theta}) = \left[\begin{array}{c|c} J_{\tau}(\boldsymbol{\theta}) & J_{\tau\alpha}(\boldsymbol{\theta}) \\ \hline J_{\tau\alpha}^{\text{H}}(\boldsymbol{\theta}) & J_{\alpha}(\boldsymbol{\theta}) \end{array}\right] = \left[\begin{array}{c|cc} J_{\tau}(\boldsymbol{\theta}) & J_{\tau\alpha^{\text{R}}}(\boldsymbol{\theta}) & J_{\tau\alpha^{\text{I}}}(\boldsymbol{\theta}) \\ \hline J_{\tau\alpha^{\text{R}}}^{\text{H}}(\boldsymbol{\theta}) & J_{\alpha^{\text{R}}}(\boldsymbol{\theta}) & J_{\alpha^{\text{R}}\alpha^{\text{I}}}(\boldsymbol{\theta}) \\ J_{\tau\alpha^{\text{I}}}^{\text{H}}(\boldsymbol{\theta}) & J_{\alpha^{\text{R}}\alpha^{\text{I}}}^{\text{H}}(\boldsymbol{\theta}) & J_{\alpha^{\text{I}}}(\boldsymbol{\theta}) \end{array}\right]. \tag{C.2}$$

The following relations will be used:

$$\frac{\partial \mu_p^*}{\partial \tau_i}\left(e^{j\omega T}\right) = j\left(\omega + \omega_p\right)x^*\left(e^{j\omega T}\right)e^{j(\omega+\omega_p)\tau_i}\alpha_i\,, \tag{C.3}$$

$$\frac{\partial \mu_p}{\partial \tau_j}\left(e^{j\omega T}\right) = -j\left(\omega + \omega_p\right)x\left(e^{j\omega T}\right)e^{-j(\omega+\omega_p)\tau_j}\alpha_j\,, \tag{C.4}$$

$$\frac{\partial \mu_p}{\partial \alpha_k^{\mathrm{R}}}\left(e^{j\omega T}\right) = x\left(e^{j\omega T}\right)e^{-j(\omega+\omega_p)\tau_k}\,, \tag{C.5}$$

$$\frac{\partial \mu_p}{\partial \alpha_k^{\mathrm{I}}}\left(e^{j\omega T}\right) = jx\left(e^{j\omega T}\right)e^{-j(\omega+\omega_p)\tau_k}\,, \tag{C.6}$$

$$\frac{\partial \mu_p^*}{\partial \alpha_\ell^{\mathrm{R}}}\left(e^{j\omega T}\right) = x^*\left(e^{j\omega T}\right)e^{j(\omega+\omega_p)\tau_\ell}\,, \tag{C.7}$$

$$\frac{\partial \mu_p^*}{\partial \alpha_\ell^{\mathrm{I}}}\left(e^{j\omega T}\right) = -jx^*\left(e^{j\omega T}\right)e^{j(\omega+\omega_p)\tau_\ell}. \tag{C.8}$$

Also, the following notations will be used to keep the complexity of the expressions in check:

$$\Upsilon_x = 2P\,\Phi_x/\sigma_\eta^2\,,\ \beta^2 = P^2\pi^2/T^2\,, \Delta\tau_{ij} = \tau_i - \tau_j, \tag{C.9}$$

$$S_{a,ij} = T\sin\left(P\pi\Delta\tau_{ij}/T\right)/P\pi\Delta\tau_{ij}\,, \tag{C.10}$$

$$C_{a,ij} = \left(\cos\left(P\pi\Delta\tau_{ij}/T\right) - S_{a,ij}\right)/\Delta\tau_{ij}, \tag{C.11}$$

$$\rho_{\tau,ij} = \beta^2 S_{a,ij} + 2C_{a,ij}/\Delta\tau_{ij}, \tag{C.12}$$

$$\rho_{\alpha,ij} = C_{a,ij}^2/\left(1 - S_{a,ij}^2\right). \tag{C.13}$$

Further, the elements of each of the sub-matrices from $\boldsymbol{J}(\boldsymbol{\theta})$ are calculated.

1). The elements of sub-matrix $\boldsymbol{J}_\tau(\boldsymbol{\theta})$ are determined by using (C.3) and (C.4) in (C.1):

$$[\boldsymbol{J}_{\tau}(\boldsymbol{\theta})]_{i,j} = \frac{T}{\pi\sigma_{\eta}^2}\int_{-\frac{\pi}{T}}^{\frac{\pi}{T}}\sum_{p=1}^{P}\mathrm{Re}\left\{\frac{\partial\mu_p^*}{\partial\theta_i}\left(e^{j\omega T}\right)\frac{\partial\mu_p}{\partial\theta_j}\left(e^{j\omega T}\right)\right\}\mathrm{d}\omega =$$

$$= \frac{T}{\pi\sigma_{\eta}^2}\sum_{p=1}^{P}\int_{-\frac{\pi}{T}}^{\frac{\pi}{T}}\mathrm{Re}\left\{\left(\omega+\omega_p\right)^2\left|x\left(e^{j\omega T}\right)\right|^2\alpha_i^*\alpha_j e^{j(\omega+\omega_p)\Delta\tau_{ij}}\right\}\mathrm{d}\omega$$

$$= \frac{T}{\pi}\frac{\Phi_x}{\sigma_{\eta}^2}\sum_{p=1}^{P}\int_{\omega_p-\frac{\pi}{T}}^{\omega_p+\frac{\pi}{T}}\mathrm{Re}\left\{\omega^2\alpha_i^*\alpha_j e^{j\omega\Delta\tau_{ij}}\right\}\mathrm{d}\omega =$$

$$= \frac{T}{\pi}\frac{\Phi_x}{\sigma_{\eta}^2}\mathrm{Re}\left\{\int_{-P\pi/T}^{P\pi/T}\omega^2\alpha_i^*\alpha_j e^{j\omega\Delta\tau_{ij}}\mathrm{d}\omega\right\}, \tag{C.14}$$

where the assumption that $\Phi_x(\omega) = \left|x\left(e^{j\omega T}\right)\right|^2$ is flat across the frequency bins was made. Computing (C.14) for $i = j$ and for $i \neq j$,

$$[\boldsymbol{J}_{\tau}(\boldsymbol{\theta})]_{i,j} = \begin{cases}\Upsilon_x\beta^2|\alpha_i|^2/3\,, & \text{for } i = j\\ \Upsilon_x\rho_{\tau,ij}\mathrm{Re}\{\alpha_i^*\alpha_j\}, & \text{for } i \neq j.\end{cases} \tag{C.15}$$

2). The elements of sub-matrix $\boldsymbol{J}_{\alpha^{\mathrm{R}}}(\boldsymbol{\theta})$ are determined by using (C.5) and (C.7) in (C.1):

$$\left[\boldsymbol{J}_{\alpha^{\mathrm{R}}}(\boldsymbol{\theta})\right]_{\ell,k} = \frac{T}{\pi\sigma_{\eta}^2}\sum_{p=1}^{P}\int_{-\frac{\pi}{T}}^{\frac{\pi}{T}}\mathrm{Re}\left\{\frac{\partial\mu_p^*}{\partial\alpha_{\ell}^R}\left(e^{j\omega T}\right)\frac{\partial\mu_p}{\partial\alpha_k^R}\left(e^{j\omega T}\right)\right\}\mathrm{d}\omega =$$

$$= \begin{cases}\Upsilon_x, & \text{for } \ell = k\\ \Upsilon_x S_{a,\ell k}, & \text{for } \ell \neq k.\end{cases} \tag{C.16}$$

3). The elements of sub-matrix $\boldsymbol{J}_{\alpha^{\mathrm{I}}}(\boldsymbol{\theta})$ can be shown to equal those of $\boldsymbol{J}_{\alpha^{\mathrm{R}}}(\boldsymbol{\theta})$.

4). The elements of sub-matrix $\boldsymbol{J}_{\alpha^{\mathrm{R}}\alpha^{\mathrm{I}}}(\boldsymbol{\theta})$ are determined by using (C.6) and (C.7) in (C.1):

$$\left[\boldsymbol{J}_{\alpha^{\mathrm{R}}}(\boldsymbol{\theta})\right]_{\ell,k} = \frac{T}{\pi\sigma_\eta^2}\sum_{p=1}^{P}\int_{-\frac{\pi}{T}}^{\frac{\pi}{T}} \mathrm{Re}\left\{\frac{\partial\mu_p^*}{\partial\alpha_\ell^R}\left(e^{j\omega T}\right)\frac{\partial\mu_p}{\partial\alpha_k^I}\left(e^{j\omega T}\right)\right\}\mathrm{d}\omega = 0. \tag{C.17}$$

5). The elements of sub-matrix $\boldsymbol{J}_{\tau\alpha^{\mathrm{R}}}(\boldsymbol{\theta})$ are determined by using (C.3) and (C.5) in (C.1):

$$\left[\boldsymbol{J}_{\tau\alpha^{\mathrm{R}}}(\boldsymbol{\theta})\right]_{i,k} = \frac{T}{\pi\sigma_\eta^2}\sum_{p=1}^{P}\int_{-\frac{\pi}{T}}^{\frac{\pi}{T}} \mathrm{Re}\left\{\frac{\partial\mu_p^*}{\partial\tau_i}\left(e^{j\omega T}\right)\frac{\partial\mu_p}{\partial\alpha_k^R}\left(e^{j\omega T}\right)\right\}\mathrm{d}\omega =$$

$$= \begin{cases} 0, & \text{for } k = i \\ \Upsilon_x C_{a,ik}\mathrm{Re}\{\alpha_i\}, & \text{for } k \neq i. \end{cases} \tag{C.18}$$

6). The sub-matrix $\boldsymbol{J}_{\tau\alpha^{\mathrm{I}}}(\boldsymbol{\theta})$ can be shown to equal $\boldsymbol{J}_{\tau\alpha^{\mathrm{R}}}(\boldsymbol{\theta})$.

Based on the expressions determined for the sub-matrices forming $\boldsymbol{J}(\boldsymbol{\theta})$, the later can be particularized for different number of multipath components, K. Then, the CRB for estimating only the parameters of interest can be determined. That is, the CRB for time delays $\boldsymbol{\tau} = [\tau_1, \ldots, \tau_K]^{\mathrm{T}}$ can be calculated as a $K \times K$ matrix: $\boldsymbol{C}_\tau(\boldsymbol{\theta}) = \bar{\boldsymbol{J}}_\tau^{-1}(\boldsymbol{\theta})$, where $\bar{\boldsymbol{J}}_\tau(\boldsymbol{\theta}) = \boldsymbol{J}_\tau(\boldsymbol{\theta}) - \boldsymbol{J}_{\tau\alpha}(\boldsymbol{\theta})\boldsymbol{J}_\alpha^{-1}(\boldsymbol{\theta})\boldsymbol{J}_{\tau\alpha}^{\mathrm{H}}(\boldsymbol{\theta})$. The CRB for amplitudes $\boldsymbol{\alpha} = [\alpha_1^{\mathrm{R}}, \ldots, \alpha_K^{\mathrm{R}}, \alpha_1^{\mathrm{I}}, \ldots, \alpha_K^{\mathrm{I}}]^{\mathrm{T}}$ can be calculated as a $2K \times 2K$ matrix: $\boldsymbol{C}_\alpha(\boldsymbol{\theta}) = \bar{\boldsymbol{J}}_\alpha^{-1}(\boldsymbol{\theta})$, where $\bar{\boldsymbol{J}}_\alpha(\boldsymbol{\theta}) = \boldsymbol{J}_\alpha(\boldsymbol{\theta}) - \boldsymbol{J}_{\tau\alpha}^{\mathrm{H}}(\boldsymbol{\theta})\boldsymbol{J}_\tau^{-1}(\boldsymbol{\theta})\boldsymbol{J}_{\tau\alpha}(\boldsymbol{\theta})$.

i). Thus, for $K = 1$,

$$\boldsymbol{J}(\boldsymbol{\theta})|_{K=1} = \Upsilon_x \left[\begin{array}{c|cc} \beta^2|\alpha_1|^2/3 & 0 & 0 \\ \hline 0 & 1 & 0 \\ 0 & 0 & 1 \end{array}\right]. \tag{C.19}$$

This leads to $\mathrm{CRB}(\tau_1)|_{K=1} = [\boldsymbol{C}_\tau(\boldsymbol{\theta})]_{1,1} = 3/\Upsilon_x\beta^2|\alpha_1|^2$ or by replacing back the notations (C.9),

$$\mathrm{CRB}(\tau_1)|_{K=1} = \frac{3}{2\pi^2}\frac{\sigma_\eta^2}{\Phi_x|\alpha_1|^2}\frac{T^2}{P^3}. \tag{C.20}$$

Similarly, $\mathrm{CRB}(\alpha_1)|_{K=1} = [\boldsymbol{C}_\alpha(\boldsymbol{\theta})]_{1,1} + [\boldsymbol{C}_\alpha(\boldsymbol{\theta})]_{2,2} = 2/\Upsilon_x$ or by replacing back the notations (C.9),

$$\mathrm{CRB}(\alpha_1)|_{K=1} = \frac{\sigma_\eta^2}{\Phi_x}\frac{1}{P}. \tag{C.21}$$

With equations (C.20) and (C.21) the proof of Theorem 2 is concluded.

ii). For $K = 2$, dropping the indices ij in notations (C.9)-(C.13) since they are fixed as $i = 1$ and $j = 2$, $\boldsymbol{J}(\boldsymbol{\theta})$ and $\bar{\boldsymbol{J}}_\tau(\boldsymbol{\theta})$ can be particularized as

$$\boldsymbol{J}(\boldsymbol{\theta})|_{K=2} = \Upsilon_x \begin{bmatrix} \beta^2|\alpha_1|^2/3 & \rho_\tau\alpha_1^R\alpha_2^{\mathrm{R}} & 0 & C_a\alpha_1^R & 0 & C_a\alpha_1^R \\ \rho_\tau\alpha_1^R\alpha_2^{\mathrm{R}} & \beta^2|\alpha_2|^2/3 & -C_a\alpha_2^{\mathrm{R}} & 0 & -C_a\alpha_2^{\mathrm{R}} & 0 \\ 0 & -C_a\alpha_2^{\mathrm{R}} & 1 & S_a & 0 & 0 \\ C_a\alpha_1^R & 0 & S_a & 1 & 0 & 0 \\ 0 & -C_a\alpha_2^{\mathrm{R}} & 0 & 0 & 1 & S_a \\ C_a\alpha_1^R & 0 & 0 & 0 & S_a & 1 \end{bmatrix} \tag{C.22}$$

$$\bar{\boldsymbol{J}}_{\tau}(\boldsymbol{\theta})|_{K=2} = \Upsilon_x \begin{bmatrix} |\alpha_1|^2(\beta^2/3 - \rho_\alpha) & \alpha_1^R \alpha_2^{\mathrm{R}}(\rho_\tau - \rho_\alpha S_a) \\ \alpha_1^R \alpha_2^{\mathrm{R}}(\rho_\tau - \rho_\alpha S_a) & |\alpha_2|^2(\beta^2/3 - \rho_\alpha) \end{bmatrix} \tag{C.23}$$

From this, $\boldsymbol{C}_{\tau}(\boldsymbol{\theta}) = \bar{\boldsymbol{J}}_{\tau}^{-\mathbf{1}}(\boldsymbol{\theta})$ and the CRB bounding the time delays estimation variance is given by $\mathrm{CRB}(\tau_1)|_{K=2} = [\boldsymbol{C}_{\tau}(\boldsymbol{\theta})]_{1,1}$ and $\mathrm{CRB}(\tau_2)|_{K=2} = [\boldsymbol{C}_{\tau}(\boldsymbol{\theta})]_{2,2}$, resulting in:

$$\begin{cases} \mathrm{CRB}(\tau_1)|_{K=2} = (\beta^2/3 - \rho_\alpha)|\alpha_2|^2/\rho_\Delta \\ \mathrm{CRB}(\tau_2)|_{K=2} = (\beta^2/3 - \rho_\alpha)|\alpha_1|^2/\rho_\Delta \end{cases}, \tag{C.24}$$

whith $\rho_\Delta = \Upsilon_x(|\alpha_1\alpha_2|^2(\beta^2/3 - \rho_\alpha)^2 - (\alpha_1^R\alpha_2^R)^2(\rho_\tau - \rho_\alpha S_a)^2)$.

Equation (C.24) gives a closed form expression of the CRB for TDE for $K = 2$ paths, favoring the analysis of the CRB variation with the inter-path separation.

REFERENCES

[1] H. Krim and M. Viberg, "Two decades of array signal processing research: the parametric approach," *IEEE Signal Processing Magazine*, vol. 13, pp. 67-94, 1996.

[2] L. C. Godara, "Applications of antenna arrays to mobile communications. I. Performance improvement, feasibility, and system considerations," *Proceedings of the IEEE*, vol. 85, pp. 1031-1060, 1997.

[3] L. C. Godara, "Applications of antenna arrays to mobile communications. II. Beam-forming and direction-of-arrival considerations," *Proceedings of the IEEE*, vol. 85, pp. 1195-1245, 1997.

[4] S. Frattasi, F. H. P. Fitzek, and R. Prasad, "A look into the 4G crystal ball," in *Proceedings of INTELLCOMM*, 2005, pp. 281–90.

[5] A. Hero, H. Messer, J. Goldberg, D. J. Thomson, M. G. Amin, et al., "Highlights of statistical signal and array processing," *IEEE Signal Processing Magazine*, vol. 15, pp. 21-64, 1998.

[6] N. E. Hurt, "Maximum likelihood estimation and MUSIC in array localization signal processing: A review," *Multidimensional Systems and Signal Processing*, vol. 1, pp. 279-325, 1990.

[7] J. F. Bull, "Wireless Geolocation," *IEEE Vehicular Technology Magazine*, vol. 4, pp. 45-53, 2009.

[8] S. Frattasi, *Mobile Positioning and Tracking: From Conventional to Cooperative Techniques*. Chichester UK: John Wiley & Sons Ltd., 2010.

[9] R. W. Klukas, "A superresolution based cellular positioning system using GPS time synchronization," *PhD Dissertation*, Department of Geomatics Engineering, The University of Calgary, Calgary, Canada, 1997.

[10] M. Aatique, "Evaluation of TDoA techniques for position location in CDMA systems," *MSc Dissertation*, Faculty of the Virginia Polytechnic Institute and State University, Blacksburg, Virginia, 1997.

[11] J. J. Caffery, *Wireless location in CDMA cellular radio systems*. Norwell MA: Kluwer Academic Publishers, 1999.

[12] J. J. Caffery and G. L. Stuber, "Overview of radiolocation in CDMA cellular systems," *Communications Magazine*, IEEE, vol. 36, pp. 38-45, 1998.

[13] T. S. Rappaport, J. H. Reed, and B. D. Woerner, "Position location using wireless communications on highways of the future," *Communications Magazine*, IEEE, vol. 34, pp. 33-41, 1996.

[14] A. H. Sayed and N. R. Yousef, "Wireless location," in *Wiley Encyclopedia of Telecommunications*, Hoboken NJ, ed: John Wiley & Sons Inc., 2003.

[15] A. H. Sayed, A. Tarighat, and N. Khajehnouri, "Network-based wireless location: challenges faced in developing techniques for accurate wireless location information," *IEEE Signal Processing Magazine*, vol. 22, pp. 24-40, 2005.

[16] N. Patwari, J. N. Ash, S. Kyperountas, A. O. Hero, III, R. L. Moses, et al., "Locating the nodes: cooperative localization in wireless sensor networks," *IEEE Signal Processing Magazine*, vol. 22, pp. 54-69, 2005.

[17] F. Gustafsson and F. Gunnarsson, "Mobile positioning using wireless networks: possibilities and fundamental limitations based on available wireless network measurements," *IEEE Signal Processing Magazine*, vol. 22, pp. 41-53, 2005.

[18] S. Gezici, T. Zhi, G. B. Giannakis, H. Kobayashi, A. F. Molisch, et al., "Localization via ultra-wideband radios: A look at positioning aspects for future sensor networks," *IEEE Signal Processing Magazine*, vol. 22, pp. 70-84, 2005.

[19] S. Gezici, "A survey on wireless position estimation," *Wireless Personal Communications*, vol. 44, pp. 263-282, 2008.

[20] D. Dardari, A. Conti, U. Ferner, A. Giorgetti, and M. Z. Win, "Ranging with ultrawide bandwidth signals in multipath environments," in *Proceedings of the IEEE*, vol. 97, pp. 404-426, 2009.

[21] C. Knapp and G. Carter, "The generalized correlation method for estimation of time delay," *IEEE Transactions on Acoustics, Speech and Signal Processing*, vol. 24, pp. 320-327, 1976.

[22] M. S. Brandstein and H. F. Silverman, "A robust method for speech signal time-delay estimation in reverberant rooms," in *Proceedings of the IEEE International Conference on Acoustics, Speech, and Signal Processing*, ICASSP, 1997, pp. 375-378, vol.1.

[23] J. Chen, J. Benesty, and Y. Huang, "Time delay estimation in room acoustic environments: an overview," *EURASIP Journal of Applied Signal Processing*, vol. 2006, pp. 170-170, 2006.

[24] C. R. Comsa, L. Jianghong, A. M. Haimovich, and S. Schwartz, "Wireless localization using time difference of arrival in narrow-band multipath systems," in *Proceedings of the IEEE International Symposium on Signals, Circuits and Systems*, ISSCS, 2007, pp. 1-4.

[25] B. M. Sadler and R. J. Kozick, "A survey of time delay estimation performance bounds," in *Proceedings of the Fourth IEEE Workshop on Sensor Array and Multichannel Processing*, 2006, pp. 282-288.

[26] R. J. Kozick and B. M. Sadler, "Bounds and algorithms for time delay estimation on parallel, flat fading channels," in *Proceedings of the IEEE International Conference on Acoustics, Speech and Signal Processing*, ICASSP, 2008, pp. 2413-2416.

[27] S. Gezici, H. Celebi, H. V. Poor, and H. Arslan, "Fundamental limits on time delay estimation in dispersed spectrum cognitive radio systems," *IEEE Transactions on Wireless Communications*, vol. 8, pp. 78-83, 2009.

[28] M. L. Fowler and X. Hu, "Signal models for TDOA/FDOA estimation," *IEEE Transactions on Aerospace and Electronic Systems*, vol. 44, pp. 1543-1550, 2008.

[29] J. Luo, S. Schwartz, and A. M. Haimovich, *Geolocation using TDOA*. Research report, New Jersey Institute of Technology, Newark, NJ, 2006.

[30] Y. Qi, H. Kobayashi, and H. Suda, "On time-of-arrival positioning in a multipath environment," *IEEE Transactions on Vehicular Technology*, vol. 55, pp. 1516-1526, 2006.

[31] Y. Qi, H. Kobayashi, and H. Suda, "Analysis of wireless geolocation in a non-line-of-sight environment," *IEEE Transactions on Wireless Communications*, vol. 5, pp. 672-681, 2006.

[32] I. Guvenc and C.-C. Chong, "A Survey on TOA based wireless localization and NLOS mitigation techniques," *IEEE Communications Surveys & Tutorials*, vol. 11, pp. 107-124, 2009.

[33] J. Khodjaev, Y. Park, and A. Saeed Malik, "Survey of NLOS identification and error mitigation problems in UWB-based positioning algorithms for dense environments," *Annals of Telecommunications*, vol. 65, pp. 301-311, 2010.

[34] A. O. Hero and S. C. Schwartz, "Topics in time delay estimation," *PhD Dissertation*, Electrical Engineering Dept., Princeton University, Princeton, NJ, 1985.

[35] X. Li and K. Pahlavan, "Super-Resolution TOA Estimation with diversity for indoor geolocation," *IEEE Transactions on Wireless Communications*, vol. 3, pp. 224-234, 2004.

[36] P. R. Hirschler-Marchand and G. F. Hatke, "Superresolution techniques in time of arrival estimation for precise geolocation," in *Conference Record of the Thirty-Sixth Asilomar Conference on Signals, Systems and Computers*, 2002, pp. 1272-1277, vol.2.

[37] R. Schmidt, "Multiple emitter location and signal parameter estimation," *IEEE Transactions on Antennas and Propagation*, vol. 34, pp. 276-280, 1986.

[38] B. D. Rao and K. V. S. Hari, "Performance analysis of root-MUSIC," *IEEE Transactions on Acoustics, Speech and Signal Processing*, vol. 37, pp. 1939-1949, 1989.

[39] P. Stoica and A. Nehorai, "MUSIC, maximum likelihood, and Cramer-Rao bound," *IEEE Transactions on Acoustics, Speech and Signal Processing*, vol. 37, pp. 720-741, 1989.

[40] J. J. Fuchs, "Multipath time-delay detection and Estimation," *IEEE Transactions on Signal Processing*, vol. 47, pp. 237-243, 1999.

[41] W. U. Bajwa, J. Haupt, A. M. Sayeed, and R. Nowak, "Compressed channel sensing: A new approach to estimating sparse multipath channels," *Proceedings of the IEEE*, vol. 98, pp. 1058-1076, 2010.

[42] C. R. Berger, Z.-H. Wang, J.-Z. Huang, and S. Zhou, "Application of compressive sensing to sparse channel estimation," *IEEE Communications Magazine*, pp.164-174, Nov. 2010.

[43] W.-J. Zeng, X. Jiang, X.-L. Li, and X.-D. Zhang, "Deconvolution of sparse underwater acoustic multipath channel with a large time-delay spread," *The Journal of the Acoustical Society of America*, vol. 127, pp. 909-919, 2010.

[44] D. Angelosante, E. Grossi, G. B. Giannakis, and M. Lops, "Sparsity-aware estimation of CDMA system parameters," *EURASIP Journal on Advances in Signal Processing*, 2010.

[45] Y. Lin, J. Chen, Y. Kim, and D. D. Lee, "Blind sparse-nonnegative (BSN) channel identification for acoustic time-difference-of-arrival estimation," in *IEEE Workshop on Applications of Signal Processing to Audio and Acoustics*, 2007, pp. 106-109.

[46] H. Liu, G. Xu, and L. Tong, "A deterministic approach to blind equalization," in *Conference Record of The Twenty-Seventh Asilomar Conference on Signals, Systems and Computers*, 1993, pp. 751-755 vol.1.

[47] L. Tong and S. Perreau, "Multichannel blind identification: from subspace to maximum likelihood methods," *Proceedings of the IEEE*, vol. 86, pp. 1951-1968, 1998.

[48] L. Perros-Meilhac, E. Moulines, K. Abed-Meraim, P. Chevalier, and P. Duhamel, "Blind identification of multipath channels: A parametric subspace approach," *IEEE Transactions on Signal Processing*, vol. 49, pp. 1468-1480, 2001.

[49] Z. He and A. Cichocki, "Robust channel identification using FOCUSS method," in *Advances in Neural Network Research and Applications*. vol. 67, Z. Zeng and J. Wang, Eds., ed: Springer Berlin Heidelberg, 2010, pp. 471-477.

[50] A. Aissa-El-Bey and K. Abed-Meraim, "Blind SIMO channel identification using a sparsity criterion," in *IEEE 9th Workshop on Signal Processing Advances in Wireless Communications*, SPAWC 2008, pp. 271-275.

[51] A. Kammoun, A. Aissa El Bey, K. Abed-Meraim, and S. Affes, "Robustness of blind subspace based techniques using l_p quasi-norms," in *Proceedings of IEEE Workshop on Signal Processing Advances in Wireless Communications,* SPAWC 2010, Marrakech, Morroco.

[52] M. Grant, S. Boyd, and Y. Ye. *CVX: Matlab Software for Disciplined Convex Programming* [Online]. Available 2010: www.stanford.edu/~boyd/cvx

[53] Y. T. Chan and K. C. Ho, "A simple and efficient estimator for hyperbolic location," *IEEE Transactions on Signal Processing*, vol. 42, pp. 1905-1915, 1994.

[54] I. Ziskind and M. Wax, "Maximum likelihood localization of multiple sources by alternating projection," *IEEE Transactions on Acoustics, Speech and Signal Processing*, vol. 36, pp. 1553-1560, 1988.

[55] J. C. Chen, R. E. Hudson, and Y. Kung, "Maximum-likelihood source localization and unknown sensor location estimation for wideband signals in the near-field," *IEEE Transactions on Signal Processing*, vol. 50, pp. 1843-1854, 2002.

[56] Y. Rui and D. Florencio, "New direct approaches to robust sound source localization," in *Proceedings of International Conference on Multimedia and Expo*, ICME, 2003, pp. I-737-40 vol.1.

[57] C. Zhang, D. Florencio, D. E. Ba, and Z. Zhang, "Maximum likelihood sound source localization and beamforming for directional microphone arrays in distributed meetings," *IEEE Transactions on Multimedia*, vol. 10, pp. 538-548, 2008.

[58] A. J. Weiss, "Direct position determination of narrowband radio transmitters," in *IEEE Proceedings of International Conference on Acoustics, Speech, and Signal Processing*, ICASSP, 2004, pp. ii-249-50,ii-251-2 vol.2.

[59] I. Guvenc, S. Gezici, and Z. Sahinoglu, "Ultra-wideband range estimation: Theoretical limits and practical algorithms," *in IEEE International Conference on Ultra-Wideband*, ICUWB, 2008, pp. 93-96.

[60] S. Gezici and Z. Sahinoglu, "Ranging in a single-input multiple-output (SIMO) system," *IEEE Communications Letters*, vol. 12, pp. 197-199, 2008.

[61] A. L. Swindlehurst, "Time delay and spatial signature estimation using known asynchronous signals," *IEEE Transactions on Signal Processing*, vol. 46, pp. 449-462, 1998.

[62] H. V. Poor, *An introduction to signal detection and estimation*, 2nd ed., New York: Springer-Verlag, 1994.

[63] N. H. Lehmann, A. M. Haimovich, R. S. Blum, and L. Cimini, "High resolution capabilities of MIMO radar," in *Fortieth Asilomar Conference on Signals, Systems and Computers*, 2006, pp. 25-30.

[64] H. Godrich, A. M. Haimovich, and R. S. Blum, "Target localization accuracy and multiple target localization: Tradeoff in MIMO radars," in *42nd Asilomar Conference on Signals, Systems and Computers*, 2008, pp. 614-618.

[65] H. Godrich, A. M. Haimovich, and R. S. Blum, "Target localization accuracy gain in MIMO radar-based systems," *IEEE Transactions on Information Theory*, vol. 56, pp. 2783-2803, 2010.

[66] H. Godrich, A. M. Haimovich, and R. Blum, "Concepts and applications of MIMO radar sysem with widely separated antenna," in *MIMO Radar Signal Processing*, John Wiley & Sons, Inc., 2008, p. 365.

[67] H. L. Van Trees, K. L. Bell, and S. Dosso, *Bayesian Bounds for Parameter Estimation and Nonlinear Filtering/Tracking*. New York: Wiley-Interscience, 2001.

[68] M. N. El Korso, R. Boyer, A. Renaux, and S. Marcos, "Conditional and unconditional Cramer-Rao bounds for near-field source localization," *IEEE Transactions on Signal Processing*, vol. 58, pp. 2901-2907, 2010.

[69] B. Steinberg, "The peak sidelobe of the phased array having randomly located elements," *IEEE Transactions on Antennas and Propagation*, vol. 20, pp. 129-136, 1972.

[70] B. Steinberg and E. Attia, "Sidelobe reduction of random arrays by element position and frequency diversity," *IEEE Transactions on Antennas and Propagation*, vol. 31, pp. 922-930, 1983.

[71] H. Ochiai, P. Mitran, H. V. Poor, and V. Tarokh, "Collaborative beamforming for distributed wireless ad hoc sensor networks," *IEEE Transactions on Signal Processing*, vol. 53, pp. 4110-4124, 2005.

[72] M. A. Haleem and A. M. Haimovich, "On the distribution of ambiguity levels in MIMO radar," in *42nd Asilomar Conference on Signals, Systems and Computers*, 2008, pp. 198-202.

[73] X. Zhuge, A. G. Yarovoy, and L. P. Ligthart, "A sidelobe reduction technique for enhancing images of UWB sparse MIMO array," in *International Radar Conference - Surveillance for a Safer World*, RADAR, 2009, pp. 1-6.

[74] A. Zeira and P. M. Schultheiss, "Realizable lower bounds for time delay estimation. 2. Threshold phenomena," *IEEE Transactions on Signal Processing*, vol. 42, pp. 1001-1007, 1994.

[75] A. Weiss and E. Weinstein, "Fundamental limitations in passive time delay estimation--Part I: Narrow-band systems," *IEEE Transactions on Acoustics, Speech and Signal Processing*, vol. 31, pp. 472-486, 1983.

[76] Q. He, R. S. Blum, and A. M. Haimovich, "Non-coherent MIMO radar for target estimation: More antennas means better performance," in *43rd Annual Conference on Information Sciences and Systems*, CISS, 2009, pp. 108-113.

[77] V. M. Chiriac, A. M. Haimovich, S. C. Schwartz, and J. A. Dabin, "Performance bound for localization of a near field source," in *Conference Record of the Forty-Third Asilomar Conference on Signals, Systems and Computers*, 2009, pp. 130-135.

[78] S. Taheri and B. Steinberg, "Tolerances in self-cohering antenna arrays of arbitrary geometry," *IEEE Transactions on Antennas and Propagation*, vol. 24, pp. 733-739, 1976.

[79] B. P. Flanagan and K. L. Bell, "Array self calibration with large sensor position errors," in *Conference Record of the Thirty-Third Asilomar Conference on Signals, Systems, and Computers*, 1999, pp. 258-262, vol.1.

[80] Y. Rockah, H. Messer, and P. M. Schultheiss, "Localization performance of arrays subject to phase errors," *IEEE Transactions on Aerospace and Electronic Systems*, vol. 24, pp. 402-410, 1988.

[81] Y. Rockah and P. Schultheiss, "Array shape calibration using sources in unknown locations--Part II: Near-field sources and estimator implementation," *IEEE Transactions on Acoustics, Speech and Signal Processing,* vol. 35, pp. 724-735, 1987.

[82] M. Vetterli, P. Marziliano, and T. Blu, "Sampling signals with finite rate of innovation," *IEEE Transactions on Signal Processing*, vol. 50, pp. 1417-1428, 2002.

[83] T. Blu, P. L. Dragotti, M. Vetterli, P. Marziliano, and L. Coulot, "Sparse Sampling of Signal Innovations," *IEEE Signal Processing Magazine*, vol. 25, pp. 31-40, 2008.

[84] K. Gedalyahu and Y. C. Eldar, "Time-delay estimation from low-rate samples: A union of subspaces approach," *IEEE Transactions on Signal Processing*, vol. 58, pp. 3017-3031, 2010.

[85] J. A. Urigüen, Y. C. Eldar, P. L. Dragotti, and Z. Ben-Haim, *Sampling at the rate of innovation: Theory and applications* [Online]. Available 2011: http://webee.technion.ac.il/Sites/People/YoninaEldar/files/mainFormat.pdf

[86] Z. Ben-Haim, T. Michaeli, and Y. C. Eldar, "Performance bounds and design criteria for estimating finite rate of innovation signals," *Arxiv preprint* arXiv:1009.2221, 2010.

[87] A. Goldsmith, *Wireless communications*. New York: Cambridge University Press, 2005.

[88] C. R. Comsa, A. M. Haimovich, S. Schwartz, Y. Dobyns, and J. A. Dabin, "Source localization using time difference of arrival within a sparse representation framework," in *IEEE International Conference on Acoustics, Speech and Signal Processing (ICASSP)*, 2011, pp. 2872-2875.

[89] C. R. Comsa, A. M. Haimovich, S. C. Schwartz, Y. H. Dobyns, and J. A. Dabin, "Time difference of arrival based source localization within a sparse representation framework," in *45th Annual Conference on Information Sciences and Systems (CISS)*, 2011, pp. 1-6.

[90] C. R. Comsa and A. M. Haimovich, "Performance bound for signal parameters estimation from low rate samples," to be submitted to the *IEEE Transactions on Signal Processing*, 2012.

[91] S. M. Kay, *Fundamentals of statistical signal processing: Estimation Theory*. Englewood Cliffs, N.J.: Prentice-Hall PTR, 1993.

[92] H. L. Van Trees, *Optimum array processing*. New York: Wiley-Interscience, 2002.

[93] S. J. Orfanidis, *Optimum signal processing: an introduction*. New York, London: Macmillan, 1985.

[94] R. T. Williams, S. Prasad, A. K. Mahalanabis, and L. H. Sibul, "An improved spatial smoothing technique for bearing estimation in a multipath environment," *IEEE Transactions on Acoustics, Speech and Signal Processing*, vol. 36, pp. 425-432, 1988.

[95] N. Shahapurkar and C. S. Ramalingam, "Threshold performance of MUSIC when using the forward-backward data matrix," *IEEE Signal Processing Letters*, vol. 13, pp. 80-83, 2006.

[96] H. Akaike, "A new look at the statistical model identification," *IEEE Transactions on Automatic Control*, vol. 19, pp. 716-723, 1974.

[97] E. Fishler and H. V. Poor, "Estimation of the number of sources in unbalanced arrays via information theoretic criteria," *IEEE Transactions on Signal Processing*, vol. 53, pp. 3543-3553, 2005.

[98] M. Wax and T. Kailath, "Detection of signals by information theoretic criteria," *IEEE Transactions on Acoustics, Speech and Signal Processing*, vol. 33, pp. 387-392, 1985.

[99] L. Li, R. Chongsen, and W. Feng, "Number of multipaths estimation by unitary transformation," in *International Conference on Communications, Circuits and Systems*, 2004, pp. 98-102 Vol.1.

[100] Z.-F. Zhong, B.-Y. Wen, Q.-D. Wang, and Q. Cao, "A new method using Gerschgorin disks for source number estimation," in *Proceedings of International Conference on Machine Learning and Cybernetics*, 2004, pp. 2086-2089 vol.4.

[101] H.-Q. Zhao, B. Zhao, H. Quan, and Y.-p. Zhang, "Source number estimation methods base on support vector machine algorithm," in *Asia-Pacific Conference on Computational Intelligence and Industrial Applications*, PACIIA, 2009, pp. 272-275.

[102] J. A. Tropp and S. J. Wright, "Computational methods for sparse solution of linear inverse problems," *Proceedings of the IEEE Special Issue on Applications of Sparse Representation and Compressive Sensing*, vol. 98, pp. 948-958, 2010.

[103] R. Giryes, M. Elad, and Y. C. Eldar, "The projected GSURE for automatic parameter tuning in iterative shrinkage methods," *Applied and Computational Harmonic Analysis*, vol. 30, issue 3, May, pp. 407-422.

[104] D. Malioutov, M. Cetin, and A. S. Willsky, "A sparse signal reconstruction perspective for source localization with sensor arrays," *IEEE Transactions on Signal Processing*, vol. 53, pp. 3010-3022, 2005.

[105] X. Huan, C. Caramanis, and S. Mannor, "Robust regression and Lasso," *IEEE Transactions on Information Theory*, vol. 56, pp. 3561-3574, 2010.

[106] H. Zou, "The adaptive Lasso and its oracle properties," *Journal of the American Statistical Association*, vol. 101, p. 12, 2006.

[107] J. Haupt, L. Applebaum, and R. Nowak, "On the restricted isometry of deterministically subsampled Fourier matrices," in *44th Annual Conference on Information Sciences and Systems (CISS)*, 2010, pp. 1-6.

[108] D. J. Torrieri, "Statistical theory of passive location systems," *IEEE Transactions on Aerospace and Electronic Systems*, vol. AES-20, pp. 183-198, 1984.

[109] K. Lui, F. Chan, and H. C. So, "Semidefinite Programming approach for range-difference based source localization," *IEEE Transactions on Signal Processing*, vol. 57, pp. 1630-1633, 2009.

[110] J. Smith and J. Abel, "Closed-form least-squares source location estimation from range-difference measurements," *IEEE Transactions on Acoustics, Speech and Signal Processing*, vol. 35, pp. 1661-1669, 1987.

[111] B. Friedlander, "A passive localization algorithm and its accuracy analysis," *IEEE Journal of Oceanic Engineering*, vol. 12, pp. 234-245, 1987.

[112] Y. Huang, J. Benesty, G. W. Elko, and R. M. Mersereati, "Real-time passive source localization: a practical linear-correction least-squares approach," *IEEE Transactions on Speech and Audio Processing*, vol. 9, pp. 943-956, 2001.

[113] K. W. K. Lui, F. K. W. Chan, and H. C. So, "Accurate time delay estimation based passive localization," *Signal Processing*, vol. 89, pp. 1835-1838, 2009.

[114] S. Boyd and L. Vandenberghe, *Convex optimization*. Cambridge Univ. Pr., 2004.

[115] E. Xu, Z. Ding, and S. Dasgupta, "Robust and low complexity source localization in wireless sensor networks using time difference of arrival measurement," in *IEEE Wireless Communications and Networking Conference (WCNC)*, 2010, pp. 1-5.

[116] K. Yang, G. Wang, and Z.-Q. Luo, "Efficient convex relaxation methods for robust target localization by a sensor network using time differences of arrivals," *IEEE Transactions on Signal Processing*, vol. 57, pp. 2775-2784, 2009.

[117] Y. C. Eldar, A. Ben-Tal, and A. Nemirovski, "Robust mean-squared error estimation in the presence of model uncertainties," *IEEE Transactions on Signal Processing*, vol. 53, pp. 168-181, 2005.

[118] H. C. So, Y. T. Chan, and F. K. W. Chan, "Closed-form formulae for time-difference-of-arrival estimation," *IEEE Transactions on Signal Processing*, vol. 56, pp. 2614-2620, 2008.

[119] Z. Lu, X. Zhang, and Q. Wan, "Biased time-of-arrival-based location dominating linear-least-squares estimation," in *2nd International Conference on Signal Processing Systems (ICSPS)*, 2010, pp. V2-313-V2-316.

[120] Y. C. Eldar, "Universal weighted MSE improvement of the Least-Squares estimator," *IEEE Transactions on Signal Processing*, vol. 56, pp. 1788-1800, 2008.

[121] V. Cevher, M. Duarte, and R. Baraniuk, "Distributed target localization via spatial sparsity," *Proceedings of the European Signal Processing Conference (EUSIPCO)*, 2008.

[122] C. D. Austin, R. L. Moses, J. N. Ash, and E. Ertin, "On the relation between sparse reconstruction and parameter estimation with model order selection," *IEEE Journal of Selected Topics in Signal Processing*, vol. 4, pp. 560-570, 2010.

[123] K. Petersen and M. Pedersen, *The matrix cookbook*, [Online], Available 2008: http://orion.uwaterloo.ca/~hwolkowi/matrixcookbook.pdf.

[124] A. Zeira and A. Nehorai, "Frequency domain Cramer-Rao bound for Gaussian processes," *IEEE Transactions on Acoustics, Speech and Signal Processing*, vol. 38, pp. 1063-1066, 1990.

[125] M. Skolnik, *Introduction to Radar Systems*. New York: McGraw-Hill, 2002.

[126] H. B. Lee, "A novel procedure for assessing the accuracy of hyperbolic multilateration systems," *IEEE Transactions on Aerospace and Electronic Systems*, vol. AES-11, pp. 2-15, 1975.

[127] M. Mishali, Y. C. Eldar, and A. J. Elron, "Xampling: Signal acquisition and processing in union of subspaces," *IEEE Transactions on Signal Processing*, vol. 59, pp. 4719-4734, 2011.

[128] Y. M. Lu and M. N. Do, "A theory for sampling signals from a union of subspaces," *IEEE Transactions on Signal Processing*, vol. 56, pp. 2334-2345, 2008.

[129] R. Roy and T. Kailath, "ESPRIT-estimation of signal parameters via rotational invariance techniques," *IEEE Transactions on Acoustics, Speech and Signal Processing*, vol. 37, pp. 984-995, 1989.

[130] A. Jakobsson, A. L. Swindlehurst, and P. Stoica, "Subspace-based estimation of time delays and Doppler shifts," *IEEE Transactions on Signal Processing*, vol. 46, pp. 2472-2483, 1998.

[131] R. Tur, Y. C. Eldar, and Z. Friedman, "Innovation rate sampling of pulse streams with application to ultrasound imaging," *IEEE Transactions on Signal Processing*, vol. 59, pp. 1827-1842, 2011.

[132] M. Unser and T. Blu, "Cardinal exponential splines: part I - theory and filtering algorithms," *IEEE Transactions on Signal Processing*, vol. 53, pp. 1425-1438, 2005.

[133] P. L. Dragotti, M. Vetterli, and T. Blu, "Sampling moments and reconstructing signals of finite rate of innovation: Shannon meets Strang-Fix," *IEEE Transactions on Signal Processing*, vol. 55, pp. 1741-1757, 2007.

[134] Y. C. Eldar, "Compressed sensing of analog signals in shift-invariant spaces," *IEEE Transactions on Signal Processing*, vol. 57, pp. 2986-2997, 2009.

[135] K. Gedalyahu, R. Tur, and Y. C. Eldar, "Multichannel sampling of pulse streams at the rate of innovation," *IEEE Transactions on Signal Processing*, vol. 59, pp. 1491-1504, 2011.

[136] W. U. Bajwa, K. Gedalyahu, and Y. C. Eldar, "Identification of parametric underspread linear systems and super-resolution radar," *IEEE Transactions on Signal Processing*, vol. 59, pp. 2548-2561, 2011.

[137] Y. C. Eldar, "Rethinking biased estimation: Improving maximum likelihood and the Cramér–Rao bound," *Foundations and Trends in Signal Processing*, vol. 1, pp. 305-449, 2008.

[138] S. M. Kay, *Fundamentals of Statistical Signal Processing: Estimation theory*. Upper Saddle River NJ: Prentice-Hall PTR, 1993.

[139] S. F. Yau and Y. Bresler, "A compact Cramer-Rao bound expression for parametric estimation of superimposed signals," *IEEE Transactions on Signal Processing*, vol. 40, pp. 1226-1230, 1992.

[140] M. Sharp and A. Scaglione, "Estimation of sparse multipath channels," in *Military Communications Conference (MILCOM)*, 2008, pp. 1-7, Orlando FL.

[141] M. J. D. Rendas and J. M. F. Moura, "Cramer-Rao bound for location systems in multipath environments," *IEEE Transactions on Signal Processing*, vol. 39, pp. 2593-2610, 1991.

[142] L. W. Couch II, *Digital and analog communication systems*. Upper Saddle River NJ: Prentice Hall PTR, 2000.

[143] M. Wax and I. Ziskind, "On unique localization of multiple sources by passive sensor arrays," *IEEE Transactions on Acoustics, Speech and Signal Processing*, vol. 37, pp. 996-1000, 1989.

[144] I. Ziskind and Y. Bar-Ness, "Localization by narrow-band autoregressive sources by passive sensor arrays," *IEEE Transactions on Signal Processing*, vol. 40, pp. 484-487, 1992.

[145] T.-J. Shan, M. Wax, and T. Kailath, "On spatial smoothing for direction-of-arrival estimation of coherent signals," *IEEE Transactions on Acoustics, Speech and Signal Processing*, vol. 33, pp. 806-811, 1985.

[146] S. J. Orfanidis, *Introduction to signal processing*. Englewood Cliffs, NJ: Prentice-Hall, Inc., 1995.

[147] B. Friedlander, "On the Cramer-Rao bound for time delay and Doppler estimation," *IEEE Transactions on Information Theory*, vol. 30, pp. 575-580, 1984.